INFORMATION TO USERS

This manuscript has been reproduced from the microfilm master. UMI films the text directly from the original or copy submitted. Thus, some thesis and dissertation copies are in typewriter face, while others may be from any type of computer printer.

The quality of this reproduction is dependent upon the quality of the copy submitted. Broken or indistinct print, colored or poor quality illustrations and photographs, print bleedthrough, substandard margins, and improper alignment can adversely affect reproduction.

In the unlikely event that the author did not send UMI a complete manuscript and there are missing pages, these will be noted. Also, if unauthorized copyright material had to be removed, a note will indicate the deletion.

Oversize materials (e.g., maps, drawings, charts) are reproduced by sectioning the original, beginning at the upper left-hand corner and continuing from left to right in equal sections with small overlaps.

Photographs included in the original manuscript have been reproduced xerographically in this copy. Higher quality 6" x 9" black and white photographic prints are available for any photographs or illustrations appearing in this copy for an additional charge. Contact UMI directly to order.

Bell & Howell Information and Learning
300 North Zeeb Road, Ann Arbor, MI 48106-1346 USA
800-521-0600

THE HOT WORKING CHARACTERISTICS OF Al-0.65% Fe, AND Al-0.5% Fe-0.5% Co CONDUCTOR ALLOYS

Kevin Conrod

A Thesis

in

The Department

of

Mechanical Engineering

Presented in Partial Fulfillment of the Requirements

for the Degree of Master of Applied Science at

Concordia University

Montreal, Quebec, Canada

August 2000

ABSTRACT

The Hot Working Characteristics of Al-0.65% Fe,
and Al-0.5% Fe-0.5% Co Conductor Alloys

Kevin Conrod

Recrystallized, rolled rods of the two conductor alloys were deformed in continuous torsion tests between 200 and 500°C and 0.02 and 5 s^{-1}, and in interrupted torsion tests at 400 and 450°C, and 0.1 and 1.0 s^{-1}. The flow stresses were found to depend on the strain rate through a hyperbolic sine function with exponents of 3.1 and 3.5, and on temperature through an Arrhenius term with activation energies of about 260 kJ/mol, much greater than Al. Flow stresses were considerably higher than commercial Al at 200°C and 300°C, consistent with their resistance to creep softening in that range. The strengthening depends upon the dispersion of the eutectic rods which were refined by Properzi casting, were fractured and dispersed by rolling, and have very low solubility. The hot ductility increased with temperature but decreased with strain rate and with rising levels of alloy addition. The strain to fracture varied inversely with the strain to steady state and hence the level of dynamic recovery. In interrupted testing, fractional softening increased with rise in temperature or hold time, or decline in strain rate. With repeated passes, the strength of the alloys declined substantially compared to continuous testing.

ACKNOWLEDGMENTS

The author wishes to thank his advisor, Professor H.J.McQueen, for his assistance and patience in a project that took far longer to complete than could ever have been imagined at the outset.

The author would also like to thank Professor J.J.Jonas of McGill University for making the hot torsion machine available for conducting the several hundred tests needed for this work. In addition, he would like to thank J.Bowles for her advice on metallographic sample preparation and micrography.

The author would also like to thank the Southwire Aluminum Company of Carrollton, Georgia for the supply and machining of the specimens, and he acknowledges with gratitude the financial support received from the Natural Sciences and Engineering Research Council of Canada.

TABLE OF CONTENTS

LIST OF FIGURES

LIST OF SYMBOLS

A	constant in hyperbolic sine law
BCC	body centred cubic
DPH	diamond pyramid hardness
DRV	dynamic recovery
DRX	dynamic recrystallization
FCC	face centred cubic
FS	fractional softening
HCP	hexagonal close packed
K	experimental constant
N	number of revolutions in torsion test
$\dot{N}$	revolution rate in torsion test
Q	activation energy
Q_{HW}	activation energy for hot working
R	universal gas constant
RH	retained hardening
R_a	reduction in area
SFE	stacking fault energy
SRV	static recovery
SRX	static recrystallization
T	temperature
T_m	melting temperature
TEM	transmission electron microscopy
Z	Zener-Holloman parameter

c	specific heat
d_s	subgrain diameter
g.s.	grain size
g.b.	grain boundary
k_s	strength coefficient in Hall-Petch equation
k_{sb}	subgrain strengthening coefficient
l	gauge length
m	strain rate sensitivity
m	constant in Hall-Petch equation
n	constant in hyperbolic sine law
n'	strain hardening exponent
r	gauge radius of specimen
t_i	interpass hold time in interrupted deformation test
s	seconds
α	constant in hyperbolic sine law
α'	constant in Zener drag law
ϵ	linear strain
$\dot{\epsilon}$	linear strain rate
ϵ_f	fracture strain
ϵ_p	peak strain
ϵ_s	strain to peak stress or plateau stress
γ	surface shear strain
γ_{gb}	grain boundary energy
$\dot{\gamma}$	surface shear strain rate
Γ	torque
Γ_m	maximum or peak torque

Γ_{m1}	final torque at the end of the first pass for RH plots
Γ_{mi}	maximum torque at the i^{th} pass in interrupted deformation tests
Γ_o	first pass yield torque in an interrupted deformation test
Γ_r	reloading torque
Γ_{ri}	reloading torque at the i^{th} interval during an interrupted deformation test
θ	angle of twist in radians
θ	subgrain boundary angle
θ	experimental constant in exponential law
ρ	density
σ	equivalent normal stress
σ_o	yield strength of a substructure free metal
σ_s	hot strength
σ_y	yield strength
τ	shear stress
Ω	electrical resistance, ohms

LIST OF TABLES

CHAPTER ONE

INTRODUCTION

Aluminum's higher conductivity to weight ratio than copper made it an attractive candidate for replacing copper conductors in applications ranging from automobiles and aerospace to electric machinery. Despite successful use in overhead transmission lines, the introduction of 1350 grade Electrical Conductor (EC) alloy into home wiring did not prove successful. Gradual loosening at the terminals occurred, leading to some well publicized electrical fires and subsequent regulatory restrictions on their use. A new series of alloys with 0.5 to 0.9% Fe content were developed to resist the creep softening around the terminal connections that occurs with EC Al. Gaining knowledge of the relationship between manufacturing process parameters and mechanical properties is important from both a scientific and industrial standpoint in order to understand and optimize manufacturing operations, and generate full confidence in the viability of the conductor alloy for household wiring in the scientific community, regulatory agencies, and general public at large.

This study deals with two of the substructure strengthened 8000 series alloys developed by the Southwire Aluminum Company, specifically an Al-0.65Fe alloy (Triple E), and Al-0.5Fe-0.5Co alloy (Super T). The strengthening mechanism which produces the required

combination of mechanical properties and electrical conductivity is a retained dynamically recovered substructure reinforced and stabilized by dispersed eutectic particles. The particles are formed as eutectic rods of $FeAl_3$, $(Fe,Co)_2Al_9$, and $FeAl_6$ during casting and are fractured and distributed during rolling and drawing.

The primary objective of the research was to quantitatively determine the effects of temperature and strain rate on the flow stress, ductility, and microstructural development at high strains (ϵ = 4,20), thus correlating the observed mechanical properties with the microstructural evolution during processing. An additional objective was to determine in what way the hot working behaviour of the particle containing alloys compared with dynamic recovery, which reduces strain hardening and raises ductility. Torsion testing was chosen to allow testing to proceed at strain intervals representative of commercial processing. Test temperatures of 200, 300, 400, 450, and 500^{o}C, also spanned the commercial process. Strain rates were varied from 0.02 sec^{-1} to 4 sec^{-1}. Interrupted deformation testing at strain rates of 0.1 and 1.0 sec^{-1}, with interpass holding times of 5 to 100 seconds were used to check for the presence of static recrystallization, and the effect of static recovery on the change in stress upon reloading.

Before presenting the results of this investigation a review will be made of the problems with Al conductors, the theoretical basis for strengthening, followed by specifics on the mechanisms operating during production processing. Once the theoretical basis has been

established for data analysis and interpretation, along with some literature associated with Al conductor alloys, the specific tools employed for analysis will be detailed in the chapter on experimental procedure.

CHAPTER 2

REVIEW OF PAST WORK

2.1 Background on Industrial Utilization

Of all the conducting elements, only aluminum and copper possess the necessary combinations of price, conductivity, and mechanical properties to serve as current carrying conductors. Aluminum was first employed for electrical purposes in Britain in 1876, entering service in overhead transmission lines in 1909. With variations on the conductor grades and cable designs, aluminum soon supplanted copper for overhead conductors.

Widespread cost driven utilization of aluminum 1350 electrical conductor (EC) alloy for branch circuits (residential wiring) began about 1965, largely influenced by the successful deployment in transmission lines. Use in household applications did not meet with the same success as some junction failures occurred due to gradual loosening at the terminals followed by connection damage and fires, attributed primarily to glow failures (arc discharge) (1, 2, 3).

Poor thermal stability meant the EC wire could not be reliably connected to the standard small steel fasteners. Loosening and relaxation was caused by three reasons; the higher coefficient of expansion of aluminum, the formation of a tenacious aluminum oxide

film on the surface of the conductor, and the lack of thermal stability of the wire under surface overload conditions (4, 5). Steps were taken by regulatory agencies to address the above points, while Al alloys were developed with additions of 1% or less to form small uniformly distributed precipitates to stabilize a fine substructure. Alloys developed include the Triple E (AA8176), Super T, and Almhoflex Al-0.6Fe-0.3Si (AA8005). Use of iron as an alloying element was highly unusual as it was typically considered an impurity to be controlled to 0.4% or less. The higher Fe contents are advantageous when the wire is to be batch annealed at 200-250^{o}C, while lower contents and a third alloying element are beneficial for flash annealing at higher temperatures for shorter times.

2.1.1 Contributing Causes of Failures in Aluminum Conductors

Electrical conductor alloy 1350 is essentially commercially pure (1100) Al with composition controlled to 99.5% Al minimum, and limits on elements such as chromium, titanium, manganese, and vanadium. The linear coefficient of thermal expansion of Al (23.6 μm/m ^{o}C) is about 43% greater than that of copper (16.5 μm/m ^{o}C) and double that of the (11.3μm/m ^{o}C) plain carbon steel fasteners originally used in branch wiring. In order to reduce the contribution of differential expansion in the creep and oxidation of rigid contacts upon service overloads at 100-200 ^{o}C, the use of wide brass screws (20 μin/in ^{o}C) was mandated by Underwriters Laboratories (UL) in 1972 (4). Glow failures were reported to occur in Al-Fe and Cu-Fe interfaces but not in Al-Brass or Cu-Brass interfaces (4). The inability to control assembly practices

and torques led to the use of standard connectors specifically for aluminum house wiring. Reduction of the thermal expansion coefficient through alloying is not feasible for electrical conductors.

Unprotected Al possesses high resistance to atmospheric corrosion due to the formation of a highly resistant non-conductive oxide layer. Uncontrollable variability in the torque applied to standard mechanical connections during installation meant a failure to destroy the surface oxide layer when the connection was fastened to the minimum torque. Creep (deformation at strain rates of 10^{-10} to 10^{-3} per sec., >0.4 T_m) allows relaxation and subsequent decrease in contact pressure. Resistance heating at the junction interface is then accelerated due to the presence of the oxide, increasing exposure of the conductor and with growth of the layer accelerated by repeated temperature cycling under load.

2.1.2 Property Requirements for Al Conductor Alloys

The properties an Al conductor must possess to be safely employed include temperature stability, for short-time service at overload conditions, ductility for bending resistance during fabrication and installation, high yield strength for creep resistance, and resistance to stress relaxation (primary or transient creep) for contact stability (1, 6, 7). An effective high tension current carrying device requires a conductivity of at least 52% of the International Annealed Copper Standard (IACS) of 1.7241 $\mu\Omega$.cm and 61% IACS for low tension wiring (6). Aluminum 1350 EC alloy has a conductivity of 61%

IACS versus 103% for pure oxygen free copper. With a density 30% of Cu, the mass resistivity is half that of copper (0.0764 $\Omega g/m^2$ vs 0.15328 $\Omega g/m^2$ for Cu) (8). The conductivity requirements limit the types of strengthening mechanisms that may be employed. The UL minimum requirements for EC grade aluminum are given in Table 2.1 (9).

2.2 Strengthening Mechanisms for Conductor Alloys

A strong stable wire that will not loosen will not be susceptible to oxide growth and increasing contact temperature. To effectively improve creep properties of an Al conductor alloy the strengthening mechanisms employed must do so with minimal loss in conductivity. In other words, the ratio of change in strength to change in resistivity, $\Delta\sigma/\Delta\rho$, must be maximized. Work hardening, solid solution strengthening, and precipitation hardening are unacceptable as primary strengthening mechanisms for Al branch wiring as some of the mechanisms are unstable at normal overload temperatures, and the others result in excessively high resistivity. Table 2.2 (7) clearly shows that substructure strengthening offers the highest ratio of increase in strength to resistivity. Subgrain strengthening must be thermally stabilized to be effective and will be discussed further on. Production processing involves the interplay of several mechanisms which will be discussed below.

Table 2.1 Comparison of Physical Properties of Selected Al Conductor Alloys (9).

AA Number (*)	Alloy	Trade Name	UTS MPa	YS MPa	EL %	Thermal Stability (**)	Conductivity (%IACS) (***)
----	Al-0.5Fe-0.5Co	Super T	132	102	18	98	61
8176	Al-0.65Fe	Triple E	121		15	92	61
1350	Al	EC	124	105	4	71	61
	UL Requirements		103	---	10	--	--

* Aluminum association alloy number

** % retention of properties, 4 hours at 250°C

*** H24 temper, minimum

Table 2.2 Comparative Effects of Different Mechanisms on Strength and Resistivity. All Values Approximate (7)

	Mechanism	Calculated or measured at room temp.	Property: Resistivity ($\mu\Omega$.cm)	Property: Strength (MPa)	$\Delta\sigma/\Delta\rho$ (MPa/$\mu\Omega$.cm)
Substructure	Grain Boundaries	D = 100μ	nil	8.8	Very high
	Dislocations	n = 2×10^{10} mm^{-2}	3	20	7
		n = 2×10^{6} mm^{-2}	3×10^{-3}	2	70
		n = 2×10^{4} mm^{-2}	3×10^{-5}	.02	700
	Cell & Subgrain boundaries	$\theta = 10^{\circ}$, d = 2μ(m=-1/2)	6×10^{-5}	30	5×10^{5}
		$\theta = 10^{\circ}$, d = 2μ(m=-1)	6×10^{-5}	36	6×10^{5}
Alloying	Solid Solution	Ag	26	390	15
		Be	0.07	4.3	61
		Cd	0.47	6.3	13
		Ce	7×10^{-4}	0.90	1300
		Cu	1.8	160	89
		Fe	0.05	2.5	51
		Ga	1.5	93	62
		Ge	1.6	43.9	27.4
		Mg	9.9	371	37.4
		Mn	5.6	26	4.7
		Ni	0.10	2	20
		Si	0.8	25	31
		Zn	15.0	294	20
		V	1.2	8.1	7
		Mg_2Si	4.21	74	17.5
	Precipitation Hardening (over values in the pure metal)				
	Deformable particles (peak hardness)				
		Ag14%, 250°C, 10hr	6.5	400	62
		Mg_2Si, 175°C, 8hr	1.4	284	203
		Cu 1.7At%, 130°C -60°C, 1000 hr	0.7	88	125
	Non-deformable particles (Orowan)(over values in the pure metal)				
		Ag14 at%, 50°C, 100hr	3.35	70	21
		Mg_2Si, 175°C, 9 days	1.3	170	130

*** Calculated at the solubility limit
θ = subgrain misorientation

2.2.1 Cold Working

Cold working a material (deformation at <0.4 T_m) strengthens it by increasing dislocation density from 10^7 /cm^2 for fully annealed material up to 10^{12} /cm^2 for heavily cold worked material. Cold working decreases the conductivity of the wire due to the interaction of the current carrying electrons with the dislocations. Dislocations in heavily cold worked material can increase the resistance 1 to 10% above that of fully annealed material, which would lower conductivity of EC Al, and Triple E from 63% to 57% IACS, below the threshold for branch wiring (7). In alloys with high stacking fault energy (SFE) such as Al, α-Fe, or Zr, the dislocations start to develop into a well defined cellular structure after 10% strain (7). Increasing deformation results in heavily cold-worked grains and dense subgrain structure that can serve as recrystallization nuclei at normal overload temperatures, thus eliminating the substructure and rendering the recrystallized wire useless from a strength standpoint (5, 7, 10-13). Thus when cold working is performed during wire drawing a recovery anneal is necessary to restore both physical and mechanical properties, restoring conductivity and gradually reducing the driving force for recrystallization.

2.2.2 Solid Solution Strengthening

Solid solution is widely applied to increase strength by interacting with dislocations through atmospheres which either pin static dislocations or at high T are dragged by gliding dislocations.

Stacking fault energy is lowered thus increasing resistance to cross-slip and climb (changing activation energy and retarding subgrain formation) (14, 15). Changes in resistivity are not solely dependant on the quantity of element addition, but on the form in which it is present (6-8). Elements in solid solution decrease conductivity substantially more than when out of solution. As seen in Table 2.3 (8), iron in solution increases resistivity 2.56 $\mu\Omega$/wt% versus 0.058 $\mu\Omega$/wt% when present as precipitates. The recovery anneal after wire drawing in the Super T and Triple E alloys precipitates out supersaturated Fe. As indicated in Table 2.3, elements such as Cr, V, Ti, and Mn must be controlled in these particle stabilized alloys to minimize electrical resistance. In the higher strength precipitation hardened overhead conductor alloy 6201 the above mentioned elements mainly affect the drawability.

2.2.3 Strengthening and Restoration During Hot Working

When a metal is deformed, dislocations interact with one another and barriers such as particles, resulting in further dislocation generation (10-13). The rising dislocation density increasingly restricts mobile dislocations resulting in a rise in stress (strain hardening). Deformation under hot working conditions (>0.5 T_m , $\dot{\epsilon}$ from 10^{-3} to 10^{3} sec^{-1}) can develop a highly recovered substructure that is not producible through any combination of cold working and annealing due to the intervention of recrystallization. When under deformation or service at high temperatures, restoration processes counteract the strengthening obtained. The dynamic restoration

Table 2.3 Effect of Elements In and Out of Solid Solution on the Resistivity of Aluminum (8).

Element	Maximum solubility In Al, %	Average increase in resistivity per wt%, μΩ.cm	
		In Solution	Out of Solution
Chromium	0.77	4.00	0.18
Copper	5.65	0.344	0.30
Iron	0.052	2.56	0.058
Lithium	4.0	3.31	0.68
Magnesium	14.9	0.54	0.22
Nickel	0.05	0.81	0.061
Silicon	1.65	1.02	0.088
Titanium	1.0	2.88	0.12
Vanadium	0.5	3.58	0.28
Zinc	82.8	0.094	0.023
Zirconium	0.28	1.74	0.044

Note : Addition to high purity Al base resistivity of 2.71 μΩ.cm at 25°C

processes, either dynamic recovery (DRV) or dynamic recrystallization (DRX) are strongly dependant on the stacking fault energy (SFE).

In face centred cubic (FCC) metals such as Al, perfect dislocations may undergo decomposition into partials with a region of stacking fault. The higher Gibbs free energy associated with the defect in atomic stacking order is the stacking fault energy, which determines the spacing between the two partials (16). The higher the SFE, the smaller the separation, and more easily that screw dislocations can cross-slip onto a different slip-plane. The amount of cross-slip and recovery, and thus the resulting cell-size increases with SFE (12, 16). With lower stacking fault energy (SFE) the cell walls become increasingly tangled to where nucleation of dynamic recrystallization is possible from grain boundary (g.b.) bulging or accumulation of subboundaries into high misorientations (17, 18).

In Al as in body centred cubic (BCC) and hexagonal close packed (HCP) materials such as α-Fe, and Zr, dynamic recovery is generally the only dynamic restoration process operating, however in certain Al alloys such as Al-5Mg-0.7Mn (19) dynamic recrystallization can result from particle enhancement. In the "microalloyed" conductor alloys DRV was expected to be the only operative dynamic restoration mechanism. FCC metals of lower SFE such as Ni, Cu, and stainless steels restore at low strains by DRV, but at higher strains by both DRV and DRX.

2.2.4 Effect of Substructure on Mechanical Properties

The room temperature strength of a material is related to the subgrain diameter d_s as follows

$$\sigma_y = \sigma_o + k_s d_s^{-m} \qquad (2.1)$$

where σ_o is the yield strength of a substructure free metal with the same grain size, k_s is the subboundary strength coefficient, and m is an empirical constant. Equation 2.1 can be re-written in a modified Hall-Petch form where m = 1/2 as :

$$\sigma_y = \sigma_o + k_{sb}\, d_s^{-1/2}$$

$$= \sigma_o + k_s d_s^{-p}\, d_s^{-1/2} \qquad (2.2)$$

The strengthening due to the subboundaries, k_{sb} is not a constant but increases as subgrain size decreases, as compared with the value of k for grain boundary strengthening which is independent of grain size (13, 20). The value of p has been reported from 1/2 to 3/2 , rising from 1/2 for statically recovered substructures to the most commonly reported value of 1 for retained hot work substructures, and is also dependant on material and processing route (13, 20, 21-23) (Figure 2.1 (24)). The value of k_s usually climbs as the dispersion of particles becomes finer and denser thus pinning dislocations and altering the structure of the boundary (25-29). Hardness has a similar inverse relationship to subgrain size as in Eqn. 2.2 but the relationship is accurate over a narrower range of hardness and subgrain sizes. Strengthening from grain boundaries has a high ratio of $\Delta\sigma/\Delta\rho$ in Table 2.2 but the effects are limited by the smallest attainable grain size in commercial processing of about 20μ. Subgrains can be commercially

a

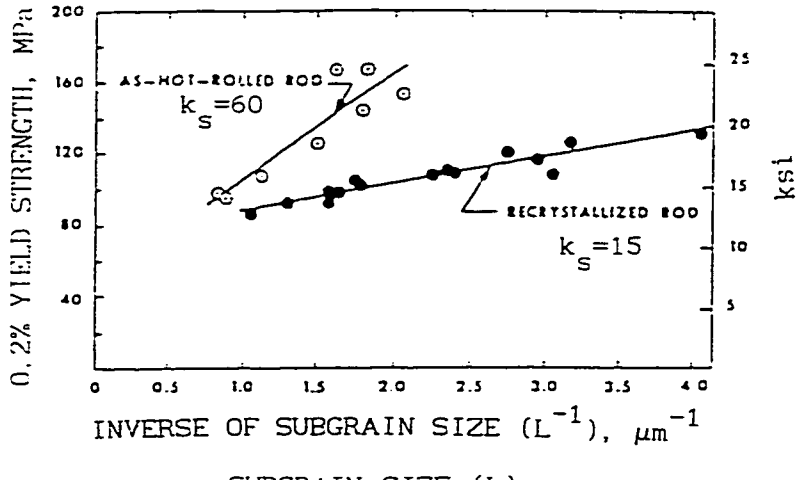

b

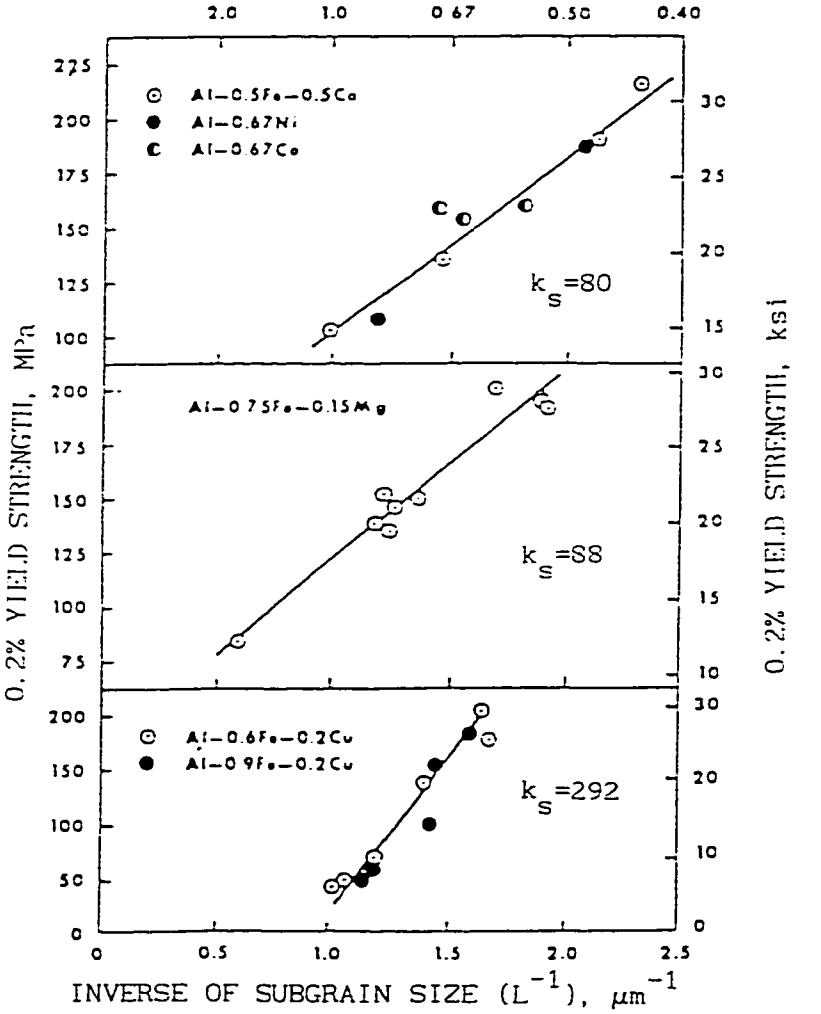

Fig. 2.1 Subgrain strengthening (a) of EC Al with continuous and conventional processing and (b) of several other dilute alloys (24).

produced with diameters of approximately 0.5μ, quadrupling the potential strengthening reported in Table 2.2.

2.3 Dynamic Recovery Flow Curve

The flow curve characteristic of metals with high SFE is shown in Figure 2.2 (17). Throughout the hot deformation, the increases in dislocation density are countered by dynamic restoration resulting in strain hardening monotonically decreasing to zero at the plateau. The plateau stress is reached after a strain of 0.2 to 0.3 when there is an equilibrium between the rate of dislocation generation and annihilation (13, 30, 31). The generation rate is dependant on the strain rate while the annihilation rate is a function of the dislocation density (and therefore the strain) and the ease of operation of recovery mechanisms such as climb, cross-slip, and node unpinning (thus temperature related) (31). With rise in DRV the hot flow stress falls and ductility climbs. Reduction of the plateau stress can occur at high strains due to deformational work heating, development of a preferred orientation, or dynamic precipitation. Strain hardening decreases as the strain rate is lowered or temperature raised. The presence of particles may reduce recovery depending on their strength, distribution, and size (6, 13, 22).

2.3.1 Dynamic Recrystallization Flow Curve

Deformation of metals with low intrinsic SFE, or SFE reduced through alloying will produce a characteristic flow curve with a

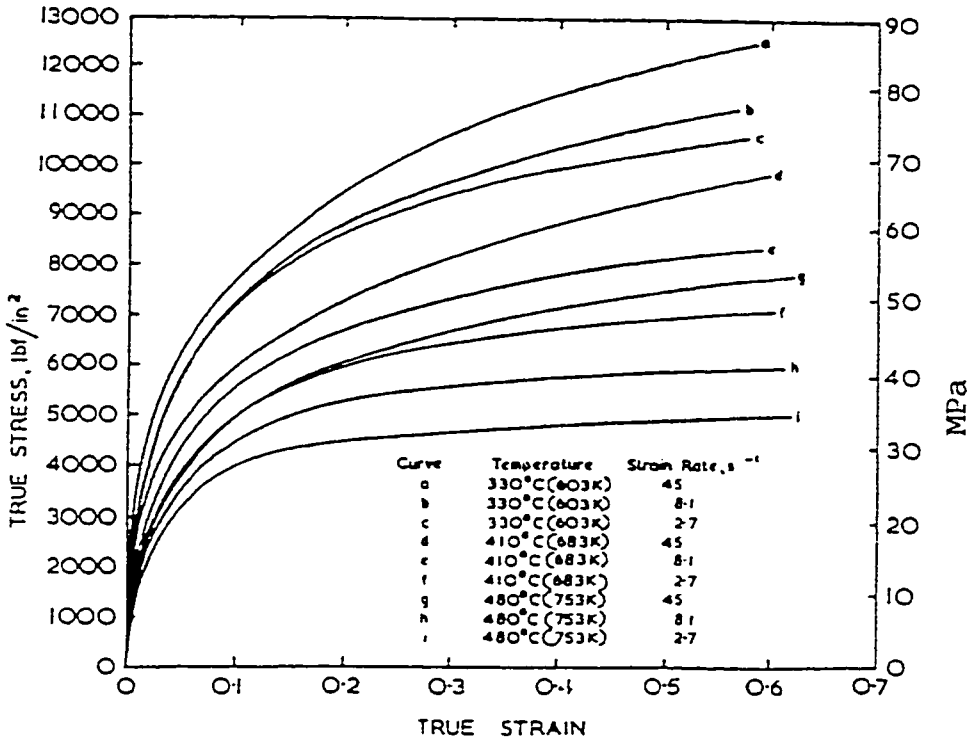

Fig. 2.2 Influence of strain rate and temperature on the shape of the flow curve of commercial purity Al, typical shape for DRV (17).

pronounced peak and decline to steady state. In these materials hardening and dynamic recovery are the only mechanisms operating until near the maximum stress, when the nucleation of dynamic recrystallization (DRX) results in a rapid decrease in strain hardening to zero at the peak strain ϵ_p, and a further decrease in the flow stress as the recrystallized grains form with lower dislocation density and less strength (30).

2.3.2 Substructure Evolution During Deformation

Substructure development in high SFE materials occurs as dislocations become entangled during strain hardening and outline a 3 dimensional cellular structure, characterized by small misorientations between cells (12, 13, 32). As the deformation temperature is increased into the hot working range subgrain formation occurs with higher misorientation (up to 2^{o}) between more dense but orderly cell walls, lower interior dislocation densities, and the formation of a stable subgrain size. The equilibrium size rises with deformation temperature and falls with the strain rate increase and is largely independent of strain during steady state (33, 34).

During large strains, the subgrains do not elongate with the grains as the cell walls continually decompose and reform in a process named repolygonization, maintaining a characteristic wall spacing and dislocation arrays (12, 13, 35-37). Dislocation generation likely occurs by the Kuhlmann-Wilsdorf model of bowing out dislocation segments from the subboundaries (38) and from the dislocation network

within the subgrains (22, 35). Increase in wall density occurs by migration of the dislocations to the cell walls where they are knitted in. Recovery occurs by annihilation of dislocations of opposite sign in the subgrain boundary and by unravelling of the boundary as dislocations are pulled out.

Equilibrium conditions of equiaxed subgrain size are achieved through continuous unravelling and knitting of dislocations at the cell walls. When the controlling variables of temperature and strain rate are changed a new stable structure will develop which is independent of the previous one (13, 22).

2.4.1 Stress, Strain Rate, and Temperature Relationships

The relationships between the strain rate $\dot{\epsilon}$, and the temperature T dependance on the stress σ obtained for both creep and constant strain rate tests are:

$$\dot{\epsilon} = A''\sigma^{n} \exp\ (-Q_{HW}/RT) \qquad (2.3)\ \text{Power Law}$$

$$\dot{\epsilon} = A'\ \exp\ \beta\theta\ \exp(-Q_{HW}/RT) \qquad (2.4)\ \text{Exponential Law}$$

$$\dot{\epsilon} = A\ (\sinh\alpha\sigma)^{n}\ \exp(-Q_{HW}/RT) \qquad (2.5)\ \text{Hyperbolic Sine Law}$$

where A, A', A'', n, θ, β, and α are experimental constants and Q_{HW} the activation energy, T the absolute temperature, and R the universal gas constant of 8.31 J/mol-K (12, 13, 22, 29, 35).

The power law is used to represent the results of creep tests as well as hot working tests at low stress (<10 MPa). For tests at higher stress levels the exponential law is used. To enable comparison of data from both creep and hot working testing, the hyperbolic sine function mathematically approximates the other two at the extreme values of the stress (12, 13, 18). A value of n from 4 to 5 was drawn from creep studies on commercial Al where the power law with exponent 4-5 was related to dislocation climb (38-40).

The activation energy for hot working has been reported to be from 150 to 156 kJ/mol for pure Al, and 154-162 kJ/mol for commercial alloys, rising with alloy content (28). Values for 1100 or 1350 EC-Al would be expected to be the same or very similar. The activation energy for hot working is commonly similar to that for self-diffusion indicating dislocation climb as the rate controlling mechanism in both creep and hot working of commercial Al.

The Zener-Hollomon parameter ($Z = \dot{\epsilon} \exp Q/RT$) or temperature compensated strain rate is used in hot working studies as it provides a constant for comparison which contains the two control variables of temperature and strain rate. Under deformation conditions with the same Z value, the flow curves and substructure are the same. The subgrain size d_s is inversely proportional to Z as follows.

$$d_s^{-1} = G + H \log Z \qquad (2.6)$$

where G and H are constants (12).

2.4.2 Hot Ductility

The ease of DRV limits the amount of W (wedge, i.e. triple junction) cracking by allowing non-uniform deformation in the grains at triple junctions, relieving stress concentrations due to grain boundary sliding. Formation of serrated grain boundaries further reduces grain boundary sliding. Fine uniformly distributed particles that stabilize the substructure by reducing DRV diminish ductility by lowering boundary mobility (10-13, 18, 20, 22-23, 30). Large particles or inclusions can act as sites for nucleation of cracks or voids.

Torsional deformation does not suffer from the necking instability present in tension testing; thus in torsion, true fracture strain is usually much higher than that in tension. The ductility in tension is defined by the equation :

$$\epsilon_f = \ln(1/1-R_a) \qquad (2.7)$$

where ϵ_f is the fracture strain and R_a the reduction in area. For $\epsilon_f > 1$ the torsion to tension ductility can be empirically related by (41):

$$\epsilon_f(\text{torsion}) = (\epsilon_f(\text{tension}))^2 \qquad (2.8)$$

2.5 Interrupted Deformation Testing

Industrial processing of alloys commonly proceeds in stages of deformation with varying interruption times, temperatures, and strain rates. Interrupted deformation tests are used to determine the type

and magnitude of restoration mechanisms. Tests can be performed with varying levels of time temperature, strain increment, and strain rate, but these are usually fixed to facilitate testing. Softening between passes reduces flow stress in the next pass and usually increases hot ductility when SRV is the only operative mechanism. Direct comparison between industrial processing and constant strain, strain rate, and constant temperature tests can be complicated due to the influence of inherited microstructure, but simulations are assumed to be valid.

2.5.1 Static Recovery

In contrast with DRV, static recovery (SRV) proceeds in the absence of strain, either between stages of deformation, at the conclusion of deformation during cooling, during a heat treat operation, or in service. Static recovery proceeds through the material via a process of annihilation and re-arrangement of dislocations in sub-boundaries. This process, termed polygonization, is followed by subgrain coalescence when decomposition of weaker sub-boundaries takes place. This process is not homogeneous and leads to a limited number of SRX nuclei. Static recovery between passes reduces the effect of inherited substructures due to the loss of mobile dislocations, usually reducing subboundary densities without changing subgrain size: in industrial processing of the Super T and Triple E alloys this loss would only be a few percent (12, 13, 22, 37).

Recovery halts by self-reduction of the driving force through creation of more stable low energy structures, or by initiation of static recrystallization (SRX). Metals of high SFE can undergo softening of 10-50% before initiation of SRX and Al can be easily cooled to room temperature to retain the substructure. The presence of fine particles on the sub-boundaries usually stabilizes them, reducing SRV and reducing or eliminating SRX. The precipitate stabilized substructure improves high temperature stability and resistance to creep (11). The particles must be large enough so that they are not sheared by dislocations, and their spacing sufficient to inhibit grain boundary mobility, but must not be so large as to act as recrystallization nuclei by creating areas of high local misorientation. Low particle solubility is necessary at the operating temperatures to maintain the pinning effect and to delay coarsening.

If the particles are not successful in inhibiting nucleation by substructure stabilization they can still slow down the migration of boundaries and sub-boundaries. Zener (42) developed a theory for the dragging effect of uniformly distributed particles on grain boundary mobility. Grain boundary migration comes to zero when particle drag equals the driving force for boundary motion. The Zener drag, Z, on a boundary is given by (28, 42-43):

$$Z = \alpha' \ (3f \ \gamma_{gb} / \ 2r) \qquad (2.9)$$

where r is the particle radius, f the volume fraction on migrating boundaries, α' a constant, and γ_{gb} the grain boundary energy. For a given volume fraction, smaller particles hinder g.b. mobility more than large ones.

2.5.2 Static Recrystallization

Static recrystallization (SRX) initiates in localized regions and proceeds by migration of high angle boundaries driven by the energy difference between the high energy of the deformed structure it is moving into, and the low energy stable structure left behind. In metals of low SFE, SRX almost always follows DRX with minimal intervention of DRV (10-13, 19, 22). The incubation time for the nucleation and growth of new high angle boundary grains of low dislocation density is dependant on DRV, and thus rises with SFE. Increasing strain, strain rate, and decreasing temperature favour SRX by increasing dislocation density and thus the driving force. Grains produced by SRX are larger and also softer than those produced by DRX due to the lack of a retained substructure. Dispersed particles will delay or prevent recrystallization if the interparticle spacing is less than 2μm by inhibiting nucleation and grain boundary migration.

2.6 Production Processing of Particle Stabilized Al-Alloys

In order to relate the strengthening mechanisms and microstructural development, the manufacturing operations and corresponding substructure development will be covered in detail. Without a dispersion of insoluble intermetallic particles to stabilize the substructure, the intervention of SRX or extensive recovery would negate any gains in strengthening. As the intermetallics are insoluble they do not respond to heat treatment. Rapid solidification during casting is the only way to control the dendritic spacing and

distribution of the precipitate (5, 9, 24, 26, 44). The initial particle dimensions and spacing determines the average stable cell size attained by thermomechanical processing, as intermediate or final wire treatments can not override the importance of the initial rod microstructure (5, 9, 24, 26, 44). One can get lower average stable cell size adding more cold work.

Continuous casting of these alloys is done on a continuous bar caster (modified Properzi type). The process ultimately yields rods and thus it is known as the Southwire continuous rod (SCR) process. Casting of 50 cm^2 bar at 16m/min on a wheel 2.5 m diameter results in a 20 μm dendrite spacing with eutectic rods of approximately 0.2 μm diameter and Fe in supersaturated solution. In Super T the rods are stable intermetallic compounds of $FeAl_6$, $(Fe,Co)Al_3$ and $(Fe,Co)_2Al_9$. In Triple E the rods are metastable $FeAl_6$ and its stable derivative $FeAl_3$. Slow solidification via conventional casting results in a 210 μm dendrite arm spacing (45, 46).

Directly from the casting wheel the bar is reduced 98.6% (ϵ = 4.33) to 0.7 cm^2 in a 13 stand rolling mill as the temperature declines from 485 to 180^{o}C and the strain rate increases from 1.6 sec^{-1} to 27 sec^{-1} at the exit of the rolling mill. After 2 passes, the 60% reduction has reduced subgrain size to 5.3 μm for Triple E. The subgrain size after each stage of deformation is larger than it would be from deformation solely at that stage as it has inherited the substructure from the previous stage where the temperature is higher and strain rate is lower (10, 13, 37). After 9 passes and 94%

reduction cell size is reduced to 1.6μm. At finishing, the sizes lie between 1.0 and 0.85 μm for Triple E and Super T respectively, versus 1.6μm for EC Al, and 4.0 μm for Super T rod produced from slowly solidified bar (5, 26, 45, 46). In production the rod is cooled before coiling to eliminate non-uniform subgrain growth. The conductivity of the as rolled Super T and Triple E alloys is 60.4% and 59.8% IACS respectively. The rod for the present testing was withdrawn at the end of the rod rolling stage and subject to recrystallization anneals as discussed in Chapter 3. Thus the eutectic rods are already broken up and fairly well distributed.

Transfer of the rod directly into wire drawing without annealing, and thus with the retained hot work substructure, is termed continuous processing. The wire drawing through 12 dies gives another reduction of 92.2% (ϵ = 2.56) to 0.052 cm^2. Cold drawing increases the uniformity of precipitate dispersion and the dislocation density thus reducing cell size to 0.8 μm for EC, 0.6μm for Triple E and 0.4 μm for Super T. Conductivity for the as drawn Super T wire is 59.1% IACS versus 61.2% for Triple E. Recovery annealing at 250-300^{o}C raises ductility to 15-20%, restores conductivity to 61% IACS minimum, and increases subgrain size to 1.6 μm (non-uniform) for EC, 1.2 μm for Triple E, and 0.8 μm for Super T. After annealing, the interparticle distance equals the average subgrain size, thus confirming the dependance of subgrain size on particle spacing (5, 9, 44). On the other hand, annealed Super T wire from slowly solidified bar has an interprecipitate spacing of 10 μm.

2.6.1 Effect of Particles on Strengthening During Processing

During the first stages of rolling the eutectic rods are resistant to shearing by dislocations but allow the matrix to flow around them. As flow stress (dislocation density and cell refinement) increases, dislocations exert bending stresses on the rods, fracturing them into segments 2 or 3 times their diameter. Continuous processing with extreme reductions leads to "stringers" of segmented rods extended through the length of the rod and wire, with interparticle spacing becoming more uniform and greatly reduced. The very short times between passes on the continuous mill limit the reduction in internal stresses thus ensuring fracture of the eutectic rods.

Particles must be sufficiently large so that they are not sheared by individual dislocations, but not large enough to act as nuclei for SRX. The size range must be from 0.06 to 0.6 μm. During rod rolling the eutectic rods are fractured into more uniform segments of 0.075-0.5 μm. For Super T and Triple E there is approximately one particle per cell, whereas only one for every two cells in EC-AL. Primary particles of $FeAl_3$ larger than 0.6 μm in diameter are not shearable by dislocations but produce complex deformation in the surrounding matrix. Small cells are produced with high misorientation walls that can transform into recrystallization nuclei upon heating. Rapid solidification with the fracturing of the eutectic rods into segments 0.2 μm in diameter in a fine dispersion inhibits both subboundary mobility and general recrystallization. At the conclusion of rolling the larger subgrain size of EC-Al (1.6 μm vs. 0.85-1.0 μm)

results from having only 40% of the particle density of Triple E and Super T in the useful range of 0.075-0.5 μm (25).

Precipitation of supersaturated iron as $FeAl_3$ particles (approx 0.01 μm dia.) takes place as the solubility of Fe in Al decreases from 0.052% at 655°C to 0.005% at 500°C. In the Al-Fe and Al-Fe-Co conductor alloys, precipitation takes place mainly on dislocations in the subboundaries, locking them in place and reducing dynamic recovery by obstructing the process of unravelling of subboundaries.

The particle stabilized substructure produces considerable increases in creep resistance and microstructural stability, as is indicated in Figure 2.3 (5). In a 100 hour stability test at 200°C the yield strength of Super T remains constant at 95 MPa whereas 1350 EC Al declines from 50 to 30 MPa and Triple E declines from 68 to 62 MPa. Increased yield and ultimate tensile strength of Super T over 1350 Al can be attributed to differences in work hardening behaviour caused by the small stable substructure. Figure 2.4 (5) shows that substructure refinement increases both strength and ductility in the alloys, with the Super T possessing nearly double the UTS of conventionally processed EC Al when annealed to provide the 15-20% ductility required in service. With rising temperature, the strengthening and stabilizing effect of the particles diminishes slowly as thermal activation increasingly facilitates motion of dislocations around the obstacles by climb or cross-slip.

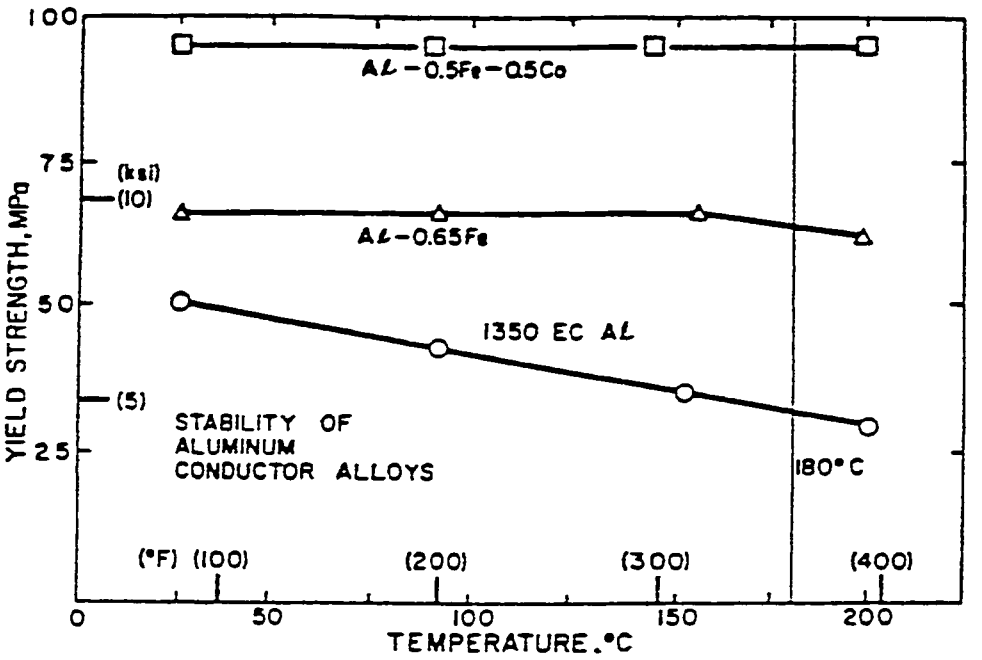

Fig. 2.3 Effect of 100 hour high temperature stability test on the yield strengths of Al conductor alloys (5).

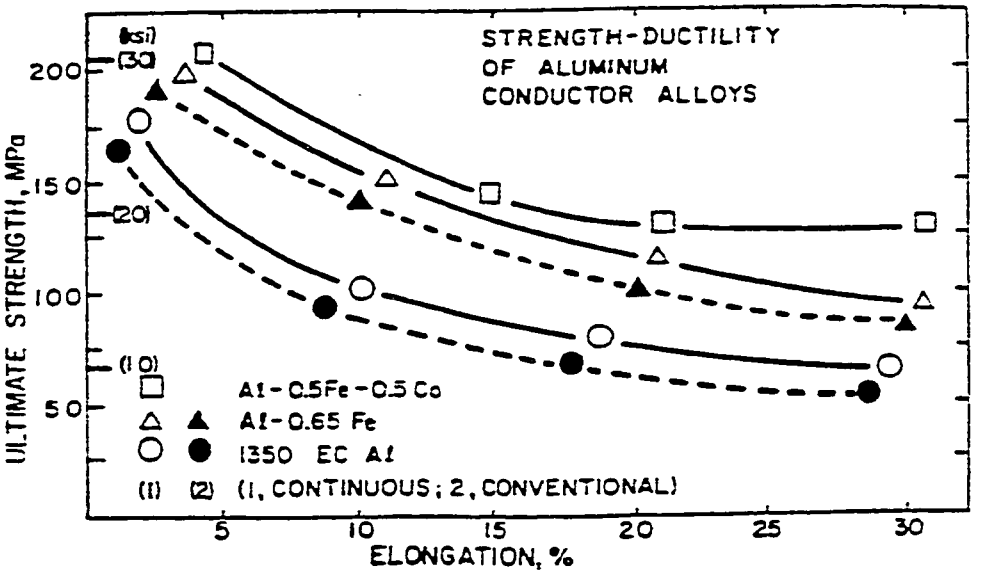

Fig. 2.4 Comparison of the relationships between ultimate strength and ductility of EC-Al and eutectic particle stabilized alloys for continuous and conventional processing (5).

CHAPTER THREE

EXPERIMENTAL PROCEDURE AND ANALYSIS OF DATA

3.1 Torsion Test Procedure

3.1.1 Torsion Equipment

The torsion machine as originally conceived was described in detail by Fulop et al (47) (Figure 3.1). Upgrades to the test rig have automated test data recording and temperature control. One end of the sample is twisted by a dual valve hydraulic motor (Figure 3.2) and the resulting torque is measured at the other end by a 100 in-lb torque cell. Two servovalves are used on the hydraulic motor to obtain reliable twist rates of 0.02 rev/sec to 1 rev/sec for the low flow servovalve, and 1 rev/sec to 10 rev/sec for the high flow valve. Output from the load cell is directed through a transducer conditioner circuit. The range of the load cell can be set to 100%, 50%, 20%, or 10% full scale to adjust the precision of the output. Rotary displacement of the motor is controlled by a closed loop system (Figure 3.3) and is measured with either a 10 turn or 50 turn potentiometer (10v full scale) which provides the feedback to the controller.

Heating of the test pieces is accomplished by an electrically heated 4 tube radiant furnace. A watercooled aluminum shell lines the furnace and focuses the radiant energy to the centerline. Unlike

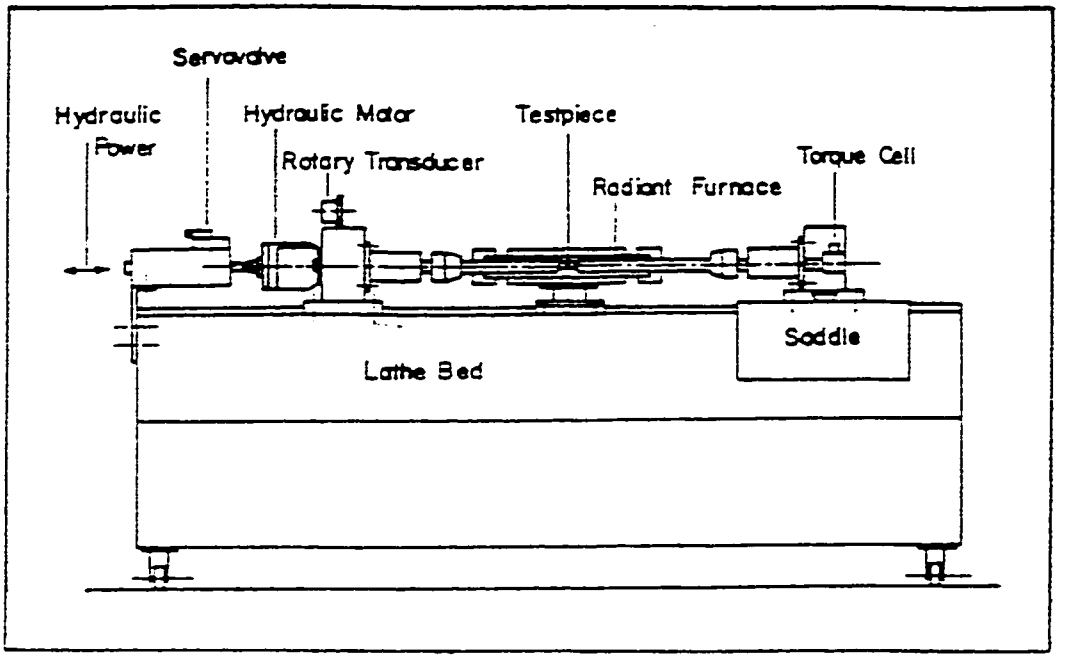

Fig. 3.1 The hot torsion machine.

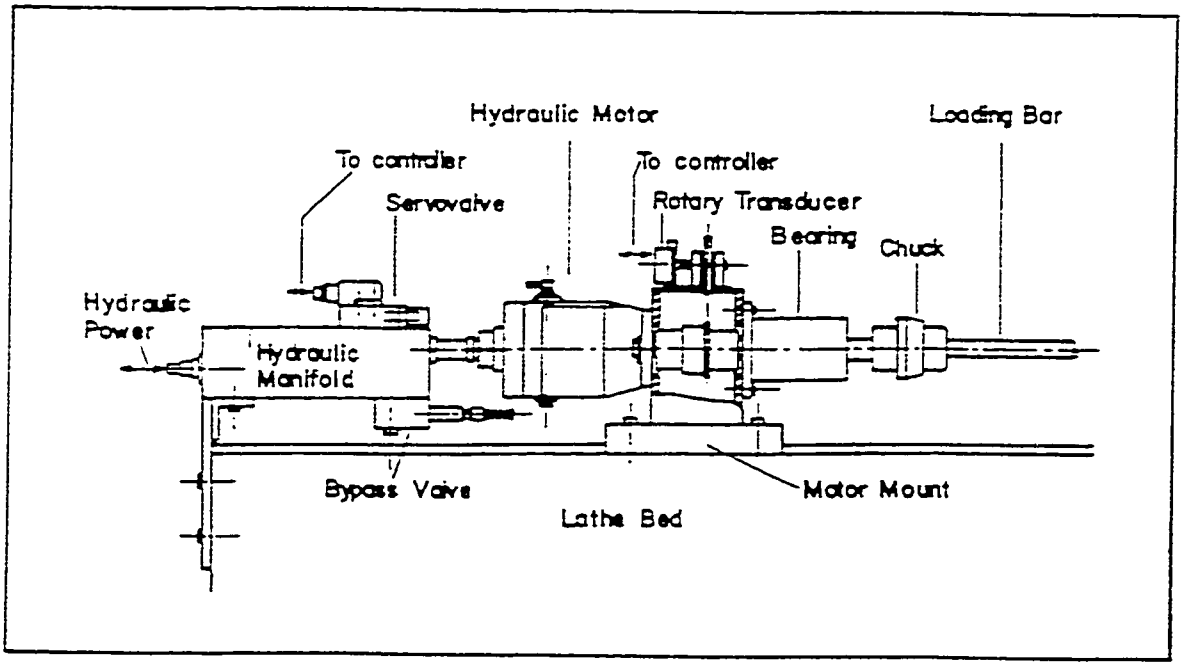

Fig. 3.2 Strain and strain rate measurement and control subsystem.

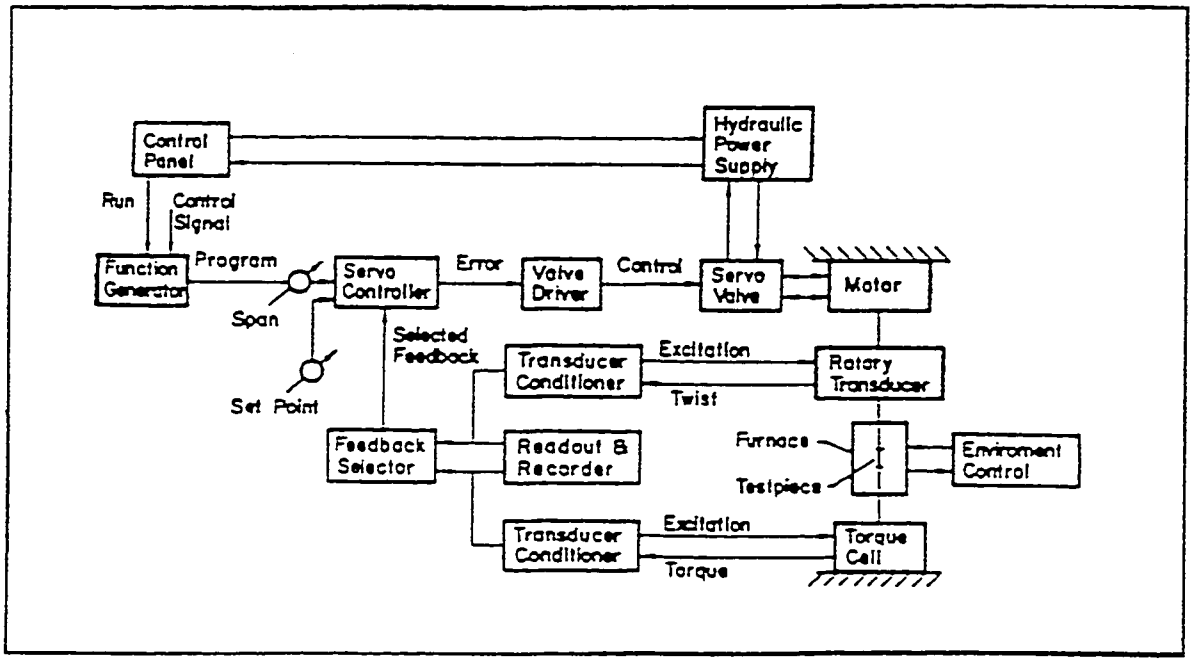

Fig. 3.3 Feedback control system.

resistance heated furnaces, there is a very low thermal inertia so rapid heating and cooling is possible. Temperature and electrical power input is also controlled through a closed loop system. The short thermal time constant of the furnace enables a fast response to increases in temperature caused by deformational work heating.

3.1.2 Mounting of Specimens

The test pieces are supported at each end by INCONEL 713C nickel based superalloy bars (48) nominally 1" in diameter with 309 stainless steel end adapters. Thrust bearings hold the self-centering three jaw chucks that grip the bars at the hydraulic motor and torque cell (Figures 3.2, 3.4). The torque bar and chuck, bearing assemblies, and torque cell are mounted on the lathe carriage which is moved axially on the lathe bed to facilitate specimen insertion and removal, and manual specimen quenching. The lathe carriage is fixed in position for the duration of the test by bolting it down to the lathe bed. Quenching is accomplished manually by removing the furnace from around the specimen and can be initiated consistently within 6 seconds.

3.1.3 Control of Test Variables

3.1.3.1 Temperature Control

Temperature control is achieved by a Leeds and Northrup model 1300 process programmer along with an Electromax 5 proportioning controller. Ramp time to test temperature and soak times at temperature are controlled by the process programmer. Feedback

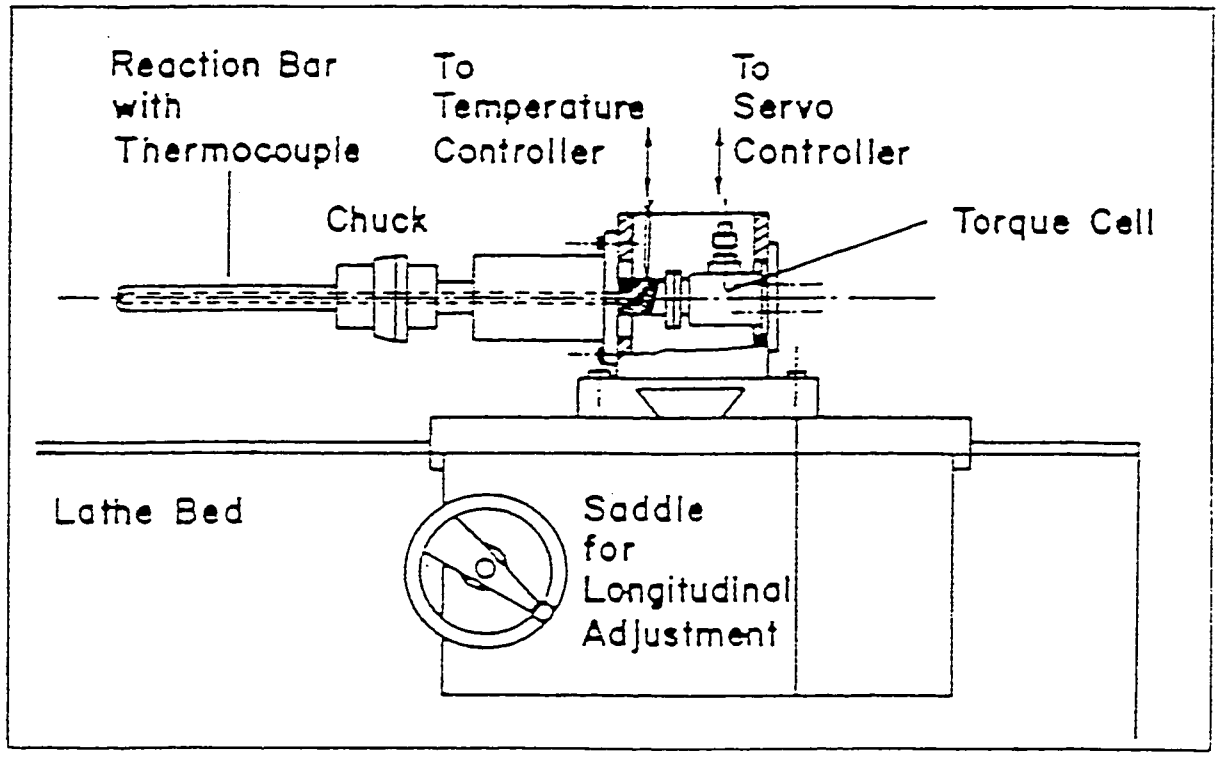

Fig. 3.4 Load cell assembly

control is used for maintaining temperature, with displays provided of set point temperature, actual temperature, and percent of maximum current drawn by the furnace. A K-type (chromel-alumel) thermocouple supplies the feedback signal to the controller. The thermocouple is held in place on the gauge section approximately 1/4" from the shoulder radius by tying it to the specimen with INCONEL wire. With the exception of the tip, the thermocouple is sheathed by an alumina tube.

Ramp times of 5 minutes were used for test temperatures of 500, 450, and 400^{0}C, 4 minutes to 300^{0}C, and 3 minutes to 200^{0}C. Specimens were soaked at test temperature for 5 minutes to equalize temperature. When test duration exceeded several seconds heat input from deformational work heating was detected by the controller and resulted in a reduction in power supplied to the furnace, lowering temperature to the set point value.

3.1.3.2 Atmosphere Control

A protective atmosphere of commercial purity argon was maintained during testing by flowing through a series of small holes uniformly distributed in the furnace walls. In trials on scrap specimens without protective atmospheres the Super T and Triple E alloys showed no visible oxidation when heated, however 6201 alloy did show some oxidation.

3.1.3.3 Control of Strain, Strain Rate, and Data Acquisition

Control of the machine is achieved by the use of a closed loop system which is schematically illustrated in Figure 3.3 (47). Conventional feedback control is used, in which a comparison is made between the command value, and the feedback signal from the rotary displacement transducer. The error signal between the two is sent to the hydraulic servo valve that moves to cancel the position error.

A PDP 11/04 minicomputer was used to record the twist and torque values at fixed intervals (200 datapoints per test) . Torque versus equivalent strain curves are displayed on a Tektronix cathode ray terminal. A Tektronix 4631 thermal printer produced copies of the screen image. Raw data is stored on hard-sectored 8" disks.

3.1.3.4 Stress and Strain Conversion

In the solid specimens used, there is a gradient of the strain, strain rate, and stress from zero at the axis to a maximum at the surface. Following the established practice in torsion testing, calculation of the equivalent linear stresses and strains were based on maximum (surface) conditions with metallographic examinations (and correlation) based on tangential sections as close to the surface as possible (49).

The surface shear strain in torsion of a solid bar is defined as

$$\gamma = r\,\theta/l \qquad (3.1)$$

and the shear strain rate as

$$\dot{\gamma} = r\,\dot{\theta}/l \qquad (3.2)$$

where r = gauge radius, l = gauge length, and θ = amount of twist in radians. Substituting for $\theta = 2\pi N$, where N = the number of revolutions, and using the von Mises criterion (41)

$$\epsilon = \gamma / \sqrt{3} \qquad (3.3)$$

where ϵ is the linear strain, leads to

$$\epsilon = [2\pi N / \sqrt{3}\,]\ (R/L) \qquad (3.4)$$

The strain rate would therefore be given by

$$\dot{\epsilon} = [2\pi N / \sqrt{3}\,]\ (R/L) \qquad (3.5)$$

With the ratio of gauge radius to length of 1:8, a strain of 4 is 8.82 revolutions, and a strain of 20 is 44.1 turns.

The measured torque Γ is equal to the moment produced by the shear stress τ acting over the specimen cross section as defined below:

$$\Gamma = F \times d = \int_{r_i}^{r_s} \tau\, 2\pi\, r\, dr$$

$$= 2\pi \int_{r_i}^{r_s} \tau\, r^2\, dr \qquad (3.6)$$

If the shear stress is assumed dependant on the shear strain and shear strain rate in the form :

$$\tau = K\ \gamma^{n'}\ \dot{\gamma}^{m} \qquad (3.7)$$

where K, n', and m are material constants, equations 3.1, 3.2, 3.6, and 3.7 become :

$$\Gamma = 2\pi K \Theta^{n'} \Theta^{m} \int r^{2+n'+m} \, dr \qquad (3.8)$$

Integrating the equation and solving for shear stress for a solid bar yields :

$$\tau = \frac{(3 + n' + m)\,\Gamma}{2\pi r^3} \qquad (3.9)$$

The strain rate sensitivity m and the strain hardening exponent n' are defined as:

$$m = \left. \frac{\partial \log \Gamma}{\partial \log \dot{\epsilon}} \right|_{\epsilon, T} \qquad (3.10)$$

and

$$n' = \left. \frac{\partial \log \Gamma}{\partial \log \epsilon} \right|_{\dot{\epsilon}, T} \qquad (3.11)$$

Using the von Mises yielding criterion

$$\sigma = \sqrt{3}\,\tau \qquad (3.12)$$

leads to the definition on the equivalent uniaxial normal stress as

$$\sigma = \frac{(3 + n' + m)}{2\pi r^3} \quad \frac{\Gamma}{\sqrt{3}} \qquad (3.13)$$

3.2 Test Material

3.2.1 Specimen Geometry

Specimens were machined with one end threaded and with the other having rectangular cross section as indicated in Figure 3.5. This configuration facilitates specimen insertion and removal without accidentally straining the test piece because the rectangular end is not constrained axially. Thermal expansion of the specimens produces

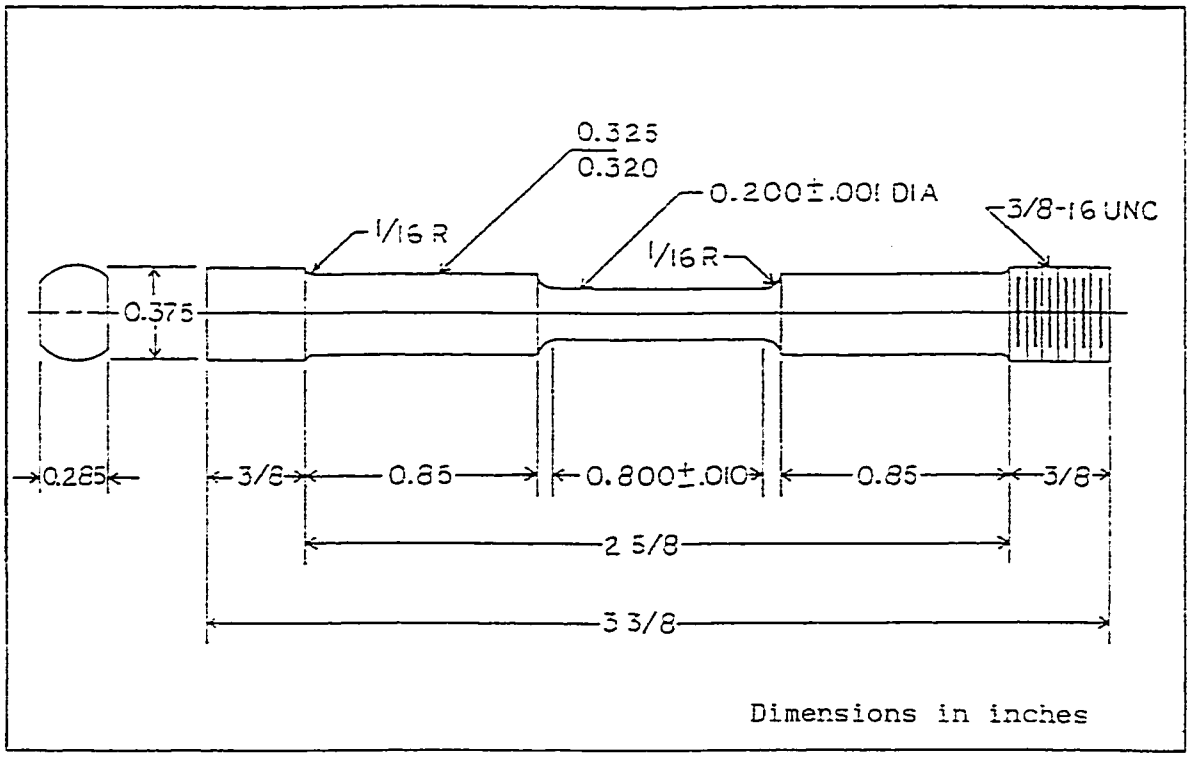

Fig. 3.5 Test Specimen Geometry.

length changes of 1/64" to 1/16". Provision is made for expansion of the specimen by positioning the slotted end of the specimen approximately 1/8" from the bottom of the recessed hole in the test bar. In addition to thermal expansion, a solid bar specimen, when twisted with free ends at high temperature, may change length, resulting in buckling or premature fracture. Texture development in the specimen with rising strain is considered to be the cause of this expansion (50).

3.2.2 Alloy Chemistry

Test specimens were supplied by the Southwire Aluminum Co of Carrollton, Georgia from a single batch of each alloy. The actual alloy chemistry is as follows:

Alloy	Al	Fe	Co	Si	Cu	Mn	Mg	Cr	Ni	Zn	Ti	V
Super T	bal	.59	.50	.04	.001	.003	.001	.001	.001	.02	.001	.005
Triple E	bal	.65	-	.038	.001	.003	.001	.001	.001	.007	.001	.001
6201	bal	.22	-	.32	.03		.44				.02	

Due to the low alloy content the melting point of the supplied batches of Super T and Triple E alloys are expected to be close to that of commercially pure (1100) aluminum (652^{o}C).

3.2.3 Heat Treatment

The test specimens were recrystallized after machining to produce uniformity of grain size (g.s.) between the three alloys and create a structure that would be stable at the highest test temperature. A Lindberg Hevi-Duty high temperature resistance furnace with argon atmosphere was used for heat treatment. On Triple E and Super T, annealing trials were conducted at : 550°C, 1 hour; 600°C, 1 hour; 625°C , 1, 2, 3 hours; and 640°C for 1 hour. Heat treatments for 6201 were: 450°C, 1hour; 500°C, 1, 2, 3 hours; 550°C, 1 hour; 575°C, 1 hour; 600°C, 1 hour. The final annealing operations producing the most similar microstructures were: Super T, 3 hours at 640°C (g.s. 85μm); Triple E, 3 hours at 625°C (g.s. 60μm); 6201, 3 hours at 500°C (g.s. 58μm). The predeformation microstructures of the Super T and Triple E alloys can be seen in Figures 3.6 and 3.7.

It was difficult to obtain a uniform grain size as the three alloys underwent non-uniform grain growth at different conditions during annealing. The non-uniform grain growth, also called secondary recrystallization, can be related to the breakdown of particle pinning of the grain boundaries, or to preferred crystallographic orientation in recrystallized material. Secondary recrystallization related to particles is pronounced in appearance only when annealed in the temperature range in which the particles gradually start to coarsen and dissolve (51).

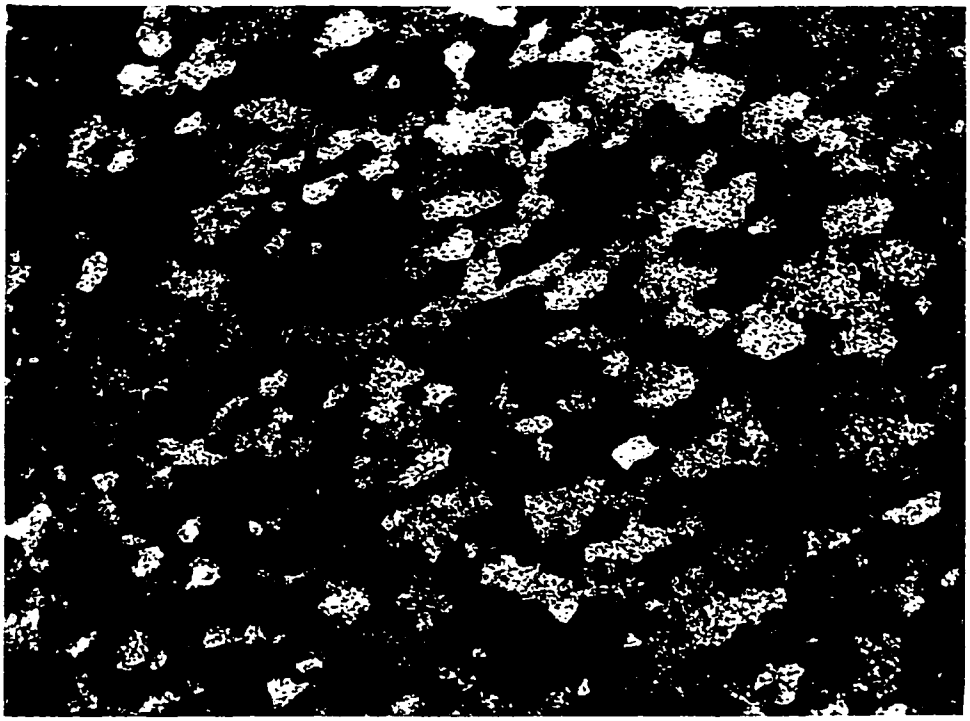

Fig. 3.6 Fully recrystallized microstructure of transverse section of Super T alloy. Annealed at 640°C for 3 hours. X50

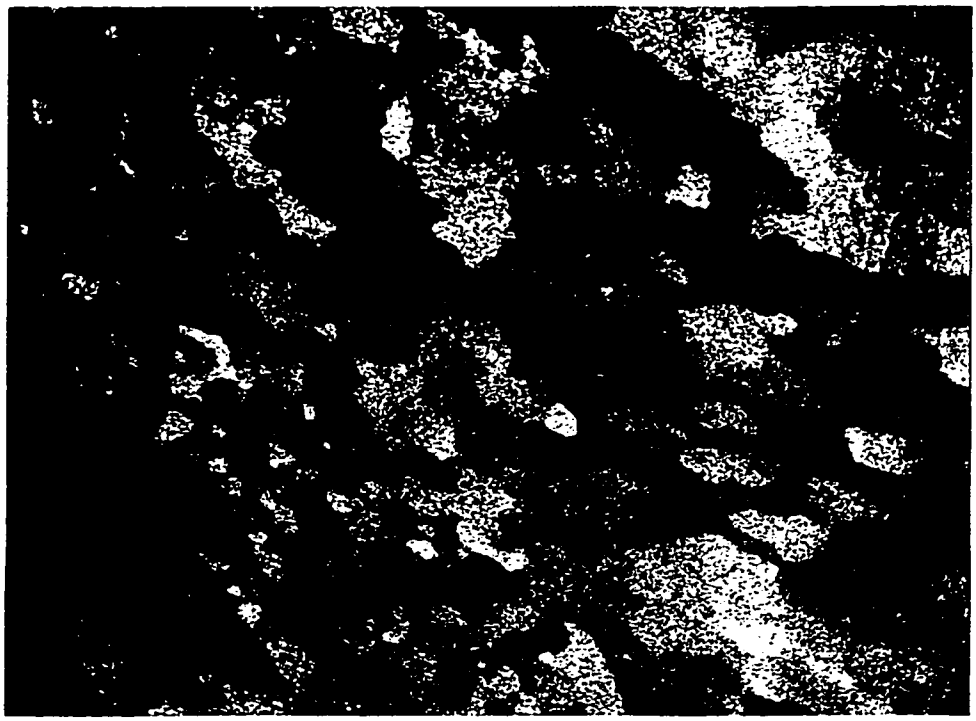

Fig. 3.7 Fully recrystallized microstructure of Triple E alloy. Annealed at 625°C for 3 hrs. X100

3.2.3.1 Grain Size Determination

Grain size determination was made by the planimetric technique (52): by counting the number of grains within an area and determining an average grain diameter. The alloys were prepared through repeated etch and polish operations, with an etchant of the following composition.

20 ml Poulton's Reagant (12 parts conc HCl)
(6 parts HNO_3)
(1 part HF)
(1 part water)

12.5 ml of HNO_3, concentrated

20 ml chromic acid solution (3g chromium trioxide per 10 ml water)

3.3 Test Matrix

The test matrix was developed to closely match the actual manufacturing process, where there is a total strain of 4.33 and the temperature declines from 485 to 180°C. Accordingly, the temperature range was 200 to 500°C and total strain of 4. Strain rates of 0.02 to 5 s^{-1} were defined by the capability of the torsion machine thus falling short of the 27 sec^{-1} in production. For ductility testing, straining proceeded to fracture or to the potentiometer strain limit of 20. Additions to the test matrix were made based on preliminary test results. The final program is illustrated in Table 3.1., and the ratios of test to melting temperatures in Table 3.2.

Table 3.1 Continuous Deformation Test Conditions

Strain Rate, s^{-1}	Equivalent Strains	Temperatures (^{o}C)
0.02	4	300, 400, 450, 500
0.1	4, 20	200, 300, 400, 450, 500
1.0	4, 20	200, 300, 400, 450, 500
4 or 5*	4, 20	200, 300, 400, 450, 500

* Strain rate was reduced from 5 to 4 to facilitate testing

Table 3.2 Homologous Temperatures (T/T_m)

Temperature (^{o}C)	T/T_m
200	0.51
300	0.62
400	0.73
450	0.78
500	0.84

During the preliminary testing, the 6201 specimens exhibited localized deformation, the degree of which increased with strain rate and temperature. Subsequent annealing treatments at different times and temperatures were unable to eliminate this problem. Moreover, the chemical composition of the material shown above indicates that the specimens supplied did not meet the specifications for 6201 alloy. Consequently, the alloy was dropped from further testing and an expanded program utilizing the remaining alloys was created.

3.4 Interrupted Deformation Tests

Interrupted deformation tests were conducted to study the effects of static recovery and recrystallization between passes. Each interrupted, or multistage, test consisted of six passes of equal strain of 0.3 to a total strain of 1.8. Strain stages of 0.3 (25% equivalent reduction per pass) paralleled the average 30% reduction in the first six passes in rod rolling ($\epsilon = 2.17$). Interpass hold times (interruption times, t_i) varied from 5 to 100 seconds. Testing was not performed at 200 and 300°C as continuous deformation testing tests had revealed a lack of rate sensitive deformation confounded with deformational heating. Testing at 500°C was not possible due to the inability to resolve the small incremental changes in stress upon reloading the specimen. Strain rates of 0.1 and 1.0 s^{-1} were employed. The test matrix for the interrupted testing is shown in Table 3.3.

Table 3.3 Interrupted Deformation Test Conditions

Temperatures (^{o}C)	Interruption Time, t_i (sec)	Strain Rates
400	5, 10, 20, 40, 100	0.1, 1.0
450	10, 20, 40	0.1

3.4.1 Analysis of Data

The term to indicate the extent of softening between passes is known as the fractional softening (FS), i.e. the extent of softening relative to hardening. Fractional softening is based on the equation

$$FS_i = (\Gamma_{mi} - \Gamma_{ri}) / (\Gamma_{mi} - \Gamma_o) \qquad (3.14)$$

where Γ_{mi} is the maximum torque at the i^{th} pass, Γ_{ri} is the torque on reloading, and Γ_o is the initial or yield torque during the first pass. Torques were used as the conversion to stress at any one condition involves only the multiplication by a constant. The two ways to calculate the stress on reloading are: the 0.1% offset or the back extrapolation method (53). The latter method was used to determine FS as there were not enough data points in the initial strain interval to accurately place a 0.001 offset strain line. Back extrapolation involves fitting the flow curve in the first pass to the reloading curve at high strains to determine Γ_{ri} at its intersection with the elastic reloading line (53). The equation does not separate the effects of static recovery and recrystallization; however, only SRV was expected at the chosen t_i.

For successive passes during a test an envelope curve can be drawn connecting the maxima, to compare with that obtained during continuous deformation. Superimposing the curves for various t_i highlights the effect of varying hold times on net hardening. Alloys that undergo SRX during the interval would have envelope curves significantly lower than the continuous case. Due to the scatter in

the magnitudes (but not ratios) of the torque (or stress) values, a superimposed plot of all of the interrupted loading curves at various interpass hold times was not possible. Another method to produce the superimposed plots for interrupted deformation was developed, by creating an envelope curve from plots of relative retained hardening (RH) versus strain. Retained hardening is defined as

$$RH = \Gamma_{mi} \; / \; \Gamma_{m1} \qquad (3.15)$$

where Γ_{mi} is the final torque at the i^{th} interval and Γ_{m1} is the torque at the end of the first pass. A hardening ratio of less than 1 represents net softening compared to the first pass, i.e. strain hardening does not match the cumulative effects of static restoration. Retained hardening greater than 1 indicates that the dislocations generated during the loading interval are not eliminated during interpass static recovery. Analyzing data in this form offers two principal advantages over fractional softening plots. Creating ratios of pass torque during each test in effect normalizes the hardening behaviour, thus the envelope curve generated is free from the observed test to test scatter in mechanical strength. It is thus possible to compare the RH envelope curve with continuous flow curve at equal strains for all test data. Additionally, as the retained hardening is based on easily observed maximum values, the calculation of the RH parameter is very precise and reproducible. The peak torque (Γ_m) and the reloading torque (Γ_r) can rise or decline together during a series of passes to indicate a more or less constant value of fractional softening (FS), while the RH graphs would indicate the occurrence of net hardening or softening and the percent difference from continuous

deformation. Thus retained hardening plots can be directly utilized to obtain the flow stresses required for deformation.

A common format is followed in the presentation of the test results in that most graphs are plotted twice, once for Super T and once for Triple E. For each graph, all the data points for that material are plotted, with selected lines or points from the other alloy included for comparison purposes. The data point symbols for Super T have the upper half filled black, or are entirely filled. For Triple E the lower half is filled, or an empty outline is used. To aid in recognition, only Triple E curves are solid, the remaining lines dotted as per the figure captions.

CHAPTER 4

EXPERIMENTAL RESULTS

4.1 Continuous Deformation Tests

Scatter in the experimental data increased as the temperature was raised to 500°C (54). Most data employed for the study of mechanical properties was taken from tests to $\epsilon = 4$, which resulted in uniformly deformed specimens with good surface finish. Tests in which procedural or experimental errors occurred such as thermocouple breakage were excluded from the analysis. Thirty nine tests at $\epsilon = 4$ were utilized for the Al-0.65Fe Triple E alloy and 36 for the Al-0.5Fe-0.5Co Super T according to the schedule in Table 3.1. Some specimens for $\epsilon = 20$ exhibited a marked decrease in smoothness of the surface as well as limited warping of the gauge section or a reduction in length. This effect was most noted at 400-500°C at $\dot{\epsilon} = 0.1\ s^{-1}$. Oxidation does not appear to be the cause of the surface effects as tests of the same duration to $\epsilon = 4$ and $\epsilon = 20$ suffered the problem exclusively in the latter case. Elevated temperature soaks on specimens without protective argon atmosphere failed to produce any noticeable oxidation. These effects are due in part to local surface instability and in part to the development of a preferred orientation in the material at high strain (50,55). For ductility tests to $\epsilon = 20$, nineteen tests were conducted on Triple E and 20 on Super T. Tests were repeated when the results were ambiguous.

4.1.1 Rate Sensitivity

Plots of log torque versus strain rate (Triple E, Fig. 4.1, Super T, Fig. 4.2) were made at the point of highest stress to determine the strain rate sensitivity, m. Similar behaviour was observed for both alloys with rate sensitivity for Super T and Triple E rising from -.022 and -.003 at 200°C up to 0.186 and 0.194 at 500° . The negative values at 200°C partially result from adiabatic heating but more likely suggest that this T is below the hot working range. Super T shows slightly higher strength and lower rate sensitivity than Triple E except at 450°C where values of m are 0.1396 versus 0.1064. If rate sensitivity is written in the form

$$(\sigma_2/\sigma_1) = (\dot{\epsilon}_2/\dot{\epsilon}_1)^m \qquad (4.1)$$

to double the stress at 500°C ($m \approx 0.19$) would require a 40 fold increase in strain rate but at 400°C ($m \approx 0.09$) an increase of about $2x10^3$ would be necessary.

The strain hardening exponent n' was calculated at the point of highest stress by averaging values for all $\dot{\epsilon}$ at a constant T (Table 4.1). Values increased from 0 at 500 & 450°C to 0.184 and 0.114 at 200°C for Triple E and Super T. Torque to stress conversions were then made with m and n' according to equation 3.13.

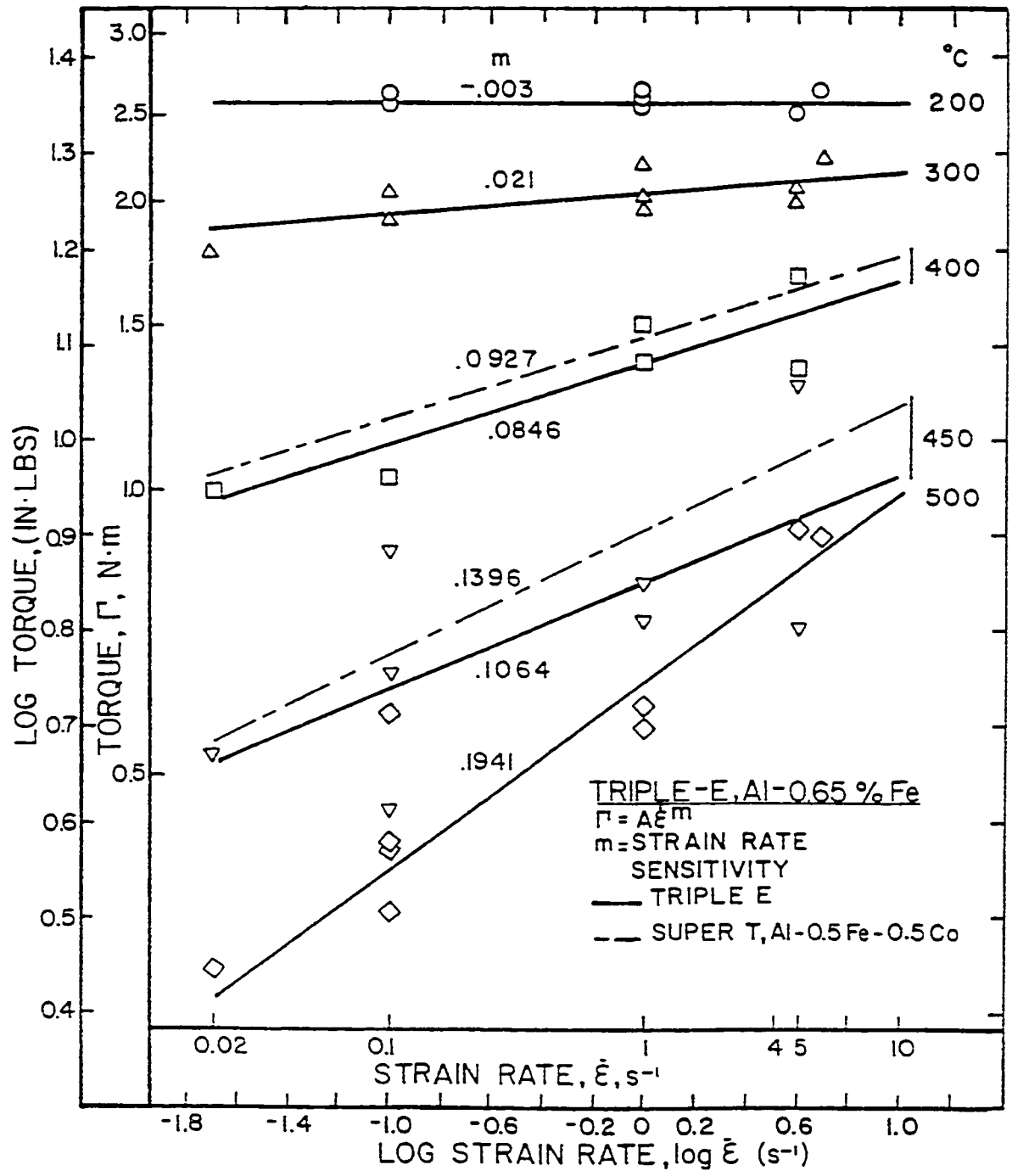

Fig. 4.1 Logarithmic dependence of torque on $\dot{\epsilon}$ for Triple E; for Super T, higher Γ but comparable m.

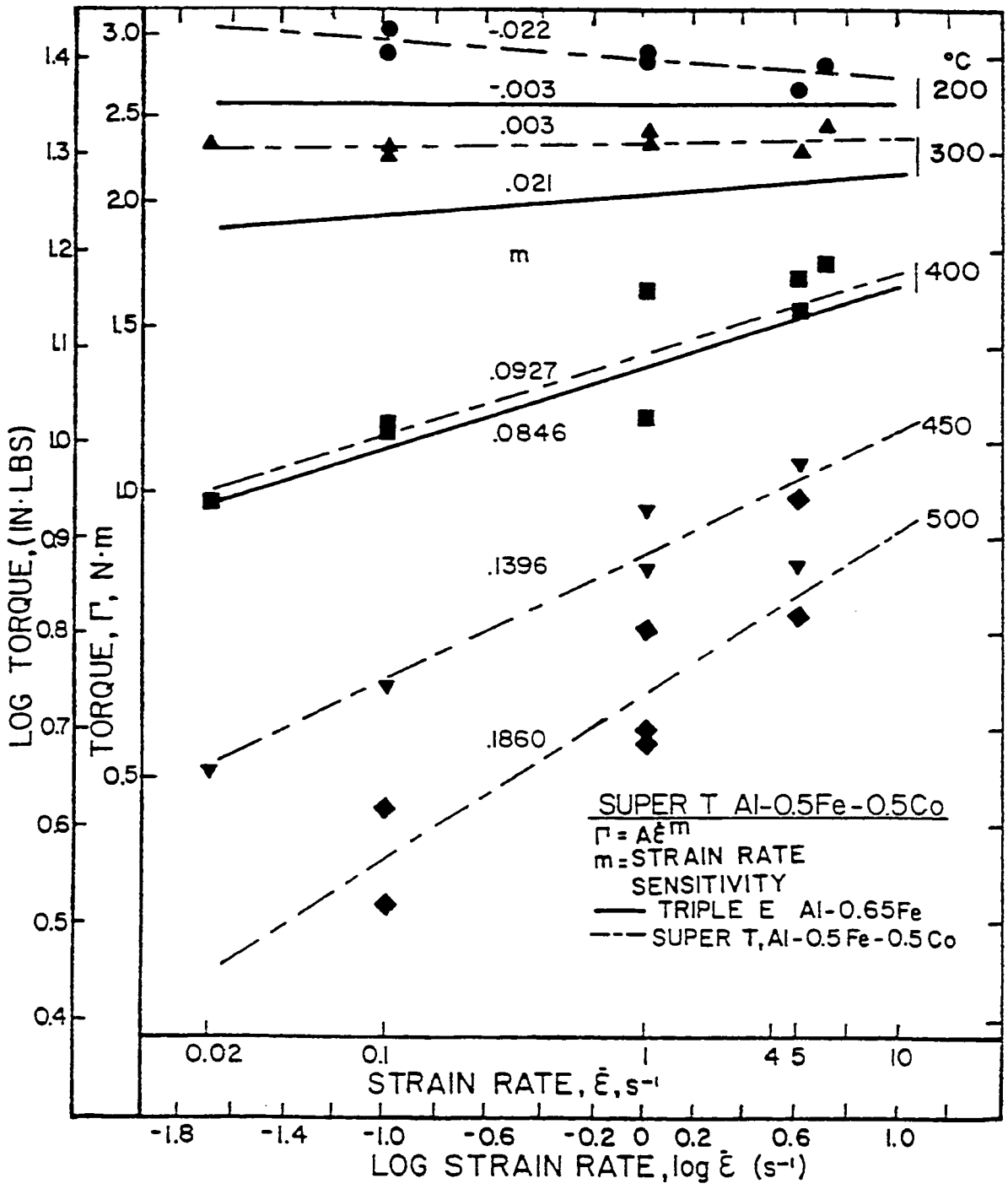

Fig. 4.2 Logarithmic dependence of torque on $\dot{\epsilon}$ for Super T

Table 4.1 Strain Hardening Exponent n'

Temperature (^{o}C)	Triple E Al-0.65Fe	Super T Al-0.5Fe-0.5Co
200	0.184	0.114
300	0.137	0.073
400	0.021	0.004
450	0	0
500	0	0

4.1.2 Continuous Deformation Flow Curves

Representative flow curves can be seen in Figure 4.3 (Triple E) and Figure 4.4 (Super T). Flow curve shape, monotonically rising to a peak or steady state stress clearly established at higher T was typical of DRV (10, 12, 13, 18). Similar behaviour was observed in tests to ϵ = 20, with a shallow decline as strain increased particularly evident at lower temperatures, attributed to texture softening or deformational heating. A rapid decline in strengthening was observed from 300 to 400°C, with the Super T slightly stronger at all temperatures.

4.1.3 Effect of Temperature & Strain Rate

The effect of temperature and strain rate on the stress was analyzed by using the hyperbolic sine law of Sect. 2.4

$$\dot{\epsilon} = A\ (\sinh\ \alpha\sigma)^n\ \exp(-Q_{HW}/RT) \qquad (4.2)$$

where A, α, and n are empirical constants, Q_{HW} the activation energy for hot working and R the universal gas constant. The value of n was obtained by the average of best fit constant T lines on a graph of log $\dot{\epsilon}$ versus log(sinh $\alpha\sigma$) (Triple E, Figure 4.5, Super T, Figure 4.6) to the test conditions where there was a clear observation of temperature dependence of the strain rate and resulting stress (i.e. stress assisted thermally activated flow). These conditions were met at 400, 450, and 500°C. As is common practice when Q_{HW} is independent of $\dot{\epsilon}$, constant temperature lines were maintained parallel to one another

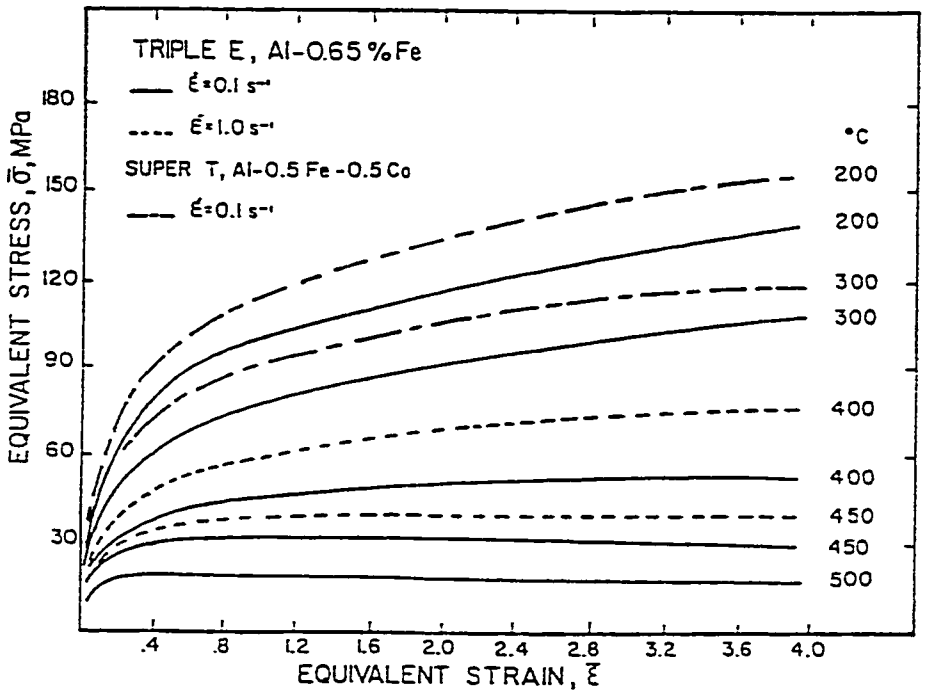

Fig. 4.3 Typical flow curves for Triple E. As T rises and $\dot{\epsilon}$ falls the strain hardening diminishes and the curves exhibit a steady state regime.

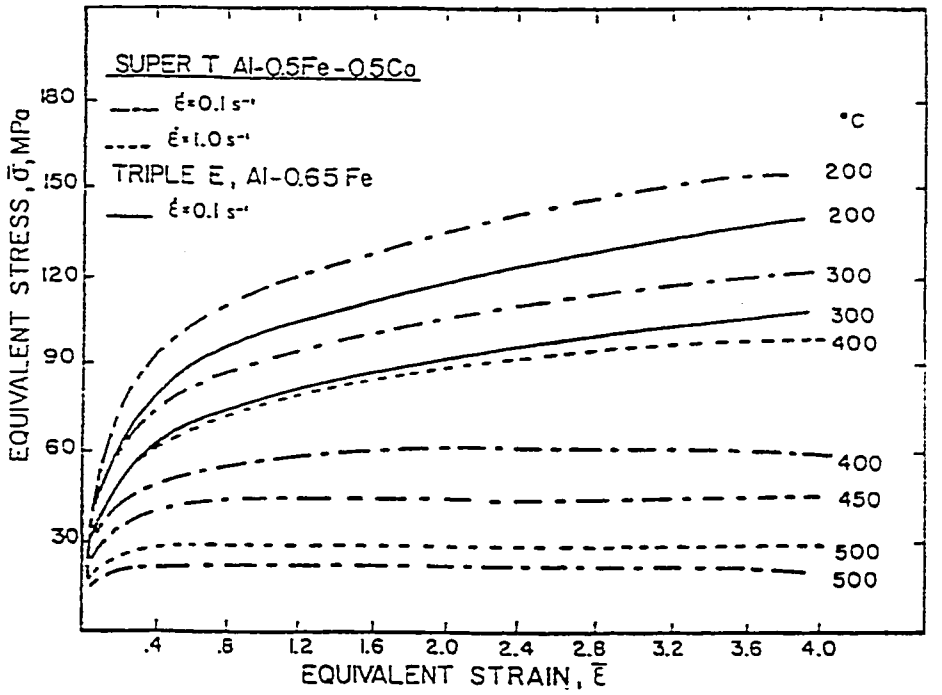

Fig. 4.4 Representative σ-ϵ curves for Super T. Flow curve shape, monotonically rising to steady state characteristic of DRV.

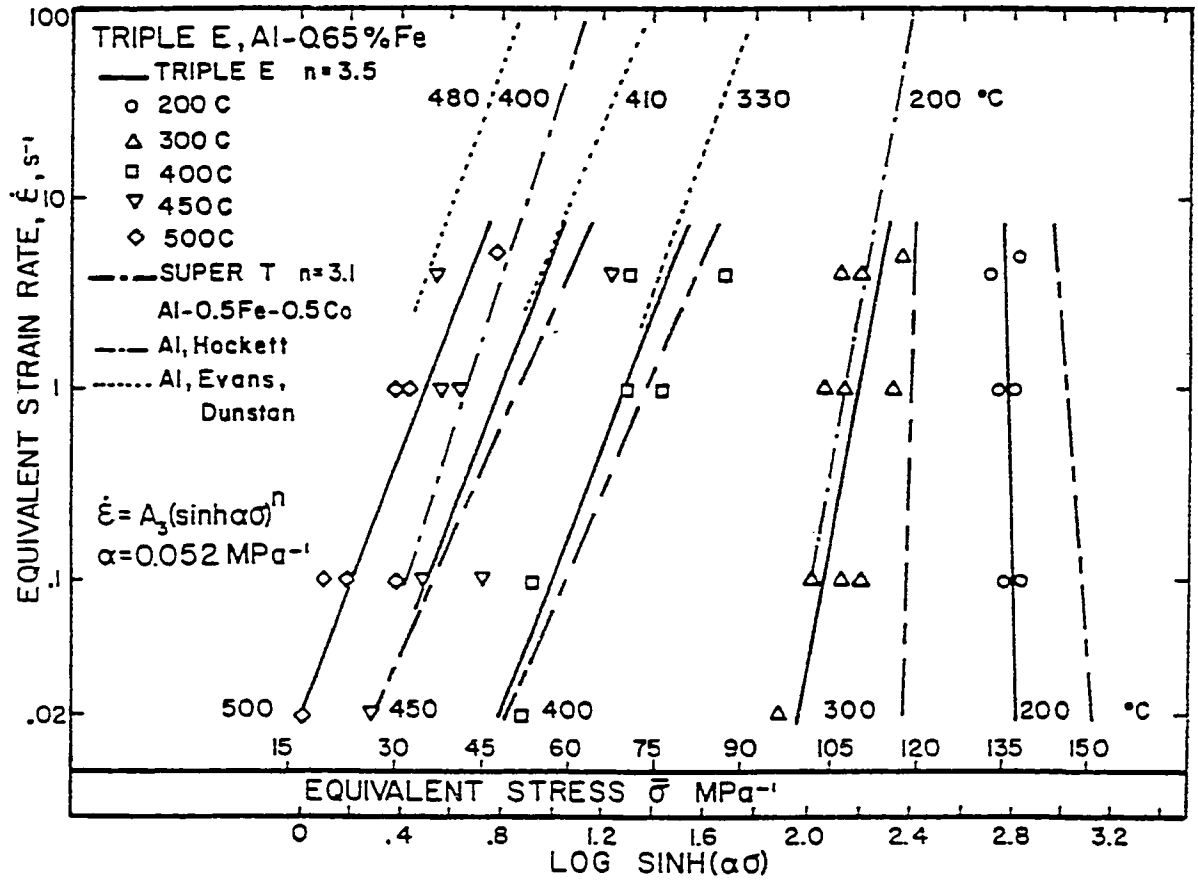

Fig. 4.5 The strain rate and temperature dependence for Triple E and Super T ; only the data points for the former are included. Comparison is made with the properties of Al.

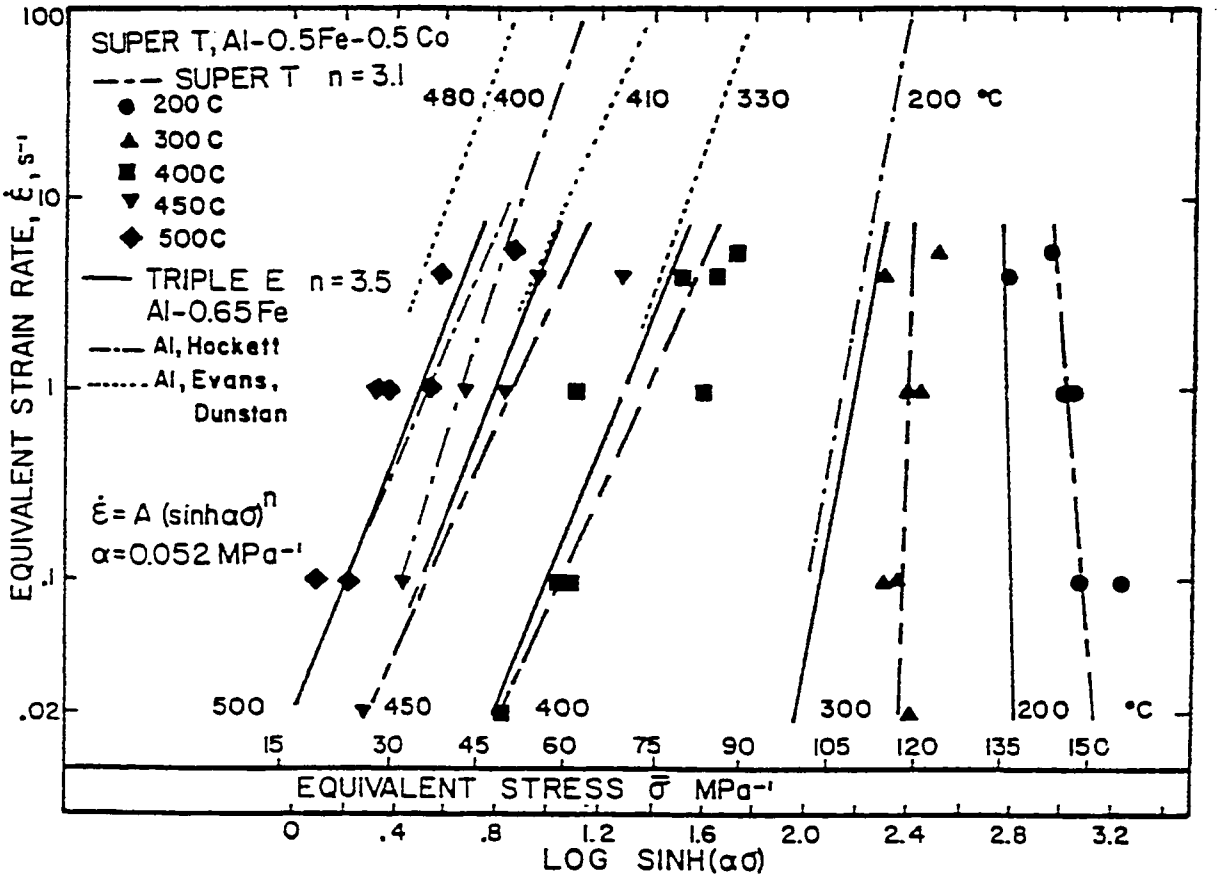

Fig. 4.6 Interdependence of $\dot{\epsilon}$ and σ of Super T and Triple E according to the hyperbolic sine law; only data points for the former are included. Strengthening by eutectic rods compared to Al.

while being fitted with this average slope, but were fit to the data at 200 and 300°C. A value of α = 0.052 MPa^{-1} was found to give the best fit to the results. The value of n of 3.5 for Triple E and 3.1 for Super T was slightly lower than the 4.0 to 4.2 for commercial purity Al. At 300°C Triple E had 10-20% lower hot strength than Super T, but comparable to Al at 200°C. At 500°C strengths of the alloys were similar, only slightly higher than Al. From the slopes for 300°C, the observation of hot working behaviour can be seen at a lower T for Triple E than Super T.

Intercepts of $\sinh(\alpha\sigma)$ were taken at $\dot{\epsilon}$ = 0.02, where no adiabatic heating was observed, and replotted in a graph of log $\mathrm{Sinh}(\alpha\sigma)$ versus 1/T (Figure 4.7). From this graph, the activation energy for hot working was determined as

$$Q_{HW} = 2.303\ R\ n\ (\text{slope of the line}) \qquad (4.3)$$

Activation energies were then calculated as 270 and 260 kJ/mol for Triple E and Super T respectively, much higher than the 150-155 kJ/mol for Al (13, 18, 22). The greater value of Q results from the rapid rise in strength of these alloys above Al as T declines.

Data from different temperatures were drawn into a plot of the Zener - Holloman parameter Z [= $\dot{\epsilon}\exp(Q_{HW}/RT)$] versus $\sinh(\alpha\sigma)$. (Triple E Figure 4.8, Super T Figure 4.9). At 200°C, (0.51 T_m) the data at all strain rates lies far above the high temperature range for both alloys supporting the observation that this temperature is not in the hot working range. The effects of deformational heating are

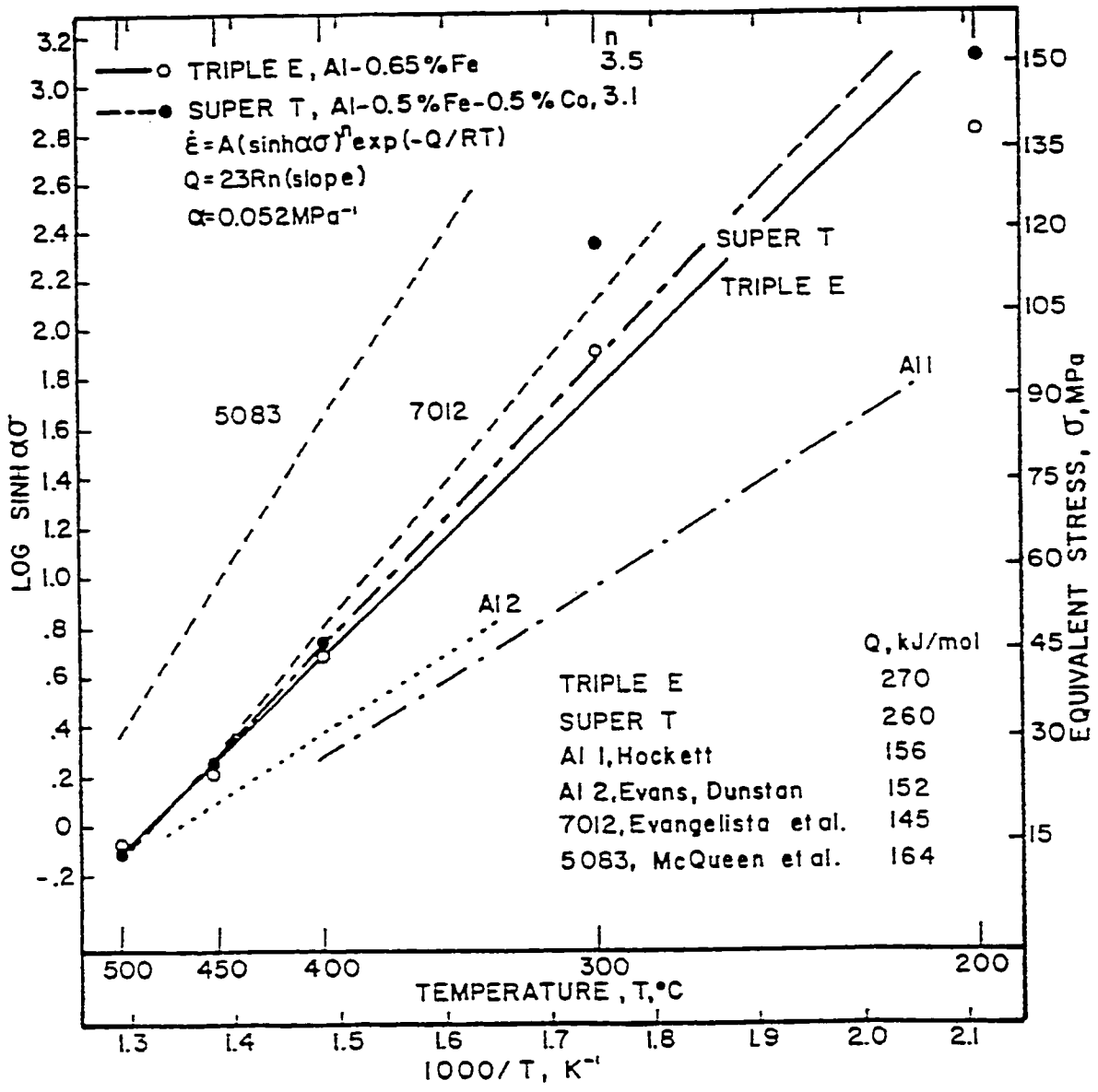

Fig. 4.7 Arrhenius relationship between $\dot{\epsilon}$, σ, and T. Particles alone provide less strengthening than with solute in 7012 (Al-6.3Zn-1.8Mg-1.1Cu-0.1Zr-0.14Mn) and 5083 (Al-4.5Mg-0.8Mn).

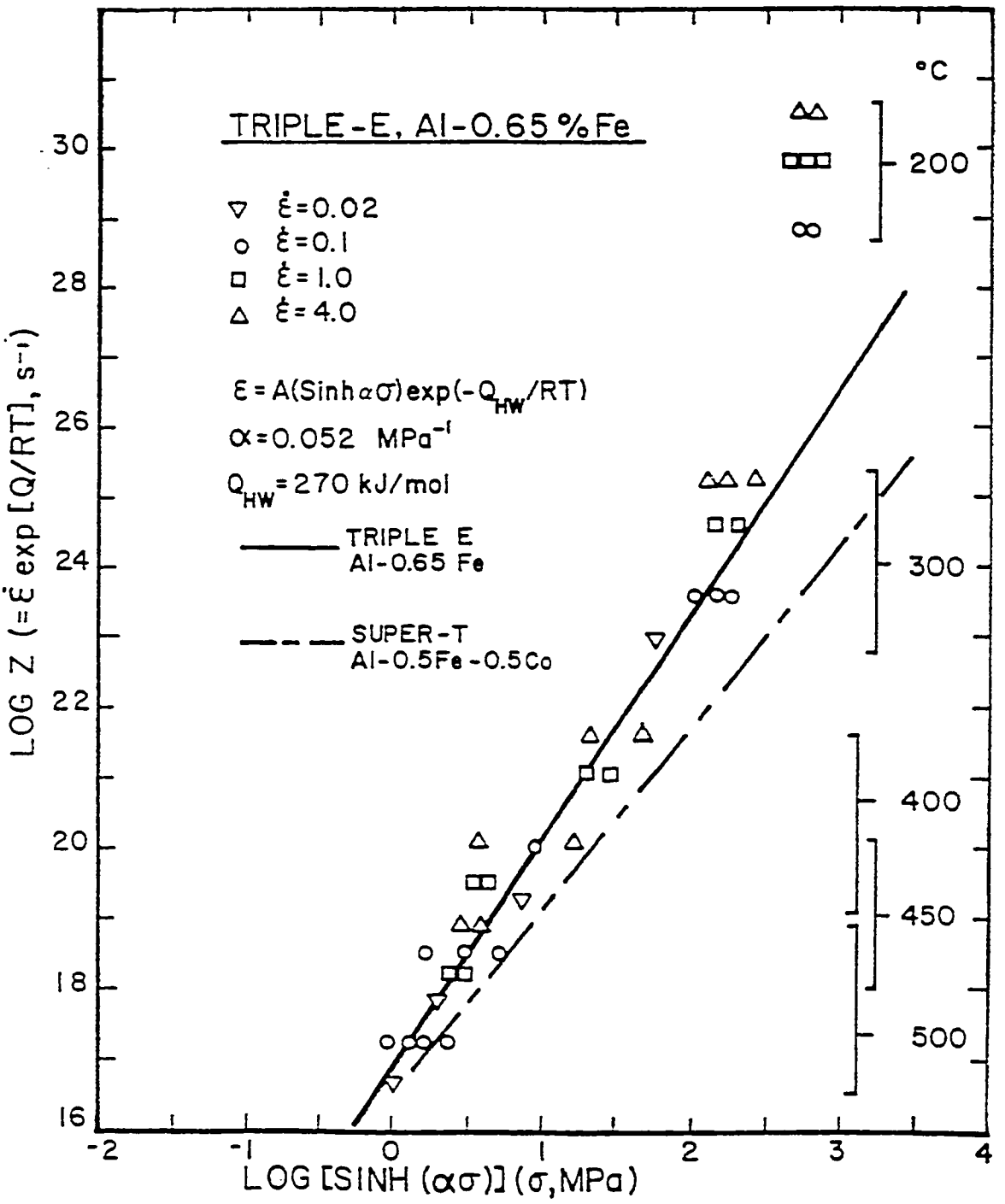

Fig. 4.8 Data from Fig. 4.5 normalized to a single line using Z parameter; only data points for Triple E shown.

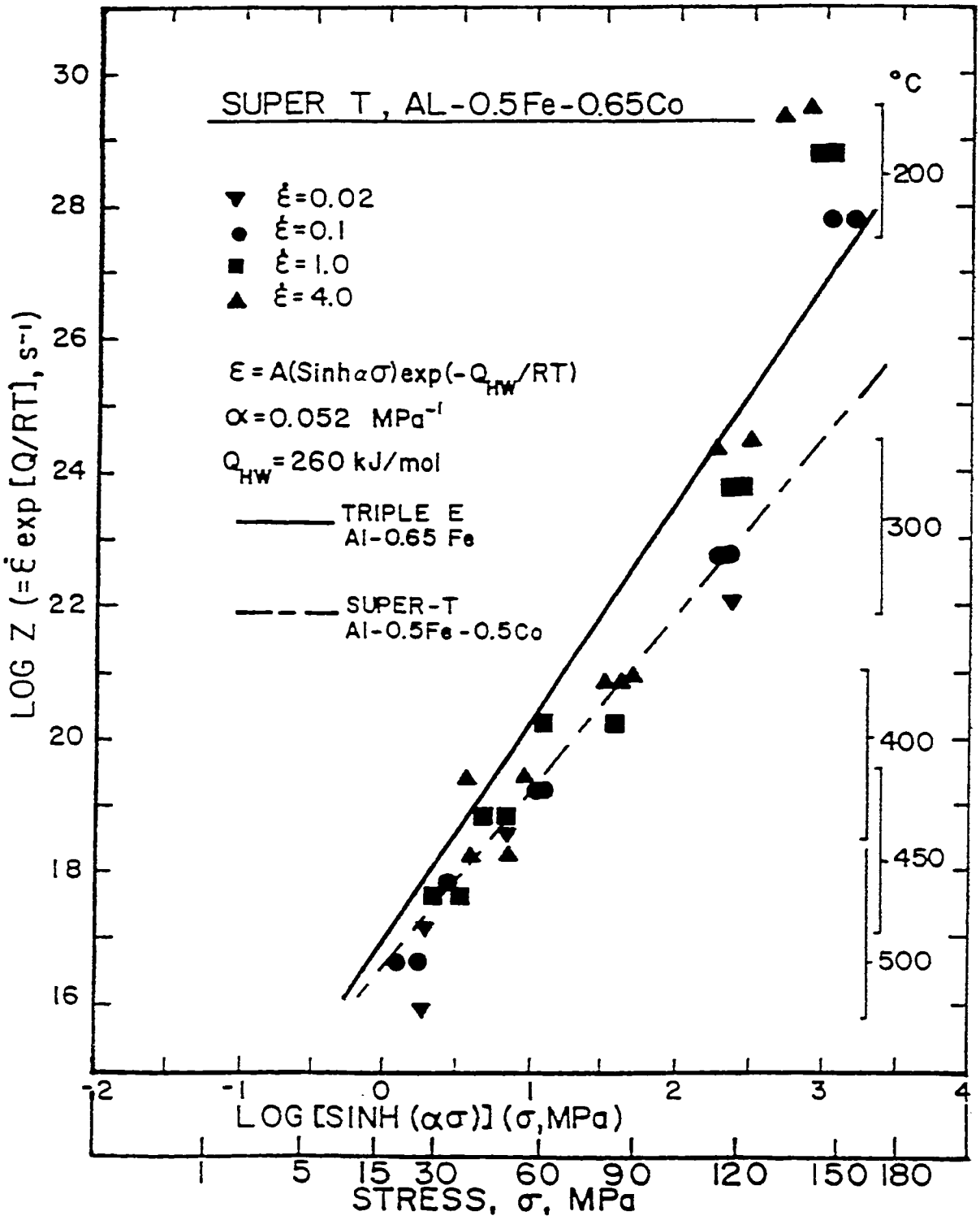

Fig. 4.9 Data from Fig. 4.6 normalized to a single line using Z parameter; lower Z values for Super T due to lower Q_{HW}.

greatest at $\dot{\epsilon}$ = 1, 4 s^{-1} at 200 and 300°C, but the 200°C, 0.1 s^{-1} data is still far above the line.

4.2 Continuous Testing to a Strain of 20

Ductility tests were carried out according to the schedule in Table 3.1. The strain to steady state (ϵ_s) and to fracture (ϵ_f) are shown as a function of T in Figures 4.10 (Triple E) and 4.11 (Super T) and versus $\dot{\epsilon}$ in Figures 4.12 (Triple E) and Figure 4.13 (Super T). For both alloys, ϵ_s and ϵ_f are inversely related with ϵ_f being maximum when ϵ_s is minimum. Steady state strain was much higher than the 0.2 to 0.5 typical for Al. At 200°C, ϵ_f for Super T was independent of strain rate (ϵ_f = 4.6-5.1) while highly rate dependant for Triple E (ϵ_f = 3.7-8.0). Strong rate dependencies for both alloys were observed at 300°C with fracture strain climbing to exceed the range of the strain sensor at 450 and 500°C. Triple E had higher ductility than Super T at 200 and 300°C but lower at 400°C.

Consistent with diminishing strain hardening exponent n', the steady state strain decreased with decreasing $\dot{\epsilon}$ and increasing T. Super T showed less rate sensitivity on ϵ_s and generally lower values than Triple E. At 200°C fracture intervened prior to the attainment of a stress plateau but by 300°C steady state conditions were established prior to failure. In Figures 4.12 and 4.13 all of the tests at $\dot{\epsilon}$ = 0.02 s^{-1} were taken to ϵ = 4, however based on the trends established at higher strain rates, fracture would not be expected to occur at this low $\dot{\epsilon}$ by ϵ = 20.

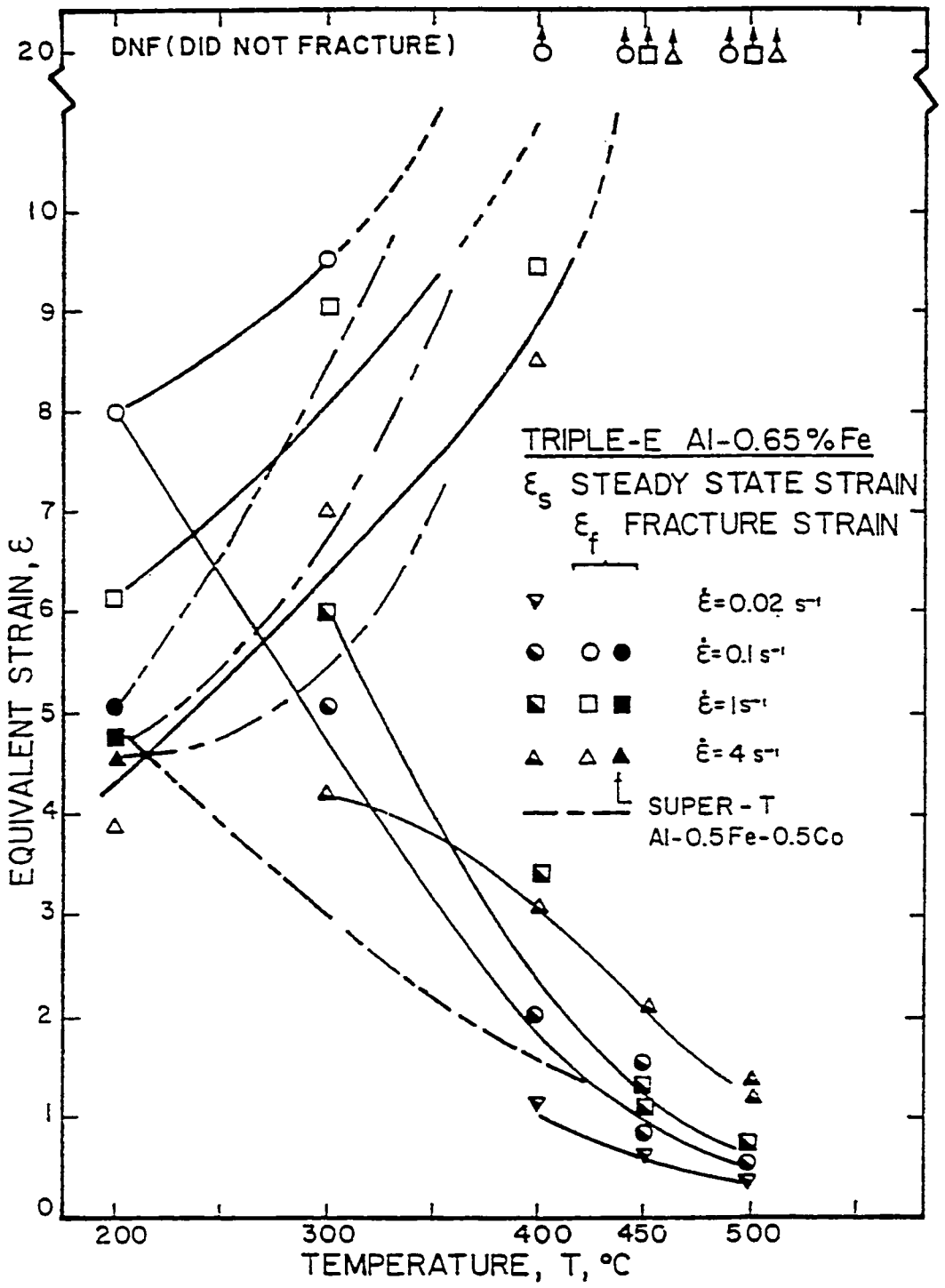

Fig. 4.10 Dependence of ϵ_f and ϵ_s on T, rising T increases DRV thus lowering ϵ_s and increasing ϵ_f. Above 400°C ϵ_f generally exceeds the range of the strain sensor (ϵ = 20).

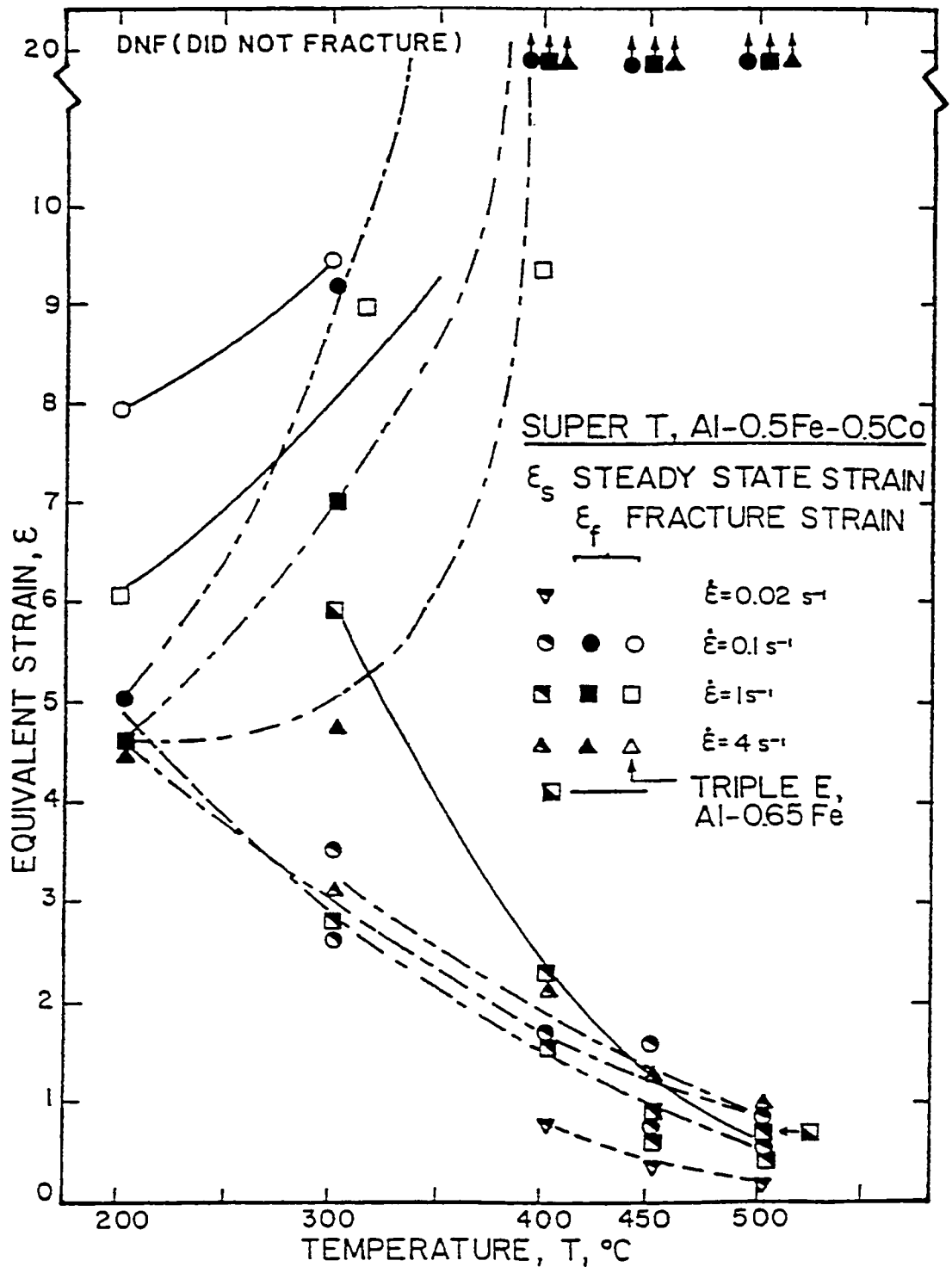

Fig. 4.11 Dependence of ϵ_f and ϵ_s on T for Super T alloy. ϵ_s lower than Triple E alloy.

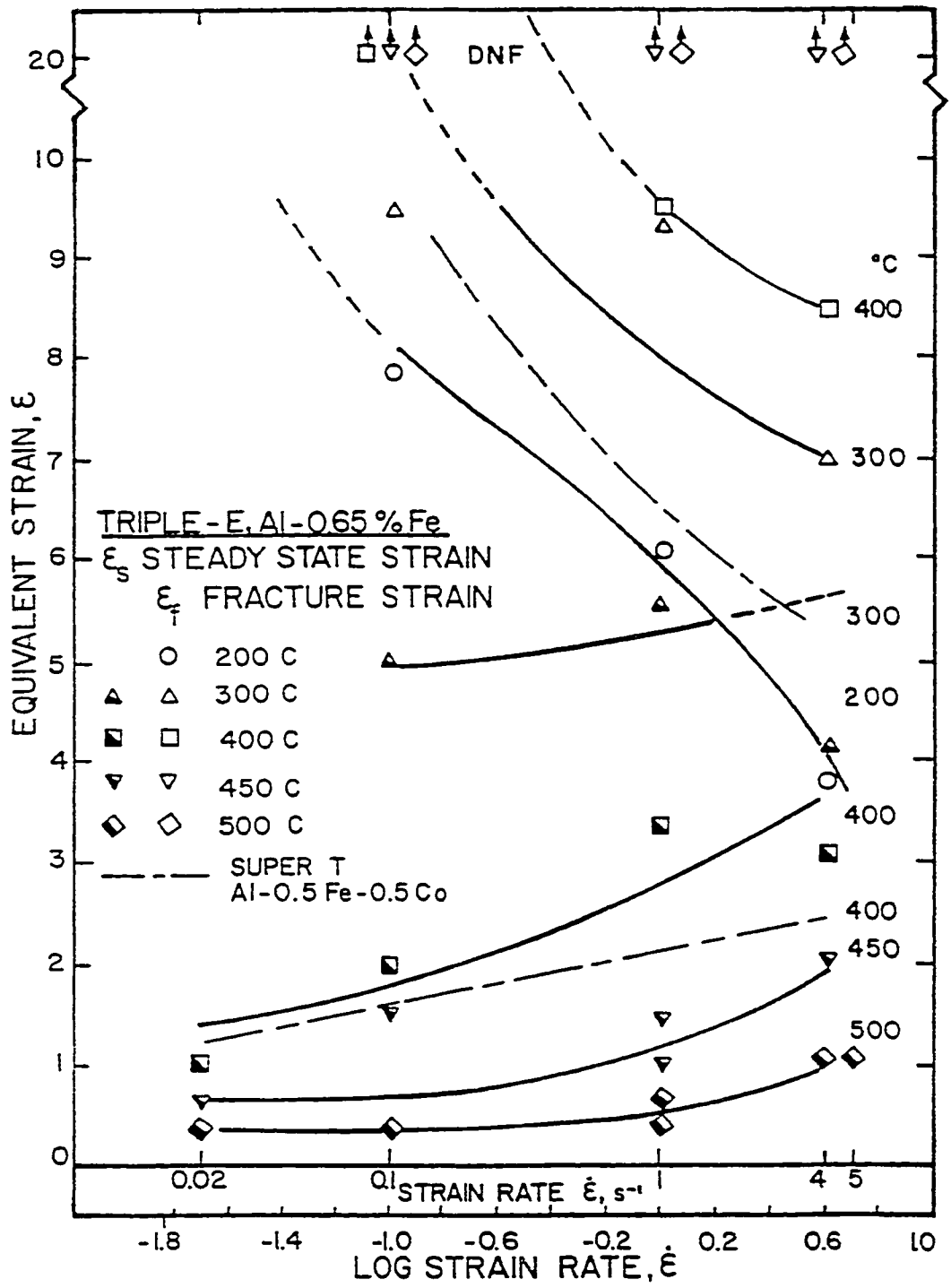

Fig 4.12 Dependence of ϵ_f and ϵ_s on $\dot{\epsilon}$; decreasing $\dot{\epsilon}$ increases DRV thus lowering ϵ_s and increasing ϵ_f.

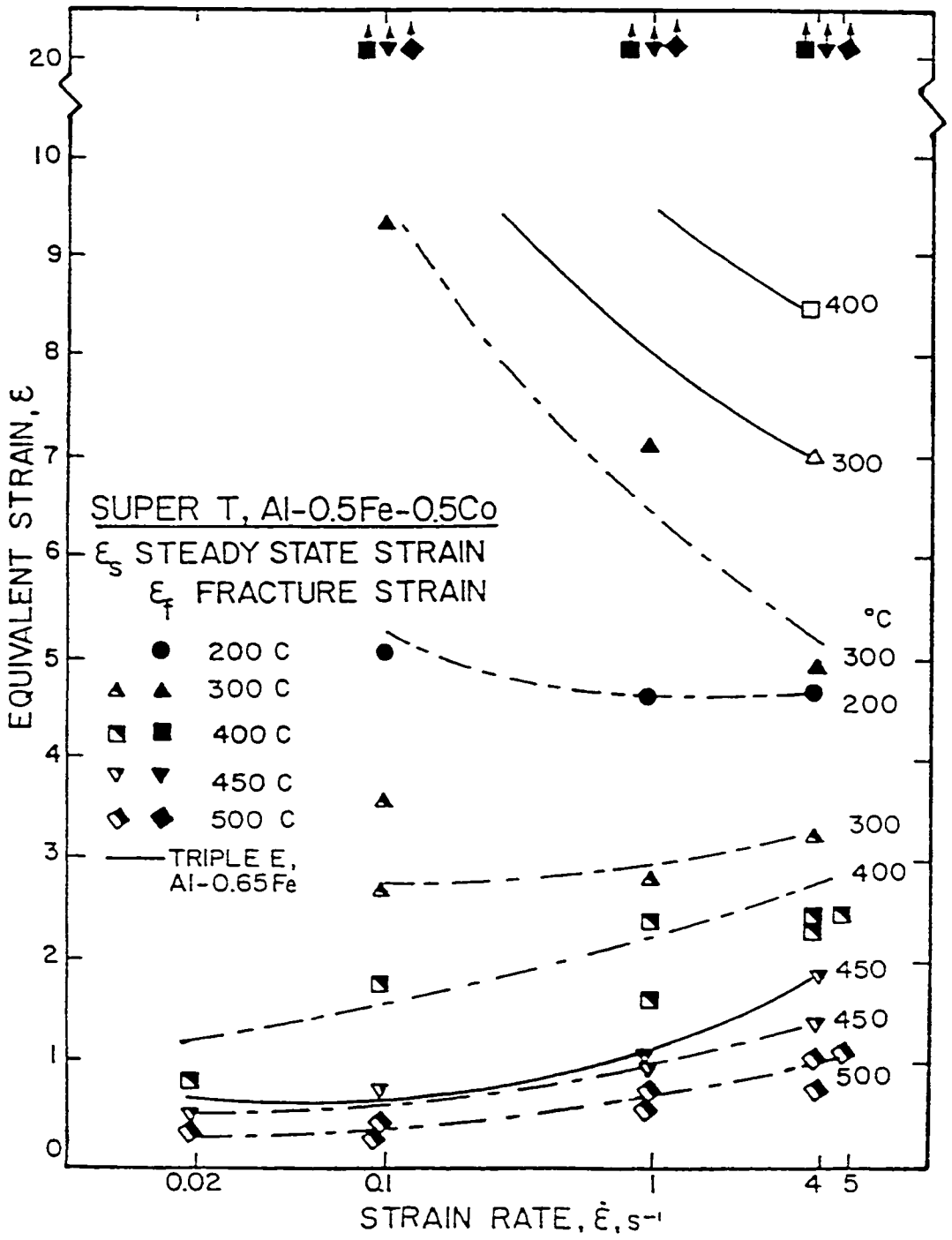

Fig. 4.13 Strain to fracture ϵ_f and strain to steady state ϵ_s as a function of strain rate for Super T. As DRV rises with declining $\dot{\epsilon}$, ϵ_s decreases and ductility ϵ_f increases.

An exhaustive attempt was made to quantify the temperature rise due to deformational work heating by refinement of test practices and analytical methods. When assisting in torsion testing of stainless steel alloys it was observed that the thermocouple routinely picked up temperature rises of over 50°C but in the lower strength Al conductor alloys the highest observed temperature rise was in the order of 5°C. The damping rate of the thermocouple controller was electronically varied, along with thermocouple location, method of attachment, and insulation, in tests at maximum $\dot{\epsilon}$ to high strains in an attempt to detect larger temperature rises, but none were found.

Steady state strain was plotted in an attempt to use the correction factor for adiabatic work heating

$$\Delta T = \int_0^{\epsilon_s} \sigma \, d\epsilon \; / \; \rho c \qquad (4.4)$$

where ρ is the density and c the specific heat. Although this equation has been used to approximate the temperature rise in aluminum (56) and stainless steel (57) it proved completely unsatisfactory for the present alloys. The equation erroneously predicted that all tests had approximately the same corrected test temperature. Due to furnace compensation the assumption of adiabatic conditions could not be made. Adiabatic conditions are approached as $\dot{\epsilon}$ is increased, however equation 4.4 did not generate realistic values for temperature rise.

4.3 Microstructure and Hardness

Subsequent to testing, a separate detailed study was made of the specimens via optical metallography to evaluate the grain and subgrain structures by normal and polarized light microscopy (58, 59). Samples were prepared from sections 0.5 mm below the surface, with one group etched to delineate grain boundaries, and the other group anodized to reveal grain and subgrain dimensions. Anodized specimens were viewed in polarized light with and without a quarter wave plate. Subgrain sizes established by optical microscopy are larger than when determined by transmission electron microscopy (TEM) (22,58). Grain structure determined by chemical etching was similar for both alloys with the grains twisted about the torsion axis, appearing on tangential sections as elongated streaks with serrated grain boundaries, and thus gave no evidence of SRX. Grain width increased with test temperature from 30-40 μm up to 70-80 μm at 500^{o}C.

Specimens were anodized and examined by polarized light with the results presented for Triple E in Figure 4.14a,b. Subgrains were irresolvable at 200^{o}C and 300^{o}C, although the grain mottling increased in both size and contrast with T. At 400^{o}C (Fig. 4.14a, (59)) the subgrains are still not clearly defined and lie in bands with nominal diameter of 2 μm. By 500^{o}C (Fig. 4.14b, (58)) the subgrains become larger, clearly defined, and equiaxed. Subgrains from Super T specimens were clearly smaller and less resolvable at all test temperatures.

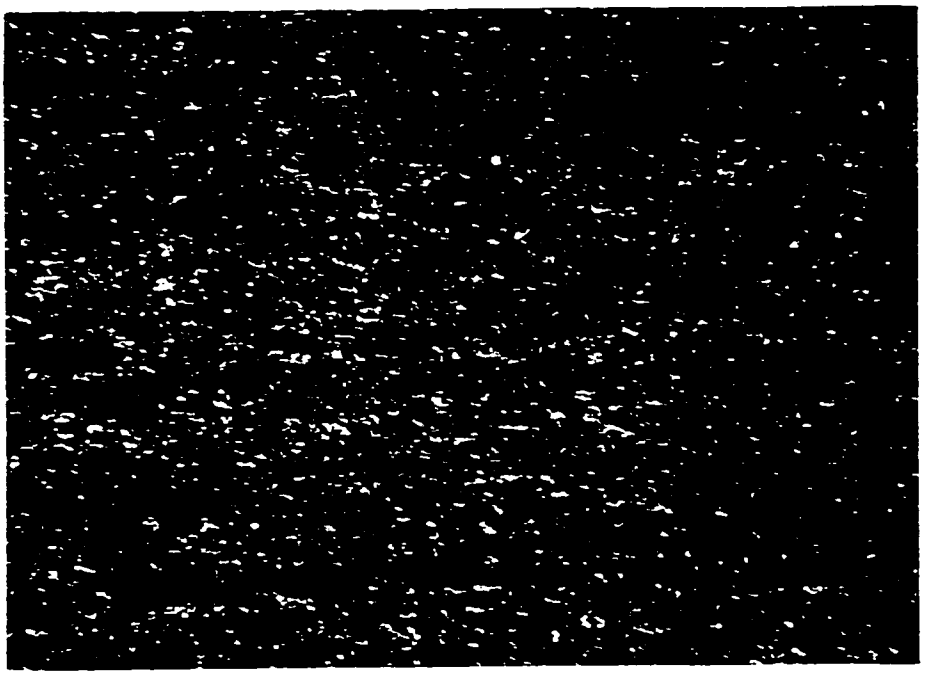

a)

b)

Fig. 4.14 Polarized light micrographs of anodized Triple E (Al-0.65Fe) alloy ($\dot{\epsilon}$ = 1 s^{-1}). Subgrains become larger and more resolvable with higher temperatures. a) 400°C, b) 500°C. (200X)

Subgrain size versus hardness is reported in Table 4.2 (58). Diamond pyramid hardness values (1kg) decrease as subgrain size increases. Hardness of Triple E slowly declines from 50 at 200°C to 46 at 300°C to 41 at 400°C, followed by rapid decline to 28 at 450°C and 25 at 500°C. Super T is generally harder at each temperature but experiences the same rapid drop at 450°C to hardness comparable to 1100 (commercial purity) Al.

Subsequent examinations of the specimens by transmission electron microscopy after continuous and interrupted deformation was carried out by another investigator and reported elsewhere (60, 61). Figures 4.15 a,b and 4.16 a,b of Super T alloy are representative of the substructure changes that occurred. Equilibrium subgrain size, d_s, followed the expected behaviour with d_s increasing with rising T or declining strain rate. Comparison of Figures 4.15a (300°C, $\dot{\epsilon} = 4s^{-1}$), 4.15b (400°C, $\dot{\epsilon} = 5\ s^{-1}$) and Fig. 4.16b (450°C, $\dot{\epsilon} = 4s^{-1}$) shows much larger subgrain size at the higher T. The increase in d_s by decreasing $\dot{\epsilon}$ at a constant T is illustrated in Figures 4.15b, and 4.16a.

The hot strengths of the Al-0.65 Fe and Al-0.5Fe-0.5Co alloys are compared in Table 4.3 with commercial (1100) Al, a particle containing solution strengthened alloy (Al-4.5Mg-0.8Mn) and electrical conductor (EC) alloy 1350 (25). Hot strength had been found to be inversely proportional to subgrain size, with the alloys stronger than Al.

Table 4.2 Hardness versus Subgrain Size

	Super-T Al-0.5Fe-0.5Co			Triple E Al-0.65Fe			1100 Al	
TEST TEMP. ^{o}C	d_s, opt. μm	d_s, TEM μm	DPH	d_s, opt. μm	d_s TEM	DPH	d_s, TEM μm	DPH
200	2.5	1.0	60	2.0	1.1	50	1.4	41
300	2.0	2.3	55	2.5	2.7	46	2.2	34
400	3.5	4.8	36	3.5	5.3	41	2.9	25
450	5.0	5.2	32	7.5	5.6	28	3.5	25
500	7.5	5.5	27	8.0	5.9	25	4.2	22

a)

b)

Fig. 4.15 TEM micrographs illustrating effect of rising T on subgrain size d_s for Super T (Al-0.5Fe-0.5Co) alloy.
a) 300°C, $\dot{\epsilon}$ = 4 s^{-1}, ϵ = 20, b) 400°C, $\dot{\epsilon}$ = 5 s^{-1}, ϵ = 4.

a)

b)

Fig. 4.16 TEM micrographs of effect of rising T and $\dot{\epsilon}$ on subgrain size for Super T; a) 400°C, $\dot{\epsilon}$ = 0.02 s^{-1}, ϵ = 4,
b) 450°C, $\dot{\epsilon}$ = 4 s^{-1}, ϵ = 20.

Table 4.3 Strength of Hot Worked Aluminum Alloys

Alloy	T ^{o}C	$\dot{\epsilon}$ STRAIN RATE s^{-1}	ϵ STRAIN	d_{sg} μm	σ_s HOT STRENGTH MPa	σ_y YIELD STRENGTH MPa
1100	200	220	0.7	1.13	110	105
Al	200	22	0.7	1.2	105	100
	400	12	0.7	2.0	57	63
	400	1.3	0.7	2.4	43	55
Al	300	1.0	4.0	1.1	185	
4.5Mg	400	1.0	4.0	2.0	130	
0.8Mn	500	1.0	4.0	3.5	75	
Al-	485-	1.6	4.33	5.9		110
0.65Fe	180	27	13 passes	1.0		
Triple E						
	200	1,4	4		136	
	300	1,4	4		110	
	400	4	4		78	
	450	4	4		56	
	500	4	4		36	
Al-	485-	1.6	4.33	5.5		120
0.5Fe-	180	27	13 passes	0.85		
0.5Co						
Super T	200	1,4	4		150	
	300	1,4	4		120	
	400	4	4		84	
	450	4	4		60	
	500	4	4		38	
EC	485-	1.6	4.33	1.6		96
1350	180	27	13 passes			

4.4 Interrupted Deformation Testing

Multistage tests were conducted as specified in Table 3.3. The output for Triple E, 400°C, $0.1s^{-1}$, 20 sec hold time is shown in Figure 4.17a full scale, and Figure 4.17b expanded scale. Stress rises during each interval to a maximum during a pass, however the maximum declines as the number of passes increases. Fractional softening (FS, eqn. 3.14) was determined by examining the output in expanded scale as in Figure 4.17b, and is shown for Triple E in Figure 4.18. At 400°C, 0.1 s^{-1} softening for 5 to 20 second interruption time t_i is about 20%. As t_i increases to 40 and 100 seconds, FS rises to approximately 30 and 37% respectively. After the first pass the FS becomes almost constant for most t_i.

For the Super T alloy (Al-0.5Co-0.5Fe) (Figure 4.19) at 400°C, $0.1s^{-1}$ different behaviour is observed. At t_i = 5 seconds, FS stabilizes at 15 %, climbing to 23 % at 10 seconds. There is no common value of FS at 5, 10, and 20 seconds as in Triple E, and at 20, 40 and 100 hold times FS continually rises with strain. For both alloys there were no significant strain rate effects. For reasons of clarity, only a single line at $\dot{\epsilon}$ = 1.0 s^{-1} was added to Figures 4.18 and 4.19. to illustrate the lack of rate sensitivity of FS.

At 450°C, 0.1 s^{-1} (Figure 4.20) little difference in interpass softening between the alloys can be noted. FS for Triple E rises from 27% at t_i = 10 to 33% at 20 sec and 50% at 40 sec. Softening for Super T was approximately the same, 27% at 10 seconds, 36% at 20

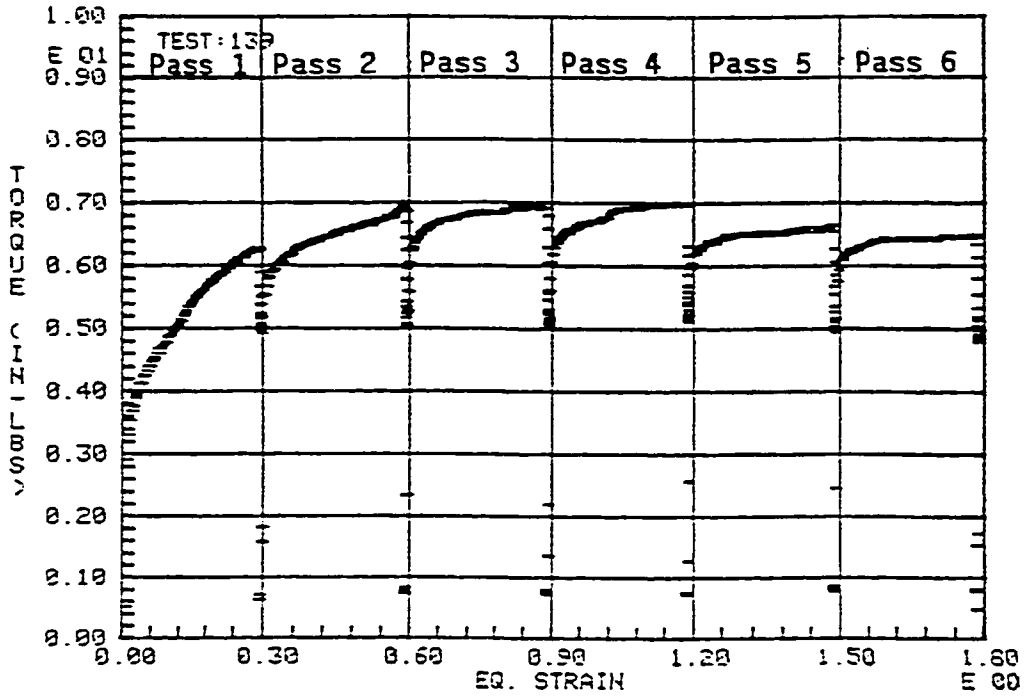

a)

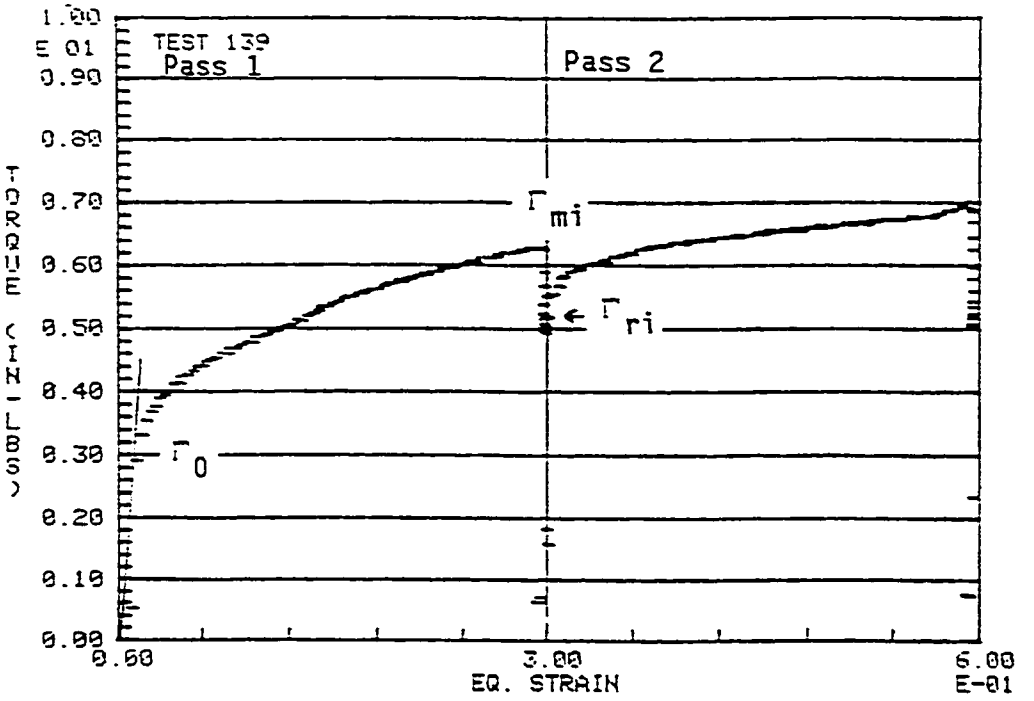

b)

Fig. 4.17 a) Interrupted deformation test on Triple E, 400°C, 0.1 s^{-1}, pass strain 0.3, interpass hold time 20s, b) same as a) with expanded scale to determine Γ_o, Γ_{mi}, Γ_{ri}.

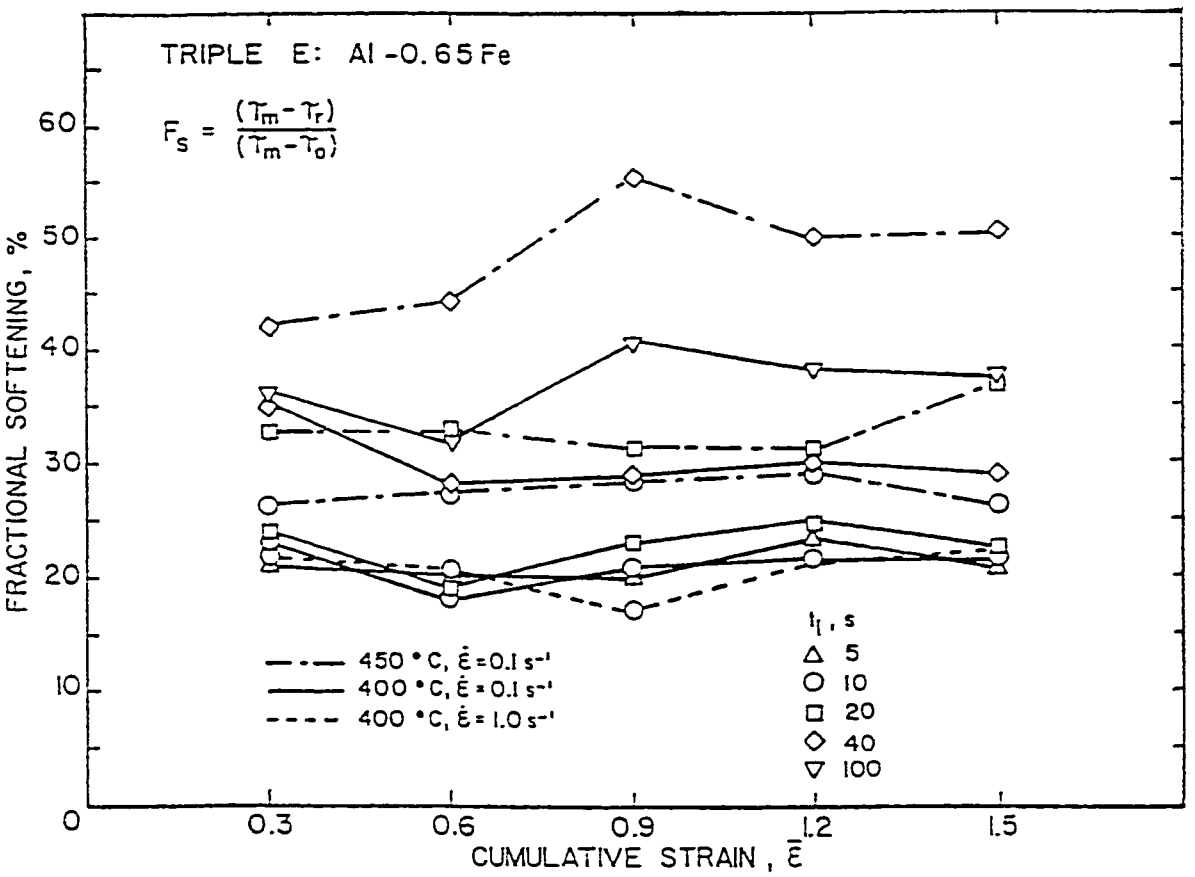

Fig. 4.18 Fractional softening for Triple E. Softening increases with hold time, temperature.

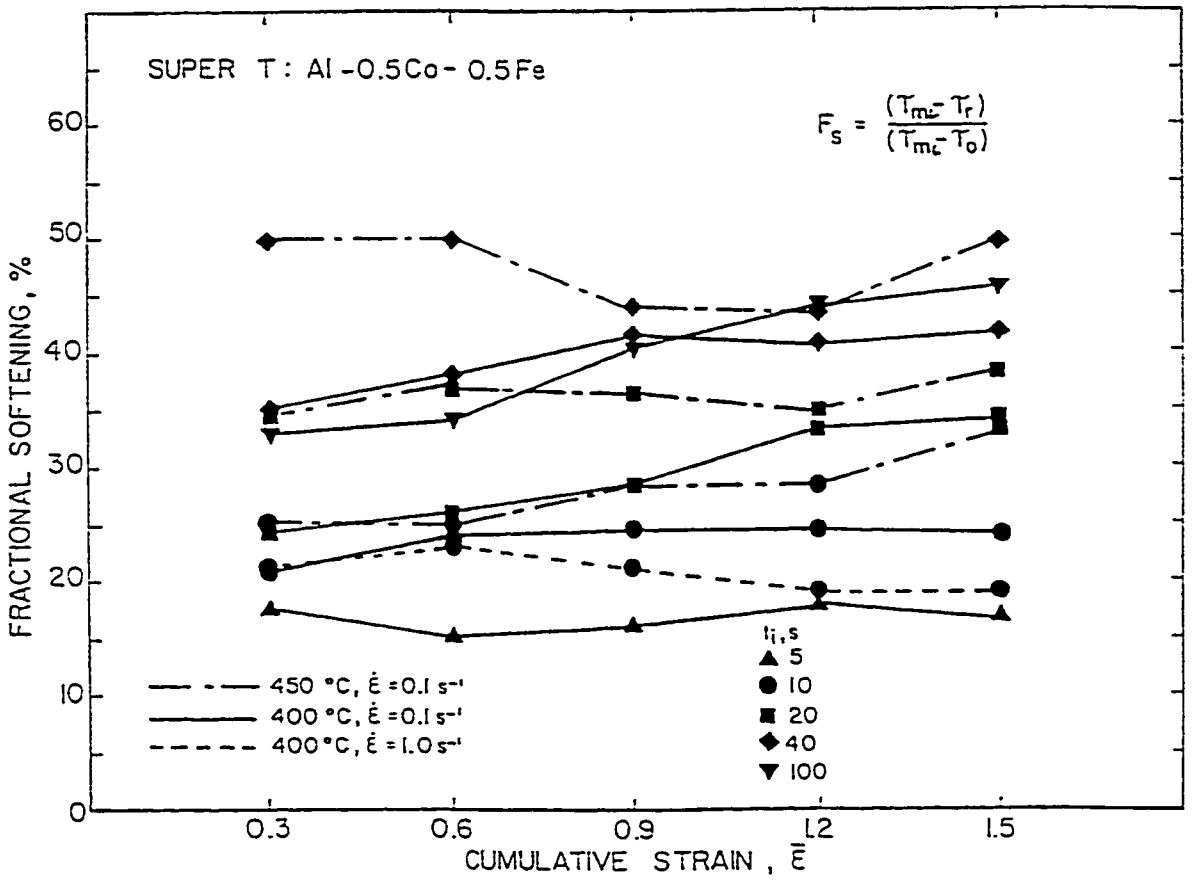

Fig. 4.19 Fractional softening of Super T during intervals (5 to 100s) of multistage tests with pass strain of $\epsilon = 0.3$ plotted versus cumulative strain.

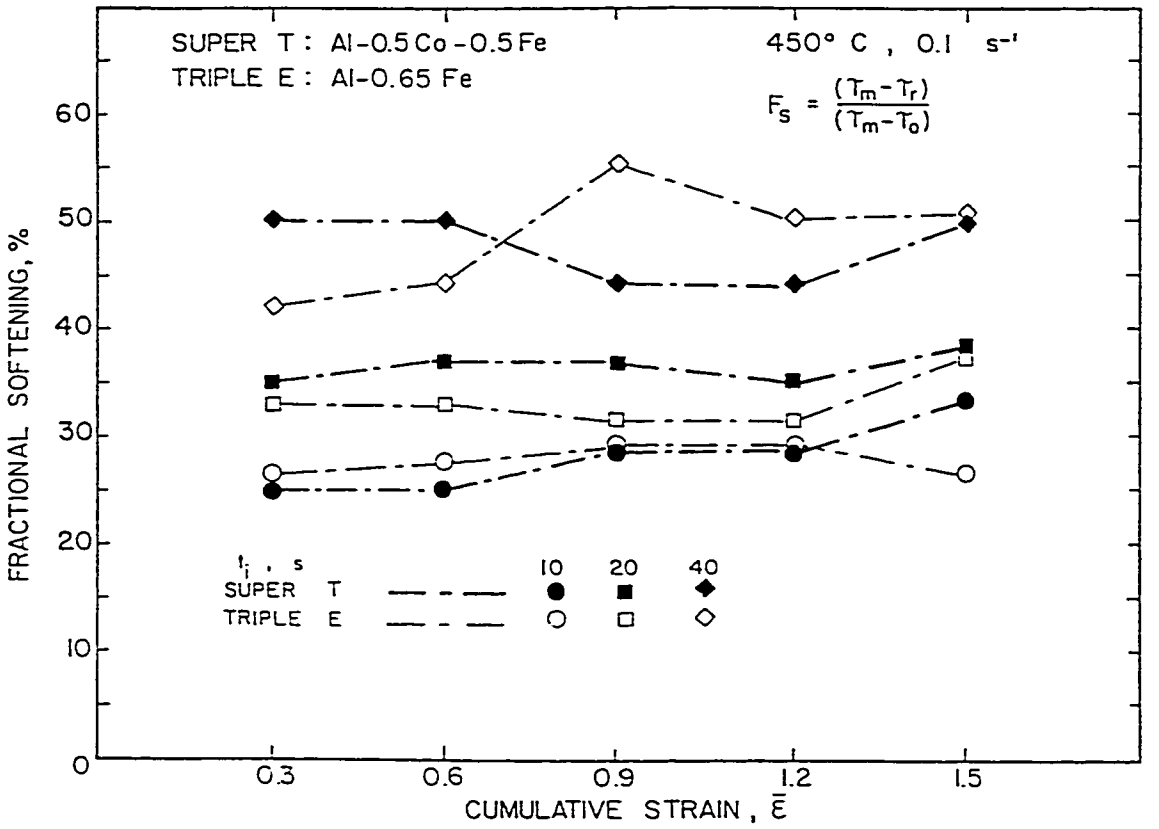

Fig. 4.20 Fractional softening versus strain for Super T, Triple E, at 450°C. Both alloys exhibit similar softening up to 50% at 100 second hold time.

seconds and 46% at 40 second hold times. By averaging all the FS data points at t_i = 10, 20, and 40 seconds (Fig. 4.18, 4.19, and 4.20), strong temperature sensitivity was noted. Increasing T from 400 to 450^{o}C raised FS an average of 21% for Super T and 48% for Triple E.

Retained hardening (RH = $\Gamma_i/\Gamma_{0.3}$, where i=0.6, 0.9 ... 1.8) curves are plotted in Figures 4.21-4.24 compared with continuous deformation flow curves. The raw data plot of a multipass test on Triple E in Figure 4.17a demonstrated typical behaviour. Maximum torque at the end of each pass rose, then declined with successive passes, never reaching the level attained in continuous deformation. The net hardening or relative retained hardening varied with strain rate and hold time. For Super T at 400^{o}C, 1.0s^{-1} (Figure 4.21) steady state conditions were reached at the conclusion of the test for 10 second pass times, with little difference from the continuous flow curve. At the same t_i, ϵ_s is 1.5 compared to 2.2 (fitted) for the continuous test (Fig. 4.11, 4.13). For 20 second pass times a steady state was observed at ϵ = 0.6 followed by a secondary steady state at ϵ = 1.8. There was no secondary steady state at t_i = 40, 100 seconds as the Super T continued to soften at these long interruption hold times. For pass times of 20 to 100 seconds, final pass RH progressively drops off to 0.88 at 100 sec, 33% lower than the continuous curve.

For Triple E at 400^{o}C, $\dot{\epsilon}$ = 1.0 s^{-1} (Fig. 4.22) the RH of 1.55 at ϵ = 1.8 for the continuous curve was higher than the RH of 1.28 for Super T under similar conditions. This is likely due to the greater

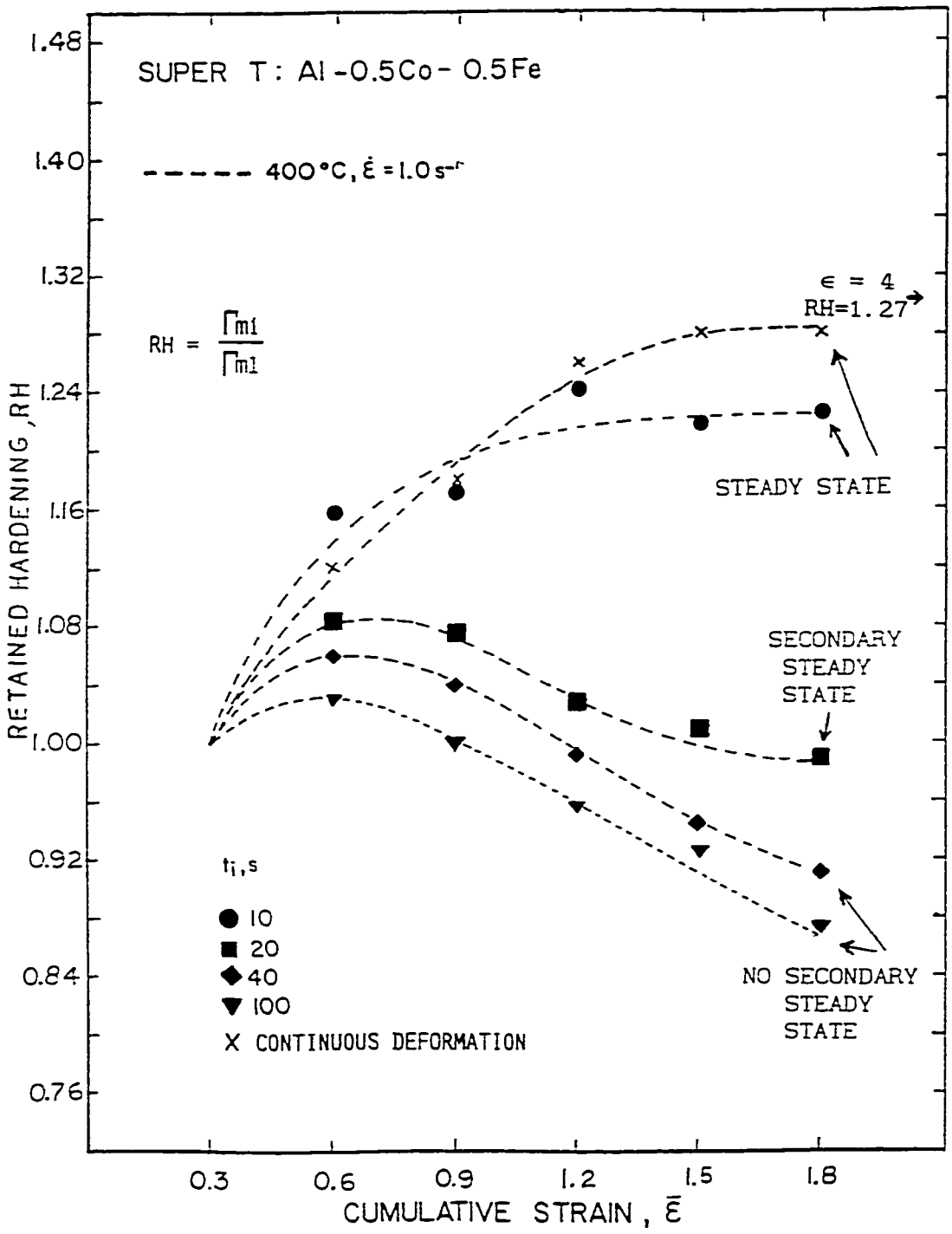

Fig. 4.21 Retained hardening versus strain for Super T alloy. Increasing $\dot{\epsilon}$ to 1.0 s^{-1} delays onset of softening due to cumulative effect of SRV.

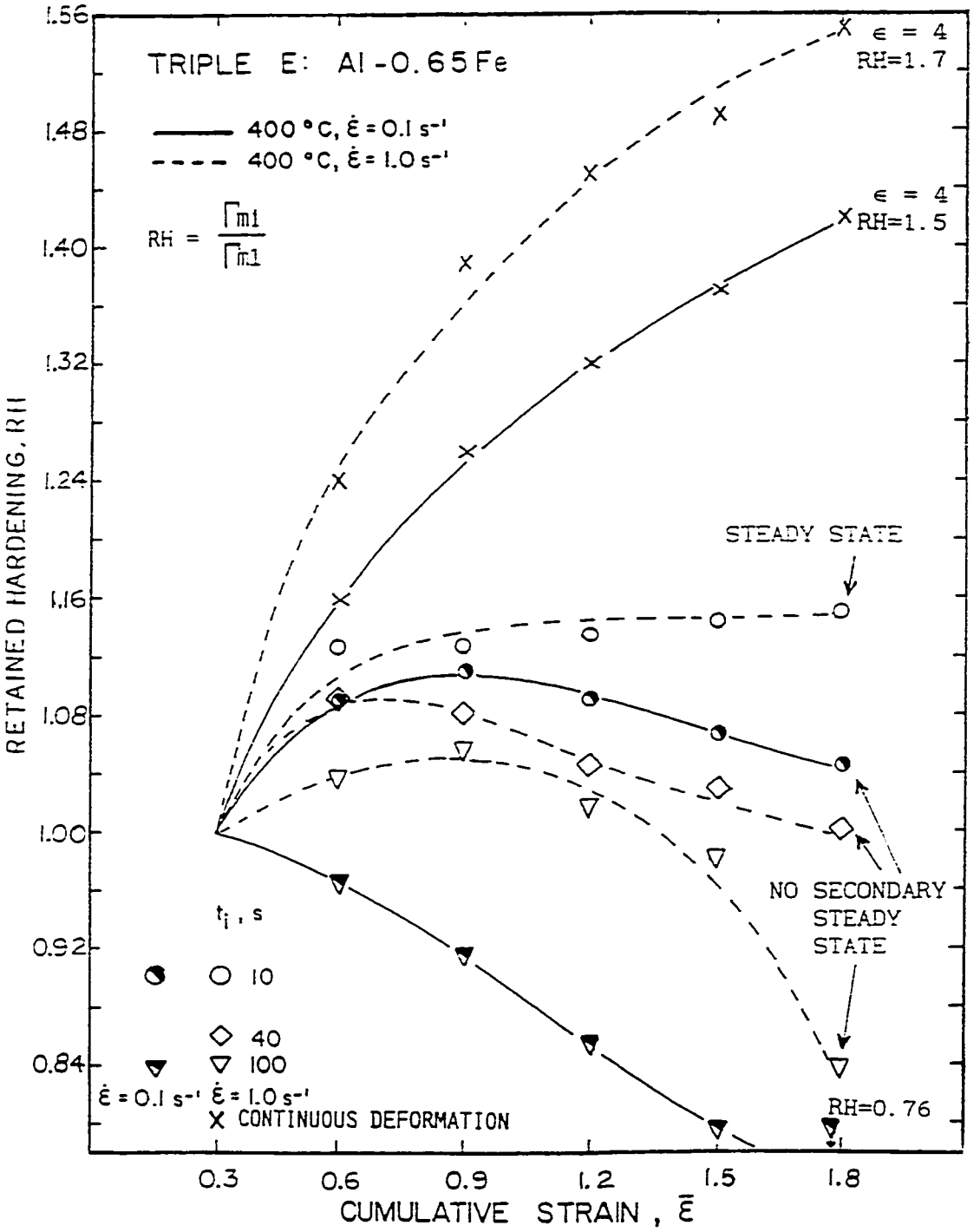

Fig. 4.22 Retained hardening versus strain at 400°C for Triple E. RH substantially less than continuous deformation, decreasing with hold time. Differences between continuous and interrupted deformation envelope curves greater than Al-0.5Fe-0.5Co alloy.

strain hardening of Super T in the first strain interval of 0.3 (lower ϵ_s), and thus increased relative hardening of Triple E in the interval from ϵ = 0.3 to 1.8. The continuous deformation steady state strain ϵ_s was 2.8 (fitted, Fig. 4.10, 4.12) for Triple E versus ϵ_s of 2.2 for Super T. There is no secondary state at t_i = 40, 100 seconds. At 100 second pass times RH drops to 0.84, similar to the 0.88 of Super T.

For Super T at 400°C, $\dot{\epsilon}$ = 0.1 s^{-1} (Fig. 4.23) RH values are all lower than at 1.0 s^{-1} (Fig. 4.21) with no secondary steady state reached at any hold time. This contrasts with the ϵ_s of 1.5 for continuous deformation (Fig. 4.11). For t_i = 10 seconds RH rises above 1 for the second and third passes indicating net hardening (relative to the first pass), then drops back to 0.99 at ϵ = 1.8, less than the 1.23 at $\dot{\epsilon}$ = 1.0 s^{-1}. At t_i of 20, 40, 100 seconds RH values are 0.90, 0.87, and 0.81 respectively, all lower than the 0.99, 0.91, and 0.88 at 1.0 s^{-1}.

As in the case of the Super T alloy, Triple E at 400°C, $\dot{\epsilon}$ = 0.1 s^{-1} (Fig. 4.22) does not develop a secondary steady state at the 10 second hold time. In continuous testing (Fig. 4.12) ϵ_s is 1.9 at 0.1 s^{-1} and 2.8 (fitted) at 1 s^{-1}. At t_i = 100 seconds RH continually declines to 0.76, comparable to the 0.81 of the Al-0.5Co-0.5Fe alloy. At this hold time the decline in RH is independent of $\dot{\epsilon}$ for both alloys. At 400°C Triple E shows greater difference between the continuous and interrupted deformation curves than the Super T alloy. At the end of the last pass at t_i = 100s, the RH value at both $\dot{\epsilon}$ drops to 54% of their values in uninterrupted straining. At the same T and

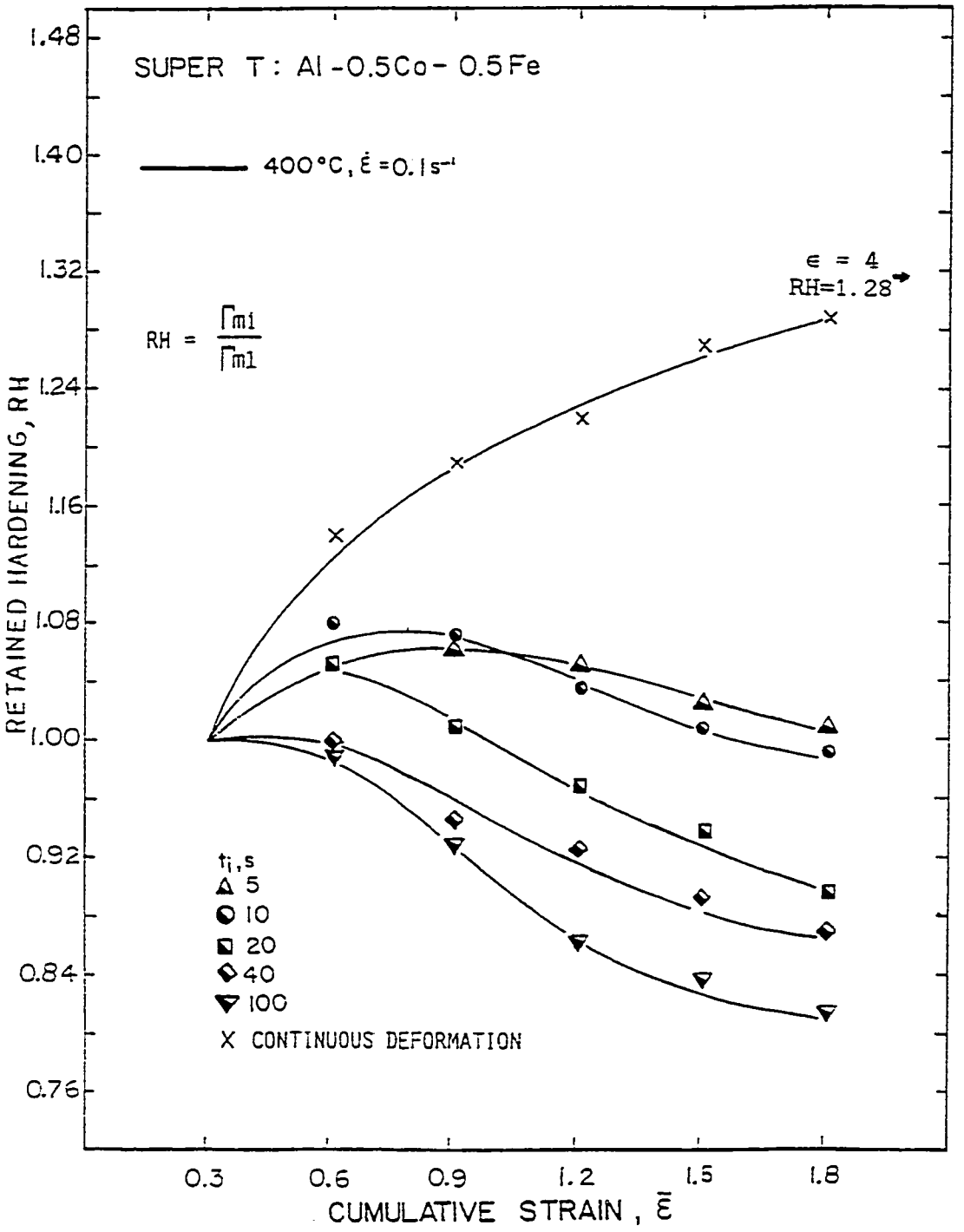

Fig. 4.23 Retained hardening (RH) versus cumulative strain for Super T during isothermal (400°C) multistage tests. RH peaks at lower strain than continuous deformation tests then drops with increasing ϵ and pass time.

t_i the RH value for Super T is 67% of the continuous curve at 1.0 s^{-1}, and 62% at 0.1 s^{-1}.

At 450°C, 0.1 s^{-1} (Figure 4.24) the differences in measured torques were at the limit of resolution with the result that the RH curves represent only general trends of an equilibrium Γ_{mi} which is lower with increase in T and t_i. As in the case of hot strength, both the Super T and Triple E exhibited similar RH at 450°C. For Super T at 450°C, t_i = 10s, hardening of 3.5% after the first pass is substantially lower than the 23% at 400°C. For Triple E at 450°C, t_i = 10 seconds, hardening is zero after the first pass, lower than the 8% gain at 400°C. Under no test conditions did the maximum pass stress fall below the yield stress.

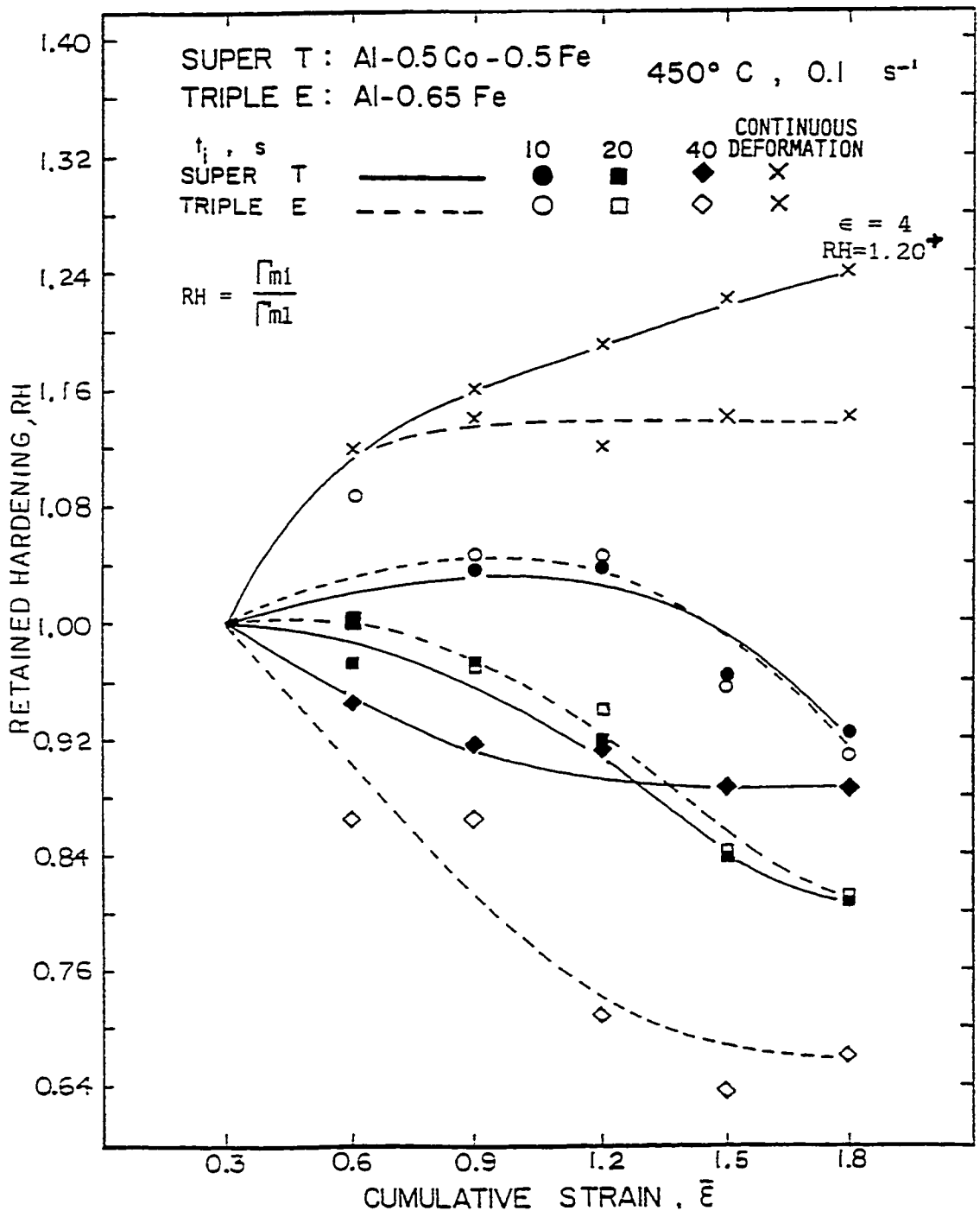

Fig. 4.24 Retained hardening (RH) versus ϵ at 450°C. RH < 1 indicates softening relative to first pass. Accumulating strain energy during pass unable to balance effects of higher cumulative SRV at higher T.

CHAPTER 5

DISCUSSION

5.1 Causes of Experimental Scatter

Although dimensional variations and differences in specimen preparation existed, the scatter in experimental results arose largely from the inhomogeneity of grain size from one specimen to another as a result of random unpinning of grain boundaries by particles. Recrystallization anneals greatly reduced the number of small grains, but grain size distribution remained inhomogeneous with specimen to specimen variations in annealing. The higher stability of the Super T alloy suggests that problems associated with non-uniform particle unpinning would occur to a lesser degree and at higher temperatures than Triple E. This was borne out by the observation of slightly higher scatter in Figures 4.1 and 4.2 at 450^{o}C and 500^{o}C for the Triple E alloy.

The effect of deformational heating in producing flow localization is usually most apparent at high T as a result of higher temperature sensitivity (62). When flow is thermally activated, rate sensitivity is related to temperature sensitivity. Instability due to localized deformational heating was not suspected as a cause of scatter as there was no temperature rise detected by the thermocouples, and only a few specimens randomly exhibited non-uniform

deformation, all at ϵ = 20, primarily at a deformation rate of 0.1 s^{-1}.

In the present case the increasing scatter with rise in T is also due to the reduction in strength to about 20% of its 200°C value at 500°C, resulting in any systematic experimental errors assuming a higher percentage of the recorded output.

5.2 Rate Sensitivity

Rising strain rate sensitivity of the torque (Fig. 4.1, Triple E, Fig. 4.2, Super T) indicated the increasing operation of the stress assisted thermally activated mechanisms responsible for recovery, specifically climb of edge dislocations, and node unpinning (13, 18, 37). Positive rate sensitivity is taken to indicate that the material is being deformed in the hot working range. As in most metals rate sensitivity in commercial Al increases with temperature; for the present alloys they are below commercial Al at 200°C but quickly rise above it. In some alloys such as precipitation hardened 2024 (Al-4.4Cu- 0.6Mn-1.5Mg) the room temperature rate sensitivity is negative and less than Al, but increases at a higher rate until it is greater in the hot working range (63). Rate sensitivities in both the present particle strengthened alloys and 2024 become positive at the same homologous temperatures, 0.62 T_m (300°C) for the former, and 0.61 T_m (200°C) for the latter.

It would be expected that temperature increases due to deformational heating would increase with σ, i.e. larger ΔT as test temperature declined to 200°C and strain rate increased to 4 s^{-1}, giving reduced torque values; however from noting the 300°C points at $\dot{\epsilon}$ = 0.02 and 0.1 s^{-1} (Super T, Fig. 4.2) where deformational heating would be virtually zero, the rate sensitivity is just marginally positive, being greater for Triple E (Fig. 4.1). This supports the observation that 200°C (0.51 T_m) is not in the hot working range as the dispersed particle stabilized substructure is delaying the onset of rate sensitive behaviour that is associated with thermally activated flow.

Comparison of Figures 4.1 and 4.2 with Figures 4.10 to 4.13 reveals the rate dependence of ductility, both strain rate sensitivity and ductility rising with temperature. Decreasing ϵ_f with increasing $\dot{\epsilon}$ is typical of materials that dynamically recover, however, unlike precipitation strengthened 7012 alloy (Al-6.3Zn-1.9Mg-1.1Cu-0.1Zr) ϵ_f continually rises with T at all strain rates. In the 7012 alloy fracture strain at 300 and 350°C was independent of $\dot{\epsilon}$, and at 5 s^{-1} ϵ_f declined with rise in T (64). This behaviour was attributed to partial solution of the (Mg,Cu) Zn_2 particles in the 7012 alloy, where as in the present alloys the particles remain insoluble. Rate sensitivities at 500°C of 0.19 are below the 0.5 associated with grain boundary sliding but above the m value of 0.1 associated with plastic flow by slip (65). Slip with DRV would produce higher m values (0.2-0.25) due to stress activation of climb and cross-slip but as rate sensitivity would be expected to be higher with significant

reduction in strain rate, a subsequent investigation was made into the potential for superplastic deformation in the alloy (66). Superplasticity was not found, which was attributed to lack of sufficient particle stabilization to initiate continuous dynamic recrystallization.

Decrease in the stress exponent n' (reciprocal of m) with increase in temperature (Table 4.1) followed the expected behaviour, as the equilibrium between dislocation generation and annihilation was shifted to a lower strain with higher T (increased annihilation rate). The work hardening rate is important in tensile testing as it determines the onset of instability but of course does not have the same significance for the torsion tests where there is no necking.

5.3 Flow Curve Shape

The stress strain flow curves (Fig. 4.3, 4.4) show the dependence on $\dot{\epsilon}$ and T typical for materials which dynamically recover; strain hardening diminishing to a steady state at lower σ with increase in T or fall in $\dot{\epsilon}$. For reasons of brevity, flow curves were not presented for all the tests but similar behaviour was observed. The significant difference observed between the alloys and pure Al or other Al alloys is in their higher strain to steady state behaviour under all conditions of T and $\dot{\epsilon}$. At 200°C, $\dot{\epsilon}$ = 0.1 or 1 s^{-1} the flow curve is still rising at ϵ = 4, whereas for many Al alloys a steady state can be obtained from ϵ = 0.2 (67) to ϵ = 1.0 (68) (extrapolated) at this T, and ϵ_s < 0.5 at higher T (13). Reference to Figures 4.10 and 4.11

at 200°C indicates ϵ_f at 4.6 to 5.1 for Super T and 3.8 to 8.1 for Triple E. Thus at low T, for the most part, the flow curve continually increased to fracture, without attaining steady state conditions.

Dynamic recovery reduces the strain hardening rate over that observed during cold working. Decrease in the hardening rate to zero, i.e. the establishment of steady state deformation conditions, results from the creation of a stable recovered substructure with uniform subgrain size. The continuous work hardening up to fracture, without achieving steady state as at 200°C for the present alloys is indicative of low temperature recovery.

For tests to $\epsilon = 4$, the flow curves which reached steady state did not exhibit the shallow decline observed by some workers at low $\dot{\epsilon}$ and attributed either to deformational heating or to work softening (69, 70). As the eutectic rods are not easily sheared and do not undergo noticeable coalescence, there is no work softening as there is in alloys such as 2024. As the temperature was raised to 500°C, the steady state strain and stress decreased (Fig. 4.3 and 4.4, Fig. 4.10 and 4.11) due to the increasing operation of the thermally activated mechanisms of dynamic recovery.

5.4 Effect of Temperature and Strain Rate on Stress

In Figures 4.5 and 4.6 the values of n in the hyperbolic sine equation were determined as 3.5 and 3.1 for Triple E and Super T

respectively. The constants in this equation are empirical but related to those in the power law (eqn. 2.3). In creep studies utilization of the power law with a stress exponent of 4 to 5 was identified with dislocation climb (38, 39, 40). Values of n near 3 have been associated with viscous drag (40) although this has not been observed in hot working. The n values are lower than the 4.1 for Al (22, 54) but greater than the 1.7 for 7012 and 5083 (19, 64).

Figures 4.5 and 4.6 illustrate the degree of strengthening in the alloys. The dependence of rising stress with rise in $\dot{\epsilon}$ or decline in T was similar for the alloys and commercial Al, with the alloys possessing strength 50% over that of pure Al at low T. Both are stronger at 300°C (0.58 T_m) than commercial Al at 200°C. The increased strength, equivalent to more than 100°C differential at 300°C, declined to 70°C at 400°C, 40°C at 450°C and 20°C at 500°C, with Super T stronger than Triple E. The substructure refinement and stabilization has been brought about largely by the 0.2μm diameter eutectic rods of $FeAl_3$ and $(Fe,Co)_2Al_9$. As the particles are insoluble in the 200°C to 500°C range and ease of particle fracture does not increase with rise in T, loss of strengthening likely occurs by the greater ease of cross-slip and climb around the particles. Minimum hot working temperature is raised by the particle content as dislocations have difficulty bypassing or deforming particles at the low end of the temperature range. The small eutectic rods also appear responsible for preventing growth of recrystallization nuclei which may form at primary particles of $FeAl_3$ with diameters of 0.6 μm or more (28, 71). The high hot strength is not unexpected given the

previously documented creep resistance, but the rapid decline in strength above 400°C ($0.72T_m$) is due to the transition in recoverability, unlike other Al alloys that would overage at high T.

Activation energies determined as 260 and 270 kJ/mol for Super T and Triple E respectively are much higher than the 150-155 kJ/mol for pure Al , the latter related to dislocation climb since it is dependent on the motion of vacancies in self-diffusion (13, 22, 35, 37, 72, 73). The higher Q_{HW} of the alloys likely results from the inhibition of DRV caused by the particles, and exhibited as subgrain refinement and increasing strength over Al as T declines to 200°C.

Figure 4.7 also illustrates the degree of strengthening conferred by the high $(Mg,Cu)Zn_2$ particle content and solute addition in 7012 (Al-6.3Zn-1.8Mg-1.1Cu-0.1Zr-0.1Mn) and 5083 (Al-4.5Mg-0.8Mn-0.15Cr) alloys (9, 64). The combined solute and particle strengthening of the 5083 alloy persists to higher temperatures than particle strengthening alone. The strength of the 7012 alloy is actually much closer to that of the 5083 as there was approximately a 10% error in omitting the corrections for rate sensitivity and strain hardening exponents. Figures 4.8 and 4.9 further illustrate that the 200°C data for Triple E and Super T lies above the line fitted to the higher temperature data, whereas commercial Al at the same T falls along the line for higher temperature points (9, 13, 37, 54, 74).

5.5 High Strain Testing

Flow curve shape exhibited the same trends as in testing to ϵ = 4, thus additional data was not presented. When deformed to ϵ = 20, the alloys did not exhibit the gradual decline with strain near ϵ = 5-10 that has been attributed to either deformational heating, or development of a preferred orientation in Al tested to high strains (74).

Steady state and fracture strain data were compiled from tests to ϵ = 4 and 20 and presented in Figures 4.10 to 4.13. The alloys exhibited improved ductility as $\dot{\epsilon}$ declines or T rises from the very low values at 200°C and 300°C. The low ductility at these temperatures, which is associated with a greater number of intergranular cracks at low T (because of higher stress concentration due to the low level of dynamic recovery), occurred as a result of the fine particle dispersion; rising ϵ_s and declining ϵ_f with increase in $\dot{\epsilon}$ is indicative of the decreasing effect of DRV (reduced dislocation annihilation rate) at lower temperatures (9, 13, 54). The close association of ductility with DRV (earlier occurrence of a balance in dislocation generation and dislocation annihilation) is confirmed by the association of high ϵ_f with low ϵ_s. With reduced DRV the difference between ϵ_s and ϵ_f is diminished until at 200°C fracture occurred before steady state was established; however, the ductility is still sufficient for commercial processing (58). The lower ductility of Super T than Triple E at 200°C and 300°C is consistent with the higher strength and lower DRV of the former. The reason for

the higher ϵ_f and lower ϵ_s of Super T versus Triple E at 400°C (Fig. 4.10, Fig. 4.11) has not been determined but it may be an artifact of the test program. Above 400°C the ductility (and strength) conform more to that of pure Al, though the strain sensor limit of 20 precluded a precise determination. Ductility is less than that of Al or Al-2Mg, but exceeds that of Al-5Mg (75). Because the particles and inclusions produced during rapid solidification are fine and well distributed they do not reduce ductility by serving as crack initiation sites, as do the larger particles produced during conventional processing. They affect ductility through reductions in DRV which is indicated by the greater activation energy for the two alloys (versus commercial Al), and thus higher σ_s and ϵ_s.

5.6 Effect of Hot Torsion on Hardness and Microstructure

Room temperature hardness (Table 4.2) declines with rising deformation T as a result of reduced dislocation density and much larger equilibrium subgrain size (58). The useful hardness increase of 25% over Al at 200°C can be attributed to the denser substructure due to the higher $FeAl_3$ content in the Triple E alloy. The 0.65% Fe level is twice the common impurity level of 0.3-0.35 Fe in commercially pure (1100) Al. At 200°C, the higher particle density of Super T produced a more refined substructure, with hardness 50% greater than Al. Deformation at 500°C reduces the incremental hardness over Al by half, to 23% for Super T, and 13% for Triple E, reflecting the reduced effectiveness of particles in stabilizing the subgrain size.

Table 4.3 quantifies the strength gains associated with declining T and rising $\dot{\epsilon}$. The Al-0.5Fe-0.5Co and Al-0.65Fe alloys are used in cold drawn and recovery annealed condition, which is similar to those of working at 200 - 300°C. The hot strength of Triple E at 200°C is 24% stronger than Al, while σ_s for Super T is 43% higher. At 200°C, the rate sensitivity for 1100 Al is low, with σ_s rising only 5% with a 900% increase in $\dot{\epsilon}$, similar to that observed in the present alloys. Electrical conductor grade alloy (EC1350) is essentially impurity controlled Al and would be expected to have mechanical properties similar to 1100. Optical micrographs failed to reveal any signs of dynamic or static recrystallization as would be expected with the short quench delay times (< 6 seconds). Subsequent TEM studies by another researcher on the tested specimens found the twisted and elongated grains with substructure associated with DRV, and confirmed and quantified the increases in subgrain size d_s with decline in $\dot{\epsilon}$ or rise in T (60, 61).

5.7 Interrupted Deformation Testing

Fractional softening graphs of interrupted deformation tests were plotted in Figures 4.18 to 4.20 to determine the presence and extent of interpass SRV and SRX. Evaluation of the degree of softening from SRV or SRX by metallography or transmission electron microscopy is extremely laborious and requires far more test specimens if subgrain structures are to be determined at each interval, rather than inferred from mechanical properties. In Al and most of its alloys, a high degree of interpass softening results from static recovery alone.

There is usually a long incubation time prior to SRX because of the highly recovered substructure from DRV. Fractional softening (FS) of up to 55% for Triple E and 50% for Super T was recorded at 450°C, due to recovery alone, since no evidence of SRX being found in subsequent metallography. The 55% FS without SRX contrasts to only 30% without SRX in the austenitic stainless steels, which also undergo DRX at high ϵ due to the low level of DRV (53, 76). As SRX times for these alloys are in the order of hours at the deformation temperature, with a maximum test t_i of 100 seconds, the upper bounds on the extent of static recovery was not established. The intervals employed were well beyond those in commercial rolling practice so SRX would not be expected during processing.

The extent of FS possible in a fixed time at constant T is dependant upon the amount of accumulated strain energy. Rising $\dot{\epsilon}$ should produce a higher dislocation density and hence a higher stored energy, which should lead to an increased restoration rate. The lack of significant strain rate effects could be an artifact of the test in that the span of strain rates was may not be large enough to demonstrate an effect. As a large temperature sensitivity on fractional softening (FS) was found, a high level of thermal activation may create an equilibrium subgrain structure via SRV and DRV that is independent of the strain rates utilized.

For the Super T alloy, there was a normal progression of continually increasing FS with t_i, from approximately 15% at t_i= 5s, to 22% at 10 s, 26% at 20 s, and 35% at 40 seconds. Triple E

displayed abnormal behaviour with an unusually high FS of approximately 19% at 5 s and an unusually low 21% FS at 20 seconds. Part of the drop in hot strength at low t_i for both alloys can be attributed to anelastic behaviour as the mobile dislocations run back from their stressed state upon the release of the load. The presence of a common value of FS at t_i= 5, 10, 20 seconds for Triple E (Fig. 4.18) may result from the above effect, its absence in Super T (Fig.4.19) may result in differences in strain hardening behaviour and thermal stability over the Al-0.65Fe Triple E alloy. Increasing the t_i from 5 to 20 s for Triple E at 400°C, 0.1 s^{-1} may not increase FS if all possible softening via SRV had already occurred by 5 s, whereas the higher stability of Super T meant that a 5 second hold time would not be sufficient to relieve the accumulated strain energy by DRV. At 400°C a critical T was observed where there was a rapid decrease in strength and increase in ductility for both alloys. At this T, dislocations can climb around particles, hence there is a likelihood of greater experimental scatter in strength or in softening due to relatively small differences in particle distributions. The higher particle density of the Al-0.5Co-0.5Fe Super T alloy is no longer pinning the cell walls but is still impeding dislocation motion to a greater extent than Triple E. As Super T retains somewhat greater strength during continuous tests at 400°C , when softening occurs due to SRV it consequently is of a greater percentage.

At 450°C higher thermal activation and ease of dislocation motion past the particles raises FS for both alloys to effectively identical values. Although no testing was done on commercial Al at 450°C,

similar values of FS would be expected, following the comparable strength of both alloys and commercial Al at this T. Unlike the alloys, commercial Al does not undergo a transition in recoverability at 400°C.

5.8 Relative Retained Hardening

Relative retained hardening (RH) plots were made for the first time for the current thesis work to address difficulties found in the analysis and presentation of the interrupted deformation test results. In RH plots, the maximum torque was precisely determined, whereas in fractional softening (FS) graphs the values of the reloading torque Γ_r and yield torque Γ_o were result of subjective interpretation. Few datapoints were available to determine Γ_o and Γ_r due to the specifics of the data recording system on the torsion machine. Additionally, as a result of the low strength of the alloys at 400°C, even a small change in the determination of the torque values resulted in a large variation in %FS. Consequently, the RH plots were made with exact values that eliminated any uncertainty over the approximate values obtained via the FS analysis. Due to the scatter in torques values a superimposed plot of all of the interrupted deformation tests could not be made, as is commonly done. By normalizing strength relative to the first pass strain (ϵ = 0.3) it was possible to follow the progress of net hardening or softening for each pass in comparison to the

continuous deformation curve via RH plots.

The behaviour exhibited in interrupted deformation testing is a function of the gross deformation and interpass softening (accumulated dislocation structure) for each selection of interpass hold time, T, $\dot{\epsilon}$, and material. For alloys of Al that only undergo DRV it is expected that the material will rapidly strain harden back up to the continuous flow curve, however other behaviour is possible. When interpass hold time is sufficient to allow SRX, then the interrupted deformation curves would be much reduced and remain below that of the continuous case. If deformational heating was a significant factor in lowering flow stress at a specific T, ϵ , and $\dot{\epsilon}$, heat rejection during the interpass hold times would result in the interrupted pass curves rising above that of continuous loading, an effect that was noted in the testing of 5083 alloy. Thus, multi-pass tests could serve to indicate the presence and extent of deformational heating, with small t_i producing results close to continuous deformation, and large t_i allowing for heat dissipation and greater strength at lower T. There was no observed rise of RH above the continuous case at 400^{o}C and 450^{o}C for the alloys, and thus it may be concluded that the temperature rise during uninterrupted straining is negligible at these conditions of T and $\dot{\epsilon}$. The above conclusion matches the experimental observations of a ΔT of only a few ^{o}C during continuous testing.

For the alloys, RH in interrupted tests was always less than that of the continuous case, that is the interrupted deformation pass curves fell below those of continuous deformation without SRX being

detected via metallography. The decline in the RH curves with successive passes likely results from inheritance of a substructure at the start of any pass that is weaker and coarser than what would have been created by uninterrupted straining to that same strain. Without detecting SRX, an RH value of 1 implies an accumulated interpass softening due to SRV which counters any strain hardening after the first interval. A rise in RH above 1 indicates net hardening relative to the first pass, and decline below 1 signifies that strength is falling below that reached in the first pass. In only one condition, 400°C, 1.0 s^{-1}, t_i = 10 s , the Super T alloy hardened up to the continuous flow curve, as if the dislocations had great difficulty bypassing the particles so that SRV was inhibited during the interval.

The decline in maximum pass stress, with or without a secondary steady state is clear on the RH plots, but not readily apparent in FS graphs, where it should appear as a rise in FS with strain. For Super T, 400°C, 0.1 s^{-1}, t_i= 100s (Fig 4.19), FS rises with ϵ matching the decline in RH (Fig.4.23). This match between plots was not consistent, probably due to the difficulties associated with determining Γ_o and Γ_r. The RH plots also display a greater range in behaviour. For the above mentioned Super T test conditions at ϵ = 0.3, FS = 33%, but ΔRH (compared to the continuous curve) is only 13%, while at ϵ = 1.8 FS = 46% versus 37% ΔRH. When the strain to peak stress is much larger than the pass strain (as in these alloys), the FS plots may overestimate the softening relative to continuous deformation. As an example, for Super T at 400°C, 1.0 s^{-1}, t_i= 10s (Fig.4.21), ΔRH is approximately 4% versus 19% FS (Fig.4.19). If FS

is constant there is no decline in the maximum pass strength, even with FS as high as the 60% associated with the SRV in Al. The RH plots show that at low $\dot{\epsilon}$ and longer hold times (40-100s not unusual for a reversing mill) the material may be substantially weaker than would be predicted from continuous curves. Thus, when there is scatter in the data, ϵ_s > pass strain, or limited data is available to reliably determine FS, the RH plots (or %RH) can be made to accurately calculate rolling forces during each pass.

In the present materials, the strain hardening in each stage at 400°C was insufficient to balance the cumulative effect of static restoration. This is particularly evident at 0.1 s^{-1} where there is a significant divergence between continuous and interrupted RH curves for both alloys, even for t_i = 10s. When compared at 400°C, $\dot{\epsilon}$ = 0.1 s^{-1}, t_i = 100s (Fig.4.22), the multistage flow stress of Triple E at ϵ = 1.8 is 50% lower than the continuous due to repeated SRV, versus 25% for Super T. The lower particle density of Triple E is unable to stabilize the substructure against SRV in the interval to the same extent as the Super T alloy. At $\dot{\epsilon}$ = 1.0 s^{-1} the higher values of RH than at 0.1 s^{-1} are attributed to the higher rate of dislocation generation which is better able to counteract the combined effects of SRV and DRV. At 1.0 s^{-1}, t_i = 20s, the Super T alloy (Fig.4.21) has a secondary steady state while the Triple E at the same conditions does not. At 100s t_i neither alloy has a secondary steady state and the decline in RH becomes independent of $\dot{\epsilon}$ due to high interpass SRV. The greater scatter in the data as well as the higher difference in RH between the interrupted and continuous data for Triple E (Fig. 4.22,

4.24) versus Super T likely results from the reduced stabilizing effect of the fewer particles in the Al-0.65Fe alloy.

At 450°C, 0.1 s^{-1} (Fig.4.23), the magnitude of stress changes were at the effective limit of resolution, therefore the plotted curves only indicate general trends. Both alloys exhibit similar behaviour at 450°C, with interrupted ϵ_s < continuous ϵ_s, and declining RH with increase in t_i, as both have passed through a transition in recoverability where the particles no longer pin the dislocations. Due to the above mentioned transition, the observed RH values at t_i= 10s and 20s were similar for the alloys, matching the observation of similar FS values. The plotted deviation between the Triple E and Super T at 40s pass times may not be significant due to the limits on the determination of the low levels of stress. The existence of an unrecrystallized structure prior to testing can be inferred from the pass curves if the maximum stress in any interval falls below the yield stress. As no datapoints met this criteria, the inference was rejected.

CHAPTER 6

CONCLUSIONS

1) The Al-0.5Fe-0.5Co Super T alloy and Al-0.65Fe Triple E Alloy undergo dynamic recovery during continuous testing. The Al-0.5Fe-0.5Co alloy is generally stronger and less ductile than the Al-0.65Fe alloy.

2) As the eutectic particles in these alloys strengthen by inhibiting dynamic recovery, activation energies for hot working are found to be much higher than Al, consistent with previously observed substructures.

3) Good hot ductility arises from DRV mechanisms as can be inferred from increases with T, decrease with $\dot{\epsilon}$, and the inverse relationship between ϵ_f and ϵ_s. Below 300°C the dispersed eutectic rods decrease ductility.

4) The temperature dependence of the alloys is much higher than Al while the strain rate dependence is about the same.

5) The hot working characteristics of the alloys are similar to Al but the relative strength rises more rapidly as $\dot{\epsilon}$ is raised and T lowered to 200°C. Triple E and Super T have the same strength at 300°C as EC-AL at 200°C.

6) The applicability of the sinh laws and Z parameter down to 300°C, instead of 200°C for Al indicates that the minimum hot working temperature is raised by the particles.

7) Below 400°C the particles significantly raise hot and cold strength over Al. As T is raised above 400°C the strength approaches Al, as a transition in recoverability at this T means the particles have reduced capability to limit subgrain size, raise hot strength, lower hot ductility, or increase final cold hardness.

8) During multipass testing the only operating restorative mechanisms are dynamic and static recovery, as confirmed by the characteristic shape of the flow curves, and subsequent metallography.

9) Fractional softening increases with rising temperature and ϵ, consistent with DRV during cumulative straining and SRV between passes.

10) In multipass deformation the strain hardening at each stage was unable to balance the cumulative effect of static restoration. This was demonstrated by the fall in retained hardening with rise in interpass hold time and strain to values far below the continuous case.

11) Due to high interpass SRV, no significant strain rate rate effects were noted under the interrupted test conditions employed.

REFERENCES

1) G.E.Leneaus and H.R.M. McPheters, Triple E and Super T Aluminum Alloys for Electrical Applications, Metals and Materials 6, 1972, pp.401-403

2) D.E.Newbury and S.Greenwald, Observations on the Mechanisms of High Resistance Junction Formation in Aluminum Wire Connections, J. of Research, vol.85, no.6, Nov-Dec 1980, pp.429-440

3) D.E.Newbury, What is Causing Failures of Aluminum Wire Connections in Residential Circuits ?, Analytical Chemistry, vol.54, no.9, August 1982, pp.1059A-1064A

4) Editors, Whatever Happened to Aluminum House Wiring, IEEE Spectrum, May 1984, p.17

5) E.H.Chia, and E.A.Starke, The Influence of Precipitates and Subgrains on the Properties of Aluminum Conductors, Aluminium 47, 1971, pp.429-431

6) F.Kutner, "Aluminium Conductor Materials", Aluminium-Verlag, Dusseldorf, 1981, pp.15-27

7) R.Iricibar, C.Pampillo, and E.H.Chia, Metallurgical Aspects of Aluminum Alloys for Electrical Applications, in "Aluminum Transformation Technology and its Application", ASM, Metals Park Ohio, 1978, pp.241-303

8) J.E.Hatch, ed, "Aluminum: Properties and Physical Metallurgy", ASM, Metals Park Ohio, 1984

9) E.H.Chia and E.A.Starke Jr., Applications of Subgrain Control to Aluminum Wire Products, Met Trans A, vol.8A, June 1977, pp.825-832

10) H.J.McQueen, The Experimental Roots of Thermomechanical Treatment for Aluminum Alloys, J.Of Metals, February 1980, pp.17-26

11) O.D.Sherby, R.H.Klundt, and A.K.Miller, Flow Stress, Subgrain Size, and Subgrain Stability at Elevated Temperature, Met Trans A, vol 8A, June 1977, pp.843-850

12) H.J.McQueen, Dynamic Recovery and its Relation to Other Restoration Mechanisms, Metalurgia I Odlewnictwo (Metallurgy and Foundary) Tom5 Zeszyt 3, 1979, pp.421-450

13) H.J.McQueen, and J.J.Jonas, Recovery and Recrystallization During High Temperature Deformation, in "Treatise on Materials Science and Technology" vol.6, ed. R.J.Arsenault, Academic Press, NY, 1975, pp.393-493

14) J.G.Morris, Dynamic Strain Aging in Aluminum Alloys, Mater. Sci. Eng. 13, 1974, pp.101-108

15) J.G.Morris and B.J.Roopchand, The Hot Working of Constitutionally Unstable Alloys, in "Proc. 4th Intl. Conf. Strength of Metals and Alloys", Vol.2, 1976, pp.617-623

16) M.A.Meyers and K.K.Chawla, "Mechanical Metallurgy, Principles and Application", Prentice-Hall, Englewood Cliffs NJ, 1984

17) R.W.Evans and G.R.Dunstan, The Hot Working and Subsequent Restoration of Commercial Purity Aluminum, J.of Inst.of Metals, vol.99, 1971, pp.4-14

18) C.M.Sellars, Hot Working Operations, in "Aluminum Transformation Technology and its Application", ASM, Metals Park Ohio, 1978 pp.405-440

19) H. J. McQueen, E. Evangelista, J. Bowles, and G. Crawford, Hot Deformation and Dynamic Recrystallization of Al-5Mg-0.8Mn Alloy, Metal Science 8, 1984, pp. 395-402

20) D. J. Abson and J. J. Jonas, Substructure Strengthening in Zirconium and Zirconium-Tin Alloys, J. Iron. Steel Inst., 1971, vol. 209, pp. 624-671

21) D. J. Abson and J. J. Jonas, The Hall-Petch Relation and High-Temperature Subgrains, Metal Sci. J., 1970, vol. 4, pp. 24-28

22) H. J. McQueen and K. Conrod, Recovery and Recrystallization in the Hot Working of Aluminum Alloys, in "Microstructural Control in Aluminum Alloys", ed. E. H. Chia and H. J. McQueen, TMS-AIME, Warrendale, Pa., 1986, pp. 197-219

23) H. J. McQueen, The Experimental Roots of Thermomechanical Treatments for Aluminum Alloys, in "Thermomechanical Processing of Aluminum Alloys", ed. J. G. Morris, TMS-AIME, Warrendale, Pa., Oct. 1978, pp. 1-24

24) D. Kalish, B. G. Lefevre, and S. K. Varma, Effect of Alloying and Processing on the Subgrain-Strength Relationship in Aluminum Conductor Alloys, Met. Trans A, vol. 8A, Jan 1977, pp. 204-206

25) H. J. McQueen, E. H. Chia, and E. A. Starke, The Microstructural Strengthening Mechanisms in Dilute Al-Fe Conductor Alloys, in "Microstructural Control in Aluminum Alloys;", ed. E. H. Chia and H. J. McQueen, AIME, Warrendale, Pa. 1986, pp. 1-18.

26) H. J. McQueen, E. H. Chia, and E. A. Starke, Fe-Particle Stabilized Aluminum Conductors, J. Met., vol. 38, 1986, pp. 19-24

27) H. J. McQueen and J. E. Hockett, Microstructures of Aluminum Compressed at Various Rates and Temperatures, Met. Trans A, vol. 1, 1970, pp. 2997-3004

28) E.Evangelista, H.J.McQueen, and E.Bonetti, Interaction Between (MnFe)Al_6 Particles and Substructure Formed During Hot Working of Al-5Mg-0.8Mn Alloy, in "Deformation of Multiphase and Particle Containing Materials", ed.J.Bilde-Sorensen, RISO Natl. Lab, Roskilde, Denmark, 1983, pp.243-250

29) D.J.LLoyd and D.Kenny, The Structure and Properties of Some Heavily Cold Worked Aluminum Alloys, Acta.Met., vol.28, 1980, pp.639-649

30) C.M.Sellars and W.J.McG.Tegart, Hot Workability, Int.Met.Rev, 1972, pp.1-24

31) J.J.Jonas, C.M.Sellars, and W.J.McG.Tegart, Strength and Structure Under Hot Working Conditions, Met.Rev., vol.14, 1969, pp.1-24

32) A.W.Thompson, Substructure Strengthening Mechanisms, Met.Trans 8A, June 1977, pp.833-842

33) W.A.Wong, H.J.McQueen, and J.J.Jonas, Recovery and Recrystallization of Al During Extrusion, J.Inst.Metals, vol.95, 1967, pp.129-137

34) J.J.Jonas, H.J.McQueen, W.A.Wong, and D.W.Demianczuk, in "Deformation Under Hot Working Conditions", Iron. Steel. Inst., 1968, pp.97-99

35) H.J.McQueen, The Production and Utility of Dislocation Recovered Substructures, Met.Trans 8A, June 1977, pp.807-824

36) H.Mecking and G.Gottstein, Recovery and Recrystallization During Deformation, in "Recrystallization of Metallic Materials", ed. F.Haessner, Dr.Riederer-Verlag, Stuttgart, 1978, pp.195-222

37) H.J.McQueen and J.J.Jonas, Role of Static and Dynamic Softening Mechanisms in Multistage Hot Working, J.Appl.Metal Working 3, 1985, pp.410-421

38) H.J.McQueen and H.Mecking, Comparison of Deformation and Failure Mechanisms in Hot Working and in Creep of Metals, in "Creep and Fracture of Engineering Materials and Structures", ed. B.Wilshire and D.R.J.Owen, Pineridge Press, Swansea, U.K., 1984, pp.169-184

39) W.D.Nix and B.Ilschner, Mechanisms Controlling Creep of Single Phase Metals and Alloys, in "Strength of Metals and Alloys (ICSMA 5)", ed.P.Haasen et al, Pergammon Press, Oxford, vol.3, 1979, pp.1503-1530

40) T.G.Langdon, Deformation at High Temperatures, in "Strength of Metals and Alloys (ICSMA 6)", ed. R.C.Gifkins, Pergammon Press, Oxford, 1982, pp.1105-1120

41) C.M.Young, and O.D.Sherby, Simulation of Extrusion Structures by Means of Torsion Testing for a High Strength Nickel Base Alloy, UDIMET 700, in "Metal Forming: Interrelation Between Theory and Practice", ed.A.L.Hoffmanner, Plenum Press, N.Y., 1971, pp.429-451

42) C.Zener, J.H.Hollomon, Effect of Strain Rate Upon Plastic Flow of Steel, J.Appl.Physics, vol.15, Jan.1944, pp.22-32

43) T.C.Rollason and J.W.Martin, The Effect of Particle Size Upon the Annealing Behaviour of Plastically Deformed Two-Phase Crystals, J.Mat.Sci. 5, 1970, pp.127-132

44) P.Fiorini, Aluminum for Electrical Conductors, Wire Industry, June 1979, pp.265-68

45) E.H.Chia, The Effect of Solidification Rate on the Properties of Al-Fe-Co (Super-T) Conductor Alloy, Wire Journal, June 1979, pp.66-70

46) E.H.Chia, S.Spooner, E.A.Starke, Microstructure and Texture of Continuously Cast and Rolled Aluminum, Aluminium 54, 1978, pp.757-761

47) S.Fulop, K.C.Cadien, M.J.Luton, and H.J.McQueen, A Servo-Controlled Hydraulic Hot Torsion Machine, J.Test.Eval 5, 1977 pp.419-426

48) T.Wolf and W.F.Brown Jr. eds., "Aerospace Structural Materials Handbook (AFML-TR-68-115)", Army Materials and Mechanics Research Center, Watertown, Mass., 1975

49) H.J.McQueen and J.J.Jonas, Hot Workability Testing Techniques, in "Metal Forming, Interrelation Between Theory and Practice", A.L.Hoffmanner ed., Plenum Press, N.Y., 1971, pp.393-428

50) F.Montheillet, M.Cohen, and J.J.Jonas, Axial Stress and Texture Development During Torsion Testing of Al, Cu, and α-Fe, Acta Met., vol.32, 1984, pp.2077-2089

51) K.Detert, Secondary Recrystallization, in "Recrystallization of Metallic Materials", ed. F.Haessner, Dr.Riederer-Verlag, Stuttgart, 1978, pp.97-109

52) G.F.Vander Voort, "Metallography: Principles and Practice", McGraw-Hill, 1984, p.445

53) H.J.McQueen, M.G.Akben and J.J.Jonas, Mechanical Metallography in Hot Working, in "Proc 5th Riso Int'l Symp.on Microstructural Character. of Materials by Non-Microscopic Techniques", ed. N.H. Anderson et al., Riso, Denmark, September 1984, pp.397-404

54) K.Conrod, and H.J.McQueen, The Hot Working Characteristics of Al-0.65%Fe, and Al-0.5%Fe-0.5%Co Conductor Alloys, in "Aluminum Alloys, their Physical and Mechanical Properties", ed. E.H.Chia, E.A.Starke, Virginia 1986, Eng.Mat. Advisory Service, Worley, U.K., vol.1, pp.435-447

55) H.J.McQueen, J.K.Solberg, N.Ryum, and F.Nes, Effect of Very High Strain on the Substructure and Texture of Aluminum, in "Aluminum Alloys, their Physical and Mechanical Properties", ed. E.H.Chia, E.A.Starke, Virginia 1986, Eng.Mat. Advisory Service, Worley, U.K., vol.1, pp.513-528

56) T.Sheppard and D.S.Wright, Determination of the Flow Stress, Part 2: Radial and Axial Temperature Distribution During Torsion Testing, Metals Technology, June 1979, pp.223-229

57) N.Ryan and H.J.McQueen, Hot Deformation of 301 Steel, in "Strength of Metals and Alloys (ICSMA 7)", ed. by H.J.McQueen et al, Pergammon Press, Oxford 1985, pp.935-940

58) I.Szkrumelak, K.Conrod, and H.J.McQueen, Substructure and Strength Development During Hot Working of Al-0.5%Fe-0.5%Co and Al-0.65%Fe Conductor Alloys, Aluminium 64, Jan 1988, pp.1151-1156

59) I.Szkrumelak, Private Communication, Concordia University, 1986

60) G.Avramovic-Cingara, and H.J.McQueen, Strain Hardening Rate and Substructure in Al-0.65Fe, in "Dispersion Strengthened Aluminum Alloys", ed. Y-W. Kim, W.M.Griffith, TMS-AIME Conference, Jan 1988, Phoenix, AZ, pp.437-450

61) G.Avramovic-Cingara, Private Communication, Concordia University, 1993

62) S.L.Semiatin and J.J.Jonas, in "Formability and Workability of Metals: Plastic Instability and Flow Localization", ASM, Metals Park, Ohio, 1984, p.109

63) D.K.Felbeck and A.G.Atkins, "Strength and Fracture of Engineering Solids", Prentice Hall, Englewood Cliffs, N.J. 1984

64) E.Evangelista, E.Bonetti, E.DiRusso, P.Fiorini, and H.J.McQueen, Hot Working Behaviour of High Strength 7012 Aluminum Alloy, in "Aluminum Technology 86", Institute of Metals, London, 1986, pp.185-196

65) O.D.Sherby and J.Wadsworth, Development and Characterization of Fine-Grain Superplastic Materials, in "Deformation, Processing, and Structure", ed G.Krauss, ASM Metals Park Ohio, 1984, pp.355-389

66) G.Avramovic-Cingara, H.J.McQueen, A.Salama, and T.R.McNelley, Hot Working and Resultant 300^{o}C Ductility of Al-Fe and Al-Fe-Co Alloys, Scripta Met., vol.23, 1989, pp.273-278

67) U.F.Kocks, Laws for Work Hardening and Low Temperature Creep, J.of Eng.Mater. and Tech., Trans ASME, Jan.1976, pp.76-85

68) J.E.Hockett, Compressive Stress versus Strain at Constant Strain Rates, Applied Polymer Symposia, no.5, 1967, pp.205-225

69) M.M.Farag and C.M.Sellars, Analysis of Double Maximum Flow Patterns in Axisymmetric Extrusion of H30 Aluminum Alloy, Met.Tech. Vol.2, 1975, pp.220-228

70) T.Sheppard and D.S.Wright, Determination of the Flow Stresses : Part 1 Constitutive Equation for Aluminum Alloys at Elevated Temperatures, Met. Tech., vol.6, 1979, pp.215-223

71) R.D.Doherty, Nucleation of Recrystallization in Single-Phase and Dispersion Hardened Polycrystalline Materials, in "Recrystallization and Grain Growth of Multiphase and Particle Containing Materials", ed. N.Hansen et al, Riso National Lab., Roskilde, Denmark, 1980, pp.55-70

72) H.J.McQueen, and J.J.Jonas, Recent Advances in Hot Working : Fundamental Dynamic Softening Mechanisms, J.Appl.Metalworking 3, 1984, pp.233-241

73) H.J.McQueen, O.Knustad, N.Ryum, and J.K.Solberg, Microstructural Evolution in Al Deformed to Strains of 60 at 400°C, Scripta Metal., vol. 19, 1985, pp.73-78

74) O.Knustad, H.J.McQueen, N.Ryum, and J.K.Solberg, Polarized Light Observation of Grain Extension in Aluminium Deformed at 400°C to Very High Strains, Pract.Metall., vol 22, 1985, pp.215-229

75) J.R.Cotner, and W.J.McG.Tegart, High Temperature Deformation of Al-Mg Alloys at High Strain Rates, J.Inst.Metals, vol.97, 1969, pp.73-79

76) D.R.Barraclough, Hot Working and Recrystallization of a Stainless and a Low Alloy Steel, Ph.D.Thesis, University of Sheffield, 1974

APPENDIX A

LIST OF PUBLISHED PAPERS

H. J. McQueen and K. Conrod, Recovery and Recrystallization in the Hot Working of Aluminum Alloys, in "Microstructural Control in Aluminum Alloys: Deformation, Recovery and Recrystallization", ed. E. H. Chia and H. J. McQueen, AIME Symposium, Warrendale, Pa., 1986, pp. 197-219

K. Conrod, and H. J. McQueen, The Hot Working Characteristics of Al-0.65% Fe, and Al-0.50% Fe - 0.5% Co Alloys, in "Aluminum Alloys, Their Physical and Mechanical Properties", (Virginia, 1986), Eng. Mater. Advisory Service, Worley, UK, vol. 1, pp. 435-447

H. J. McQueen, K. Conrod, and E. H. Chia, The Processing, Microstructure and Properties of Eutectic Particle Stabilized Al Alloys, in "Proc. 5th Yugoslav Int. Symposium on Aluminum", A. Paulin ed., April 23-25, 1986, pp. 525-542

I. Szkrumelak, K. Conrod, and H. J. McQueen, Substructure Formed During Hot Working of Al-0.5%Fe-0.5%Co and Al-0.65%Fe Conductor Alloys, in "Proc. 8th Light Metal Congress", Leoben, Vienna, 1987, pp. 539-544

I. Szkrumelak, K. Conrod, and H. J. McQueen, Substructure and Strength Developed During Hot Working of Al-0.5%Fe-0.5%Co and Al-0.65% Fe Conductor Alloys, Aluminum 64, Jan 1988, pp. 1151-1156

H. J. McQueen, G. Avramovic-Cingara, K. Conrod and I. Szkrumelak, Statically Recovered Substructures and Static Recrystallization in Hot Worked Al-0.65Fe and Al-0.5Fe-0.5Co Alloys, Microstructural Science, Vol. 17, 1989, pp. 375-392

H. J. McQueen, K. Conrod, and G. Avramovic-Cingara, The Hot Working Characteristics of Eutectic Rod Stabilized Conductor Alloys, Can. Met. Quart, 1993, vol. 32, pp. 375-386

G. Avramovic-Cingara, K. Conrod, A. Cingara and H. J. McQueen, Static Softening Between Passes of Rolling Simulations of Al Alloys, in "Intl. Symp. on Light Metals Processing and Applications", ed. C. Bickert, Met. Soc. CIMM, Quebec City, 1993, pp. 495-510